

ANALYSIS OF FIBER-REINFORCED COMPOSITE PLATES UTILIZING CURVILINEAR FIBER TRAJECTORIES

by

Yannick P. H. FIERLING

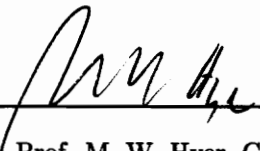
Thesis submitted to the faculty of the
Virginia Polytechnic Institute and State University
in partial fulfillment of the requirements for the degree of

MASTER OF SCIENCE


in

Engineering Mechanics

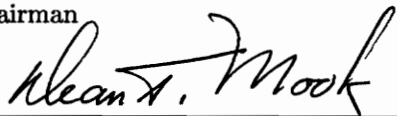
APPROVED:



Prof. M. W. Hyer, Chairman



Prof. E. R. Johnson



Prof. D. T. Mook

May, 1995

Blacksburg, Virginia

C.2

LD
E055
V055
1995
FE47
C.2

ANALYSIS OF FIBER-REINFORCED COMPOSITE PLATES UTILIZING CURVILINEAR FIBER TRAJECTORIES

by

Yannick P. H. FIERLING

Committee Chairman: Prof. M. W. Hyer

Engineering Mechanics

(ABSTRACT)

Four plates with centrally located circular holes were manufactured using a fiber placement technique. With two plates the fibers were steered around the holes in curvilinear trajectories. With the two other plates the fibers were placed in the conventional straight line format. For the case of the curvilinear trajectories, the fibers were continuous from one end of the plate to the other, whereas for the straight trajectories the fibers were cut by the presence of the hole. Two plates, a curvilinear fiber plate and a straight fiber plate, were tested in tension. The two other plates were tested in compression. The straight fiber plates were considered as baseline cases. Since the plates were thin, compression testing resulted in buckling and postbuckling. The current work focuses on the analysis of these four plates and a comparison between the analysis and experimental results. Because of a spatial dependence of the A and D stiffness matrices for the curvilinear fiber cases, the analyses were conducted using finite element methods, and included a failure criterion. A scheme to improve the plate design is also considered.

ACKNOWLEDGEMENTS

I wish to express my gratitude and appreciation to my advisor Pr. M.W. Hyer for his advice and guidance throughout the development of this thesis. I would also like to thank Pr. R. Mahan and the “Université de Technologies de Compiègne” for giving me the opportunity to pursue my higher education at the Virginia Polytechnic Institute and State University.

My sincere gratitude goes to the “Ministère des Affaires Etrangères Françaises” for honoring me with the Lavoisier scholarship for my program of study.

Funds from NASA Grant NAG-1-343 from the Langley Research Center were used for partial support of this thesis. That support is greatly appreciated.

Thanks are also due to my friends, Nachiketa Tiwari, Marie-Laure Dano, Danniella Muheim, Reza Karkehabadi and Frederick Just for their encouragements.

I would also like to thank Mr. D. Taylor for his assistance in computer related matters.

Last but not the least, I wish to express my deep appreciation to my parents and especially my sister Alexandra, for their encouragement and love from the very beginning. Without their support, this work would not have been possible.

Contents

1	INTRODUCTION	1
2	LITERATURE REVIEW	4
2.1	Tensile Load	5
2.1.1	Determination of the fiber angle	5
2.1.2	Results	6
2.2	Buckling Resistance	8
2.3	Design, manufacturing, and testing of plates utilizing curvilinear fiber tra- jectories	12
2.3.1	Plate Manufacturing	15
3	Representation of fiber trajectories	21
3.1	Finite element approach	21
3.1.1	Mesh	22
3.2	Modeling of the curvilinear fiber path	22
4	EXPERIMENTS WITH PLATE COUPONS	28
4.1	Plate thickness	29
4.2	Material Characterization Testing	33
4.2.1	Coupon Geometry	33
4.3	Strength Measurements	41

4.3.1	Coupon Geometry	41
4.4	Design of coupon used in present study	45
4.5	Coupons with straight fibers	48
4.5.1	Finite-Element analysis - strain concentration factor	48
4.5.2	Experiments	48
4.5.3	Failure location	52
4.6	Coupons with curvilinear fibers	52
4.6.1	Results	52
4.6.2	Finite element analysis	54
4.6.3	Failure location	56
4.7	Closure	56
5	TENSION TESTS	58
5.1	The Finite Element Approach	58
5.1.1	Preprocessing	58
5.2	Processing	61
5.2.1	Material Properties	63
5.2.2	Validity of the finite element programs	63
5.3	Strain gages	66
5.3.1	Summary of experimental results	66
5.3.2	Analysis of figures 5.3 and 5.4	66
5.4	Failure analysis of tensile specimens	72
5.4.1	Stress Computation	72
5.4.2	Failure criteria	74
5.5	Investigation into failure resulting from possible manufacturing features . .	80
5.6	Validity of the failure analysis: Another interpretation of results	85
5.7	Improved plate	87
5.7.1	Results	90

5.7.2	Closure	95
6	Compression tests	96
6.1	Preprocessing	96
6.1.1	Geometry of the plate used in compression	96
6.1.2	Fiber angles	97
6.1.3	Loading	97
6.1.4	Boundary conditions	99
6.1.5	Material properties	99
6.2	Processing	99
6.2.1	Eigenvalue Buckling Prediction	101
6.3	Postbuckling	106
6.3.1	Imperfection	106
6.3.2	Nonlinearity and ABAQUS	107
6.3.3	Results of the postbuckling analysis	108
7	Summary, conclusions, and recommendations	116
7.1	Detailed summary and conclusions	116
7.2	Recommendations	119
A	FORTTRAN program used in section 5.7	123
B	Sample of an ABAQUS input file	151

List of Figures

2.1	Plate geometry and nomenclature in refs. [1-6]	4
2.2	Finite element mesh used in refs. [1-5]	5
2.3	Example of fiber path proposed in refs. [1-5]	7
2.4	Partition into 18 regions for the sensitivity study in ref. [6]	10
2.5	Fiber angles in the curvilinear layers from buckling load sensitivity study for a $(\pm 45/C_6)_s$ plate in ref. [6]	11
2.6	Partition into six radial regions in ref. [6]	13
2.7	Fiber angles in the curvilinear layers that maximize buckling load in a $(\pm 45/C_6)_s$ plate in ref. [6]	14
2.8	Data provided by Cincinnati Milacron for the fiber paths in ref. [7]	16
2.9	Dimensions of test plates in ref. [7]	18
3.1	Finite element mesh for plates loaded in tension	23
3.2	Node numbers and integration point numbers for a serendipity element . . .	24
3.3	Curve fitting for fiber trajectories	26
3.4	Superposition of the finite element mesh and curvilinear fiber paths	27
4.1	Pictures of the broken plates tested in tension	30
4.2	Location of the coupons and location of the thickness measurements	31
4.3	Variation of the thickness within a coupon	32
4.4	Geometry for elastic property characterization coupons	35

4.5	Experimental results for the coupon using straight fibers	36
4.6	Variation of E_x with respect to the fiber volume fraction	39
4.7	Fiber orientation of a curvilinear ply within the coupon	42
4.8	Predicted longitudinal strain field in the straight-sided curvilinear fiber coupon during tensile testing	43
4.9	Coupons currently used in the industry	46
4.10	Geometry for strength measurement coupons	47
4.11	Strain in the loading direction in the straight fiber strength coupons	49
4.12	Failure location in strength coupons	51
4.13	Experimental results for the coupons using a curvilinear fiber format	53
4.14	Strain in the loading direction of the curvilinear fiber strength coupons . . .	55
5.1	Boundary conditions for analysis of tensile plates	59
5.2	Comparison between the results provided by ABAQUS and FEM2D	65
5.3	Results obtained at strain gage locations considering a uniform load	68
5.4	Results obtained at the strain gage locations considering concentrated loads	70
5.5	Finite element locations near net section	75
5.6	Possible manufacturing features: Cases 1 and 2	82
5.7	Possible manufacturing features: Cases 3 and 4	83
5.8	Load vs. axial displacement characteristic during tensile testing of curvilinear and straight fiber plates	86
5.9	Iteration algorithm for improved plate design	91
5.10	Fiber angles for improved plate design	92
5.11	Fiber angles for improved plate design in the hole area	93
6.1	Finite element mesh used to model the compression test	98
6.2	Boundary conditions of the model for compression	100
6.3	Difference in the deformed shape of plate according the boundary conditions	104

6.4	Variation of the buckling load of the curvilinear fiber and straight fiber plates as a function of the boundary conditions	105
6.5	End-shortening and out-of-plane deflection relations for the curvilinear fiber plate	109
6.6	End-shortening and out-of-plane deflection relations for the straight fiber plate	110
6.7	Strain gages measurements for the straight fiber plate	113
6.8	Strain gages measurements for the curvilinear fiber plate	114

List of Tables

2.1	Failure loads of curvilinear plate in tension, from refs. 1-5	9
4.1	Results from elastic property characterization testing of the straight fiber coupon	37
4.2	Variation of the material properties with respect to the fiber volume fraction for a typical graphite-epoxy composite	38
4.3	Estimates of the elastic properties at the ply level	39
4.4	Straight fiber coupons: Results from the strength measurements	50
4.5	Curvilinear fiber coupons: Results from the strength measurements	54
5.1	ABAQUS keyword definition for tension test	64
5.2	Fiber failure for the straight fiber plate: maximum stress criterion	76
5.3	Matrix failure for the straight fiber plate: maximum stress criterion	76
5.4	Fiber failure for the curvilinear fiber plate: maximum stress criterion	76
5.5	Matrix failure for the curvilinear fiber plate: maximum stress criterion	77
5.6	Fiber failure for the straight fiber plate: maximum strain criterion	77
5.7	Matrix failure for the straight fiber plate: maximum strain criterion	78
5.8	Fiber failure for the curvilinear fiber plate: maximum strain criterion	78
5.9	Matrix failure for the curvilinear fiber plate: maximum strain criterion	79
5.10	Failure of the straight fiber plate using Tsai-Hill failure criterion	80
5.11	Failure of the curvilinear fiber plate using Tsai-Hill failure criterion	80

5.12 Failure load of the improved plate 94

6.1 Comparison between the experimental and analytical buckling loads 103

Chapter 1

INTRODUCTION

The extensive use of fiber-reinforced composite materials dates back to the '60's with the appearance of several space programs. Since then, its field of application has broadened, though the way to utilize and manufacture fiber-reinforced composite materials has remained basically the same. The main barriers for further use of composite materials lies in the fact that manufacturing of composites is often costly and technically difficult, and actual gains made in structural efficiency using conventional designs have been moderate. Conventional structural designs consist of using multiple plies of fibers embedded in a matrix. At the ply level fibers are parallel to each other and straight. The orientation of the fibers usually differs from ply to ply, each ply contributing in some way to the mechanical characteristics of the structure. With this approach, stiffness and strength properties can be tailored by utilizing fiber orientation effects. However, with straight fibers, varying the structural tailoring from point to point in a flat plate, for example, can only be accomplished by dropping or adding plies at specific locations.

In the 1980's Cincinnati Milacron developed the concept of a fiber placement machine which provided more flexibility to fiber orientation at the ply level. Specifically, the Cincinnati Milacron fiber placement machine allowed the fiber orientation of a ply to vary from point to point within the ply. Utilization of such a concept could result in significant gains in

structural efficiency. On the other hand, allowing the fiber path to vary from point to point within a ply complicates any analysis technique used to predict the structural response. Indeed, the A B D stiffness matrices change from point to point instead of remaining constant for the entire laminate. This spatial dependence of the A B D matrices makes an analytical solution very difficult to find. Therefore, most of the analyses for curvilinear fiber structures have been done with finite element based methods. Although almost all structural designs have precluded the use of the curvilinear fiber format, several investigations have been performed to evaluate any gains that might be possible by using this fiber format. In most of the investigations, a plate with a centrally located hole was considered as a prime candidate. However, the results found could be extended to other geometric discontinuities, such as windows in an airplane fuselage and access panels in wings. Conventional designs simply cut the fibers at these discontinuities, creating a stress concentration. On the other hand, a curvilinear fiber path could distribute the load more effectively around the hole, perhaps minimizing or eliminating stress concentrations.

In 1988 Hyer and Charette [1-4] and Charette [5] investigated the contribution of the curvilinear fiber format in flat plates to resistance in tension. Several proposed designs utilizing the curvilinear format were presented. In 1991 the gains in buckling performance of flat plates using the curvilinear fiber format were explored by Hyer and Lee [6]. To follow in the next chapter is a literature review in which these studies will be detailed. These investigations motivated the manufacturing of four plates with a centrally located hole. The plates were manufactured by Cincinnati Milacron with a fiber placement machine. Two of the plates used the curvilinear format, while the two others represented baseline straight fiber counterparts. Two plates, a curvilinear fiber plate and a straight fiber plate, were tested in tension. The two other plates were tested in compression. Since the plates were thin, compression testing resulted in buckling and postbuckling. Since the steering radius of fiber placement machines was limited, the designs proposed in refs. [1-6] could not be followed. The philosophy used was to manufacture a curvilinear format plate consistent with the manufacturing constraints of the Cincinnati Milacron fiber placement machine.

The plates were then tested at the NASA Langley Research Center. The testing of these plates constitutes one of the rare sources of data regarding the utilization of curvilinear fiber format.

The goal of the present work is to analyze and explain the results provided by the tested plates. A finite element approach, including a failure criterion, was adopted to predict the response. Chapter 2 begins by briefly reviewing the work of Hyer and Charette [1-4], Charette [5], and Hyer and Lee [6]. Chapter 2 also describes details concerning the plate manufacturing and testing. As will be discussed in Chapter 2, though there was a small observed gain in buckling performance of the curvilinear fiber plate, the expected improvement in performance for the curvilinear fiber plate was not realized for the tension testing. The curvilinear fiber plate failed in tension at a load considerably less than the straight fiber plate. This prompted an investigation of the material properties of the curvilinear and straight fiber plates. This investigation of the material properties is discussed in Chapter 4. However, to put the material property testing results into context, information regarding the trajectories of the curvilinear fibers and the material property requirements for the finite element analyses is necessary. This information is presented in Chapter 3.

Chapter 5 describes the modeling of the plates loaded in tension, including the boundary conditions, the loading, and the fiber angles for the curvilinear plies. The data provided by the strain gages are compared with the strains obtained by the finite element analysis. This chapter also contains a comprehensive description of the failure criterion and the schemes used to predict the plate ultimate load. An optimal fiber path was also computed using a recursive scheme presented by Hyer and Charette [1-4] and Charette [5].

Chapter 6 presents the analysis of the compression tests. The chapter emphasizes the boundary conditions of the tests, computes the buckling loads, and models the postbuckling behavior of the plates. A final discussion in Chapter 7 will summarize the main conclusions of this work.

Chapter 2

LITERATURE REVIEW

This chapter provides a brief summary of the investigation of Hyer and Charette [1-4], Charette [5] , Hyer and Lee [6], and Hyer et al. [7] of curvilinear fiber plates. Interest in curvilinear fiber format is recent. This explains the limited number of papers available in the open literature.

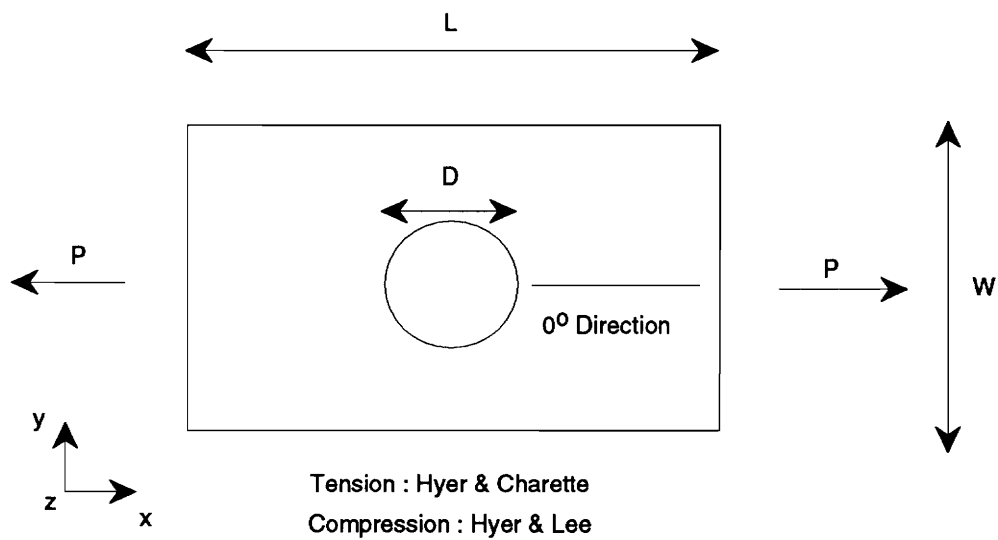


Figure 2.1: Plate geometry and nomenclature in refs. [1-6]

2.1 Tensile Load

References [1-5] investigated the influence of the curvilinear fiber format on the tensile capacity of a plate with a centrally located circular hole. Figure 2.1 illustrates the planform geometry of the plate under consideration. The plate was limited to 16 plies. The contribution of a curvilinear format was investigated for a variety of lay-ups and plate geometries. An analysis using finite elements, a failure criterion, and a recursive scheme enabled these researchers to study the influence of curvilinear fiber paths. The finite element mesh for the quarter plate model used in refs. [1-5] is presented on the figure 2.2 . The mesh consisted of 120 8-node quadrilateral elements. Recall from Figure 2.1 that the loading was in the x-direction. Lines AA' and BB' were taken to be lines of symmetry.

2.1.1 Determination of the fiber angle

The key to the designs in refs. [1-5] was to align the fiber paths in the curvilinear plies with the principal stress directions in those plies. In the analysis the fiber angle was assumed to be constant within each element of the finite element mesh. The concept of principal directions in a laminate had to be applied carefully, as the principal stresses directions vary from ply to ply. For the first iteration, the fiber angle in the curvilinear plies was set equal to zero. The stresses in each element were computed and principal stress directions in the curvilinear plies determined. Then the fibers in these plies were aligned with these principal stress directions and the stresses and the principal stress directions recomputed. By using incremental changes, the principal stress directions and fiber angles in each element were aligned to within a certain tolerance. The iteration was stopped once

$$(\phi - \theta)/\theta \leq 0.01, \quad (2.1)$$

where θ denotes the principal direction and ϕ the fiber orientation.

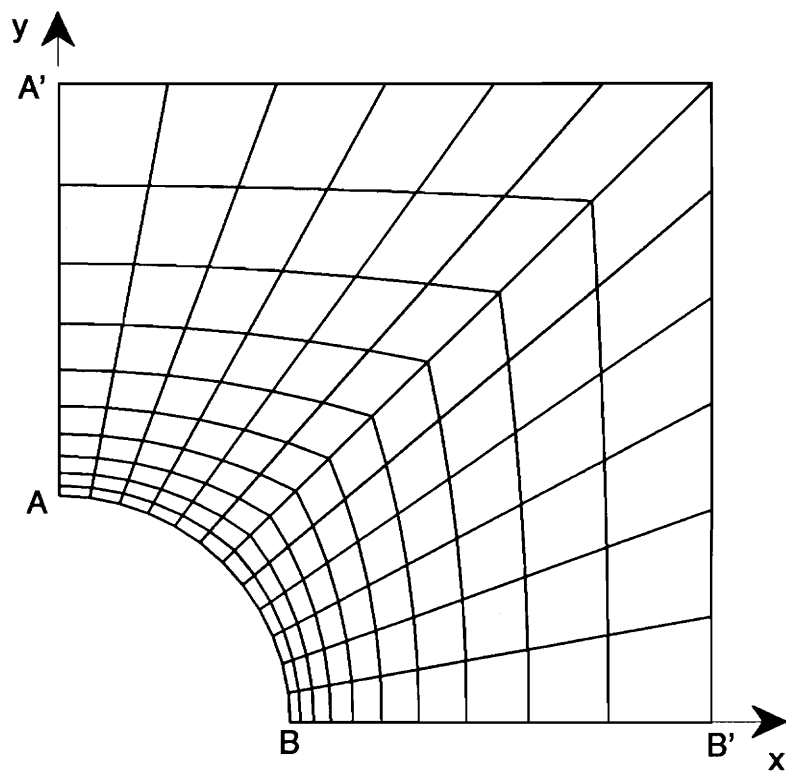


Figure 2.2: Finite element mesh used in refs. [1-5]

2.1.2 Results

Somewhat independent of the orientation of the other plies, the fiber trajectories in the curvilinear plies which satisfied equation 2.1 were computed as shown in figure 2.3. To provide a baseline for comparison, results were all normalized by results obtained for a quasi-isotropic $(\pm 45/0/90)_2$ plate with an identical geometry. The maximum strain criterion was used to estimate the ultimate load. The main results from the work are shown in Table 2.1. The table illustrates the tensile failure load, normalized by the failure load for the quasi-isotropic laminate, for nine laminates and various plate length to plate width, L/W , ratios and various hole diameter to plate width, D/W , ratios. It was assumed that the load was applied uniformly on opposite ends of the plate. The failure mode and the location of failure are indicated. Unless otherwise indicated, failure was due to fiber tensile failure. It can be seen from the table that a pure unidirectional laminate, laminate no. 2, was considerably weaker than the baseline (normalized loads less than 1). A pure curvilinear design, laminate no. 3, was stronger than the baseline, but only marginally so for larger holes. For all curvilinear designs, the fiber orientation in the vicinity of the net section was essentially 0° , so the fiber architectures of the curvilinear designs and the straight fiber designs were virtually identical in the net section regions. A design with 2 of 16 plies orthogonal to the primary curvilinear load-carrying plies, laminate no. 4, was quite effective. Design no. 6 studied further the influence of these orthogonal plies on the load-carrying capacity by increasing their number. However, designs no. 4 and 6 were very sensitive to shear loading and manufacturing of such plates would be very difficult. To ease manufacturing problems, the idea of using $(\pm 45/C_6)_s$ was pursued, i.e., laminate no. 5, and offered an interesting compromise. The straight fiber $(\pm 45/0_6)_s$ counterpart, laminate no. 7, was also studied. Both laminates 5 and 7 failed near the hole edge. Although the stacking arrangement of the two plates were identical in this area, the load capacities were different. An explanation was provided by considering the stress resultant distribution and its magnitude. Essentially, the curvilinear fibers moved the load away from the hole.

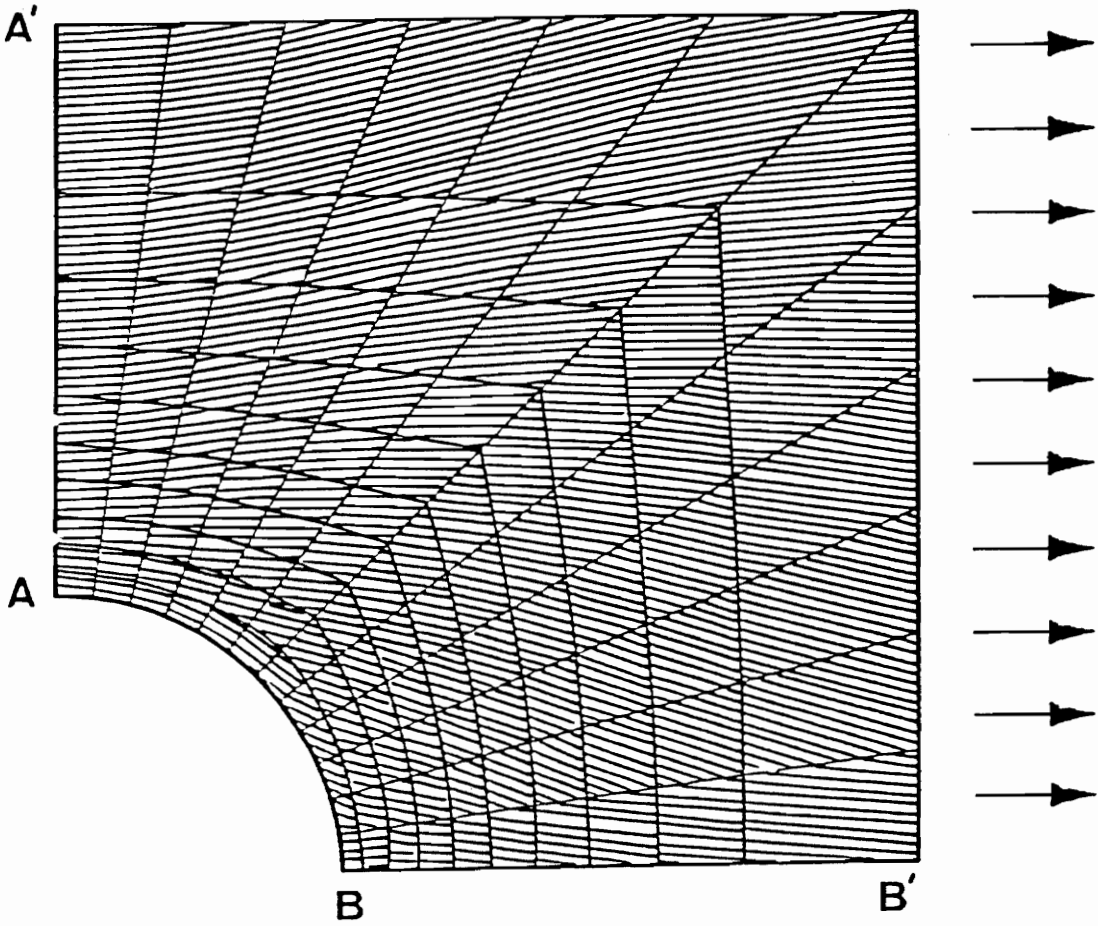


Figure 2.3: Example of fiber path proposed in refs. [1-5]

Laminates nos. 8 and 9 further illustrated this point. Despite having exactly the same design at the net section, the curvilinear fiber plate bore more load than the straight fiber plate.

The influence of a curvilinear format on buckling resistance was briefly investigated by Hyer and Charette [1-4] and Charette [5]. The study was not too comprehensive but preliminary conclusions could be drawn. Generally, the improvement of tensile performance was at the expense of buckling performance. Nevertheless, the penalty was not worse, and in fact less, than other straight fiber designs. This issue was pursued further by Hyer and

Lee [6] by considering a different approach. These results are presented in the next section.

2.2 Buckling Resistance

Hyer and Lee [6] studied the gain in buckling resistance that the curvilinear fiber format could achieve. A simply supported square plate with a centrally located hole was considered, as in refs. [1-5]. The finite element method was again used. Because of the work of Hyer and Charette [1-4], aligning the fiber path with the principal directions in the curvilinear plies was judged not to be an appropriate approach to improve buckling resistance. Instead, a sensitivity study and a gradient search technique using fiber orientation as a design parameter were conducted.

The finite element mesh consisted of 120 elements. These 120 elements were grouped in 18 different regions. The partition into regions is shown on figure 2.4. The fiber angle was considered to be constant within a region and buckling was assumed to occur due to uniform inplane displacement, Δ , at opposite edges of the plates. The other two edges were traction free. Quarter symmetry was again assumed, though this can be inaccurate for large values of D_{16} and D_{26} .

The first step of the sensitivity study consisted of setting the fiber angle in the curvilinear plies in all 18 regions equal to zero. Then the fiber angle in the curvilinear plies in one of the 18 regions was allowed to vary, while the fiber angles remained fixed at 0° for the remaining 17 regions of the plate. The buckling load of the plate was computed as a function of the fiber orientation in each region. The fiber orientation which resulted in the highest buckling load was then assigned to each region. The fiber angle in all the regions were then returned to zero and the study was repeated for another of the 18 regions. The process was repeated for each of the 18 regions. The curvilinear plies were then assumed to consist of these 18 regions, each with their own fiber orientation. Figure 2.5 shows the orientation in the 18 regions of the curvilinear ply computed by this sensitivity scheme. For a $(\pm 45/C_6)_s$, the buckling load was 2.23 times greater than the buckling load for a $(\pm 45/0_6)_s$ laminate.

Table 2.1: Failure loads of curvilinear plate in tension, from refs. [1-5]

Laminate Number	Lay-up	failure mode location	L/W=1 D/W=1/6	L/W=2 D/W=1/6	L/W=2 D/W=1/3
1	$(\pm 45/0/90)_s$	0 ply/net section hole edge	1.00	1.00	1.00
2	$(0_8)_s$	shear failure/net section	0.83	0.76	0.59
3	$(C_8)_s$	matrix failure/away from hole	1.26	1.18	1.01
4	$(O/C_7)_s$	C ply/net section hole edge	2.29	2.21	1.89
5	$(\pm 45/C_6)_s$	C ply/net section hole edge	1.84	1.79	1.60
6	$(O_2/C_6)_s$	C ply/net section hole edge	2.09	2.03	1.79
7	$(\pm 45/0_6)_s$	0 ply/net section hole edge	1.43	1.38	1.27
8	$(\pm 45/0_2)_{2s}$	0 ply/net section hole edge	1.29	1.26	1.20
9	$(\pm 45/C_2)_{2s}$	C ply/net section hole edge	1.47	1.44	1.33

L: length of the plate

W: width of the plate

D: hole diameter

C: curvilinear ply

O: ply with fibers orthogonal to curvilinear plys

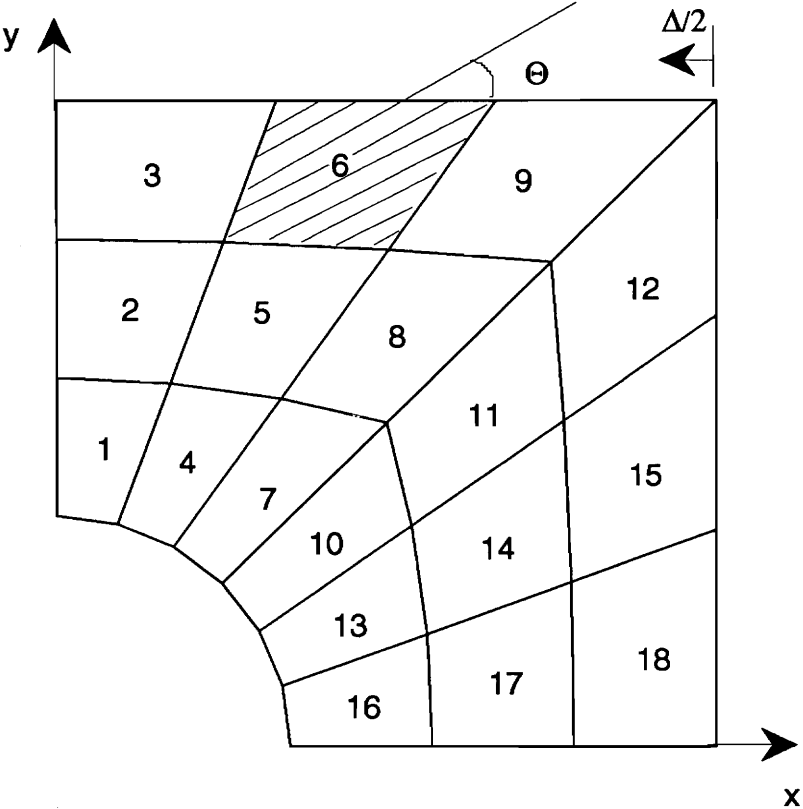


Figure 2.4: Partition into 18 regions for the sensitivity study in ref. [6]

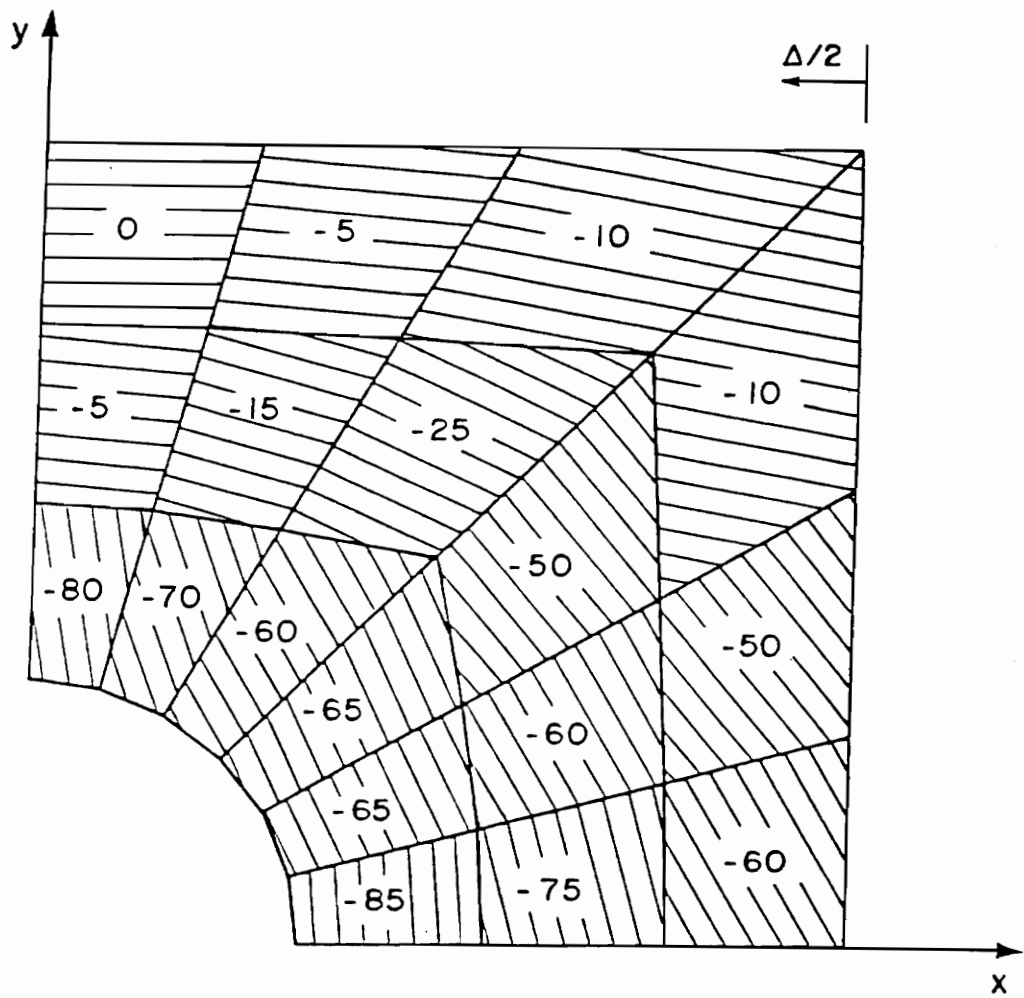


Figure 2.5: Fiber angles in the curvilinear layers from buckling load sensitivity study for a $(\pm 45/C_6)_s$ plate in ref. [6]

The sensitivity method does not take in consideration the interaction between the different regions. Therefore, results from such an approach can be somewhat misleading. Hyer and Lee [6] considered a second approach using a optimization method called the gradient search technique. This second analysis optimized the combination of the 18 different angles. This design achieved a buckling load almost three times higher than the one for the quasi-isotropic case. The orientation of the fibers in each region found by the gradient search technique was similar to the orientation found by the sensitivity analysis.

Neither the design resulting from the sensitivity scheme nor the design resulting from the gradient search scheme could reasonably be judged manufacturable. The difference in fiber angles between two adjacent regions was too large even for a smoothing scheme. A new design was achieved by partitioning the plate into six radially oriented regions. These regions are illustrated on figure 2.6. The buckling load from the gradient search design with these six regions was 1.85 greater than the buckling load for the quasi-isotropic case. The fiber angle for each of the 6 regions are shown in figure 2.7. The prebuckling stress contours showed that curvilinear fibers moved a significant portion of the inplane compressive load away from the hole. Unfortunately, designs which significantly improved the buckling load gave poor results for a tension loading. However, for some lay-ups buckling load and tensile load could both be improved by the curvilinear format. For instance, the sequence $(\pm 45/0/90/C_4)_s$ reached a buckling load and a tensile load 1.3 times greater the ones obtained for a quasi-isotropic plate. The later design was somewhat similar to the design provided by Cincinnati Milacron.

2.3 Design, manufacturing, and testing of plates utilizing curvilinear fiber trajectories

The results obtained by Hyer and Charette [1-4] and Charette [5], Hyer and Lee [6] encouraged the development of the curvilinear fiber format. Manufacturing and testing plates utilizing this concept were the next steps of the overall study. Four plates were manu-

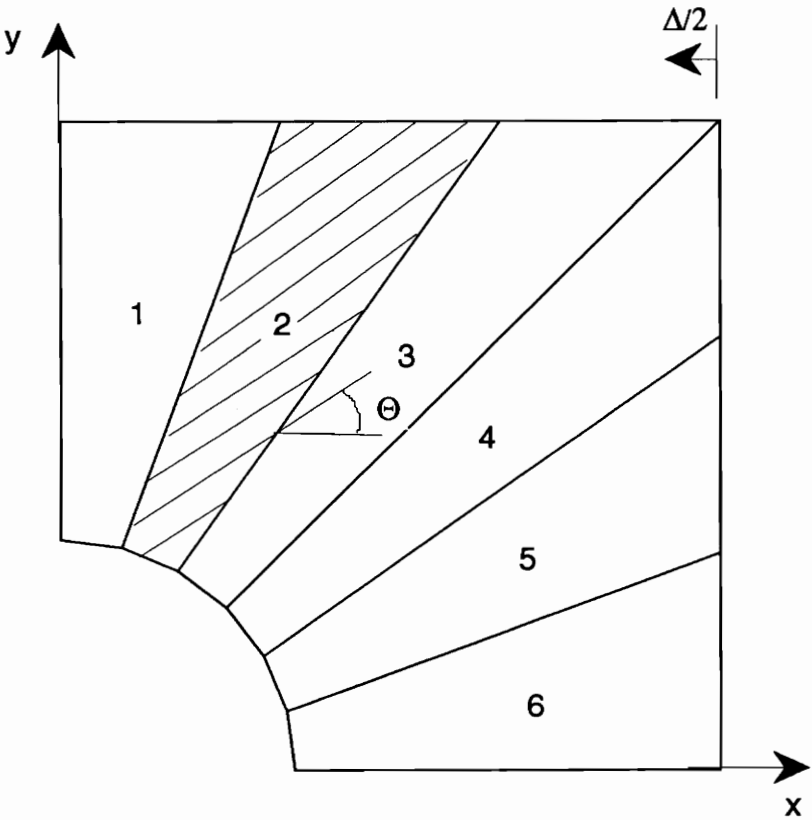


Figure 2.6: Partition into six radial regions in ref. [6]

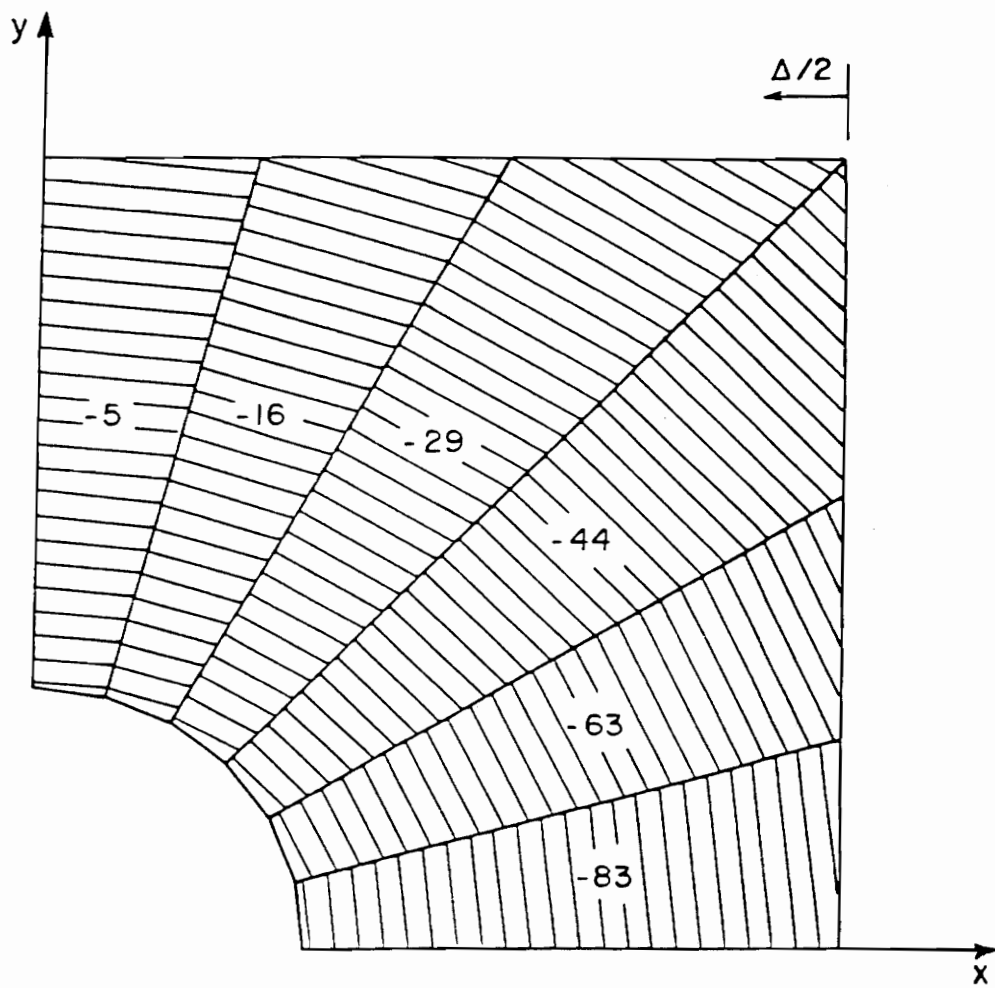


Figure 2.7: Fiber angles in the curvilinear layers that maximize buckling load in a $(\pm 45/C_6)_s$ plate in ref. [6]

factured with a Cincinnati Milacron fiber placement machine [7]. Two of them used the curvilinear fiber format, one for a tensile test and the other for a compression test. The two other plates were designed with straight fiber format for comparison. The Cincinnati Milacron fiber placement machine was designed to manufacture large structures, i.e., approximately 30-50m. To study the curvilinear fiber concept, laboratory size specimens, i.e., 1m, were felt to be more appropriate. Unfortunately, the order of magnitude smaller laboratory specimens could not take full advantage of the curvilinear capabilities of the large Cincinnati Milacron machine. The minimum radius of curvature of a steered path using the machine was 0.380m. Thus using hole diameters of 0.1 to 0.2m in plates 1m square presented a problem if any of the proposed curvilinear designs of refs. [1-6] were to be manufactured. Rather than make large plates, which required very large loads to test, laboratory size specimens with rough approximations to the curvilinear designs proposed in refs. [1-6] were fabricated by Cincinnati Milacron. The plates actually manufactured will be described in the next section.

2.3.1 Plate Manufacturing

The four plate specimens were produced on Cincinnati Milacron's 12 tow FPS fiber placement machine with an A975F control. This machine was a joint development effort between Cincinnati Milacron and Thiokol Corporation. The plates were produced using Fiberite FX13F77-2 graphite-epoxy tow material. The tow material was 0.28mm thick, with a nominal width of 3mm. The fiber placement machine uses 7 axes of motion to compact the tow onto the mold surface. As stated previously, the 0.380 m steering radius dictated the minimum size of the specimen fabricated. Figure 2.8 provides details of the curvilinear fiber trajectories used. The program used to define the fiber trajectories in the curvilinear plies allowed only fiber courses that extended from one end of the panel to the other to be machine laid. The curvilinear courses that did not extend the full length of the panel were filled in by hand. The corners of the ± 45 plies contained tows that were too short to be machine laid due to the cut length limitation were also placed by hand. As shown in

figure 2.8, some of the curvilinear courses that steered around the hole extended outside the panel dimensions.

As can be seen comparing figure 2.8 with figure 2.7 and figure 2.3, the design adopted by Cincinnati Milacron was neither the one proposed by Hyer and Charette [1-4] and Charette [5], nor the one proposed by Hyer and Lee [6]. The design developed by Cincinnati Milacron was similar to the one developed by Hyer and Lee [6] for the regions 1, 2 and 3 shown in figures 2.6 and 2.7. The fiber angle of both designs are approximately equal to zero at the net section of the plate and the magnitude of the fiber angles increased when going from the region 1 to 2, and 2 to 3. Passing region 4, the fiber angle keeps increasing for Hyer and Lee's [6] design, reaching almost -90° near the x -axis. On the other hand, for the design developed by Cincinnati Milacron, the magnitude of the fiber angle began to decrease after passing region 4, to reach an angle close to 0° near the x -axis. In other words, the fiber angle gradient kept increasing by passing from region 1 to 6 for Hyer and Lee's [6] design, while it first increased and then decreased for the curvilinear plies manufactured by Cincinnati Milacron.

The design developed by Cincinnati Milacron was similar to that proposed by Hyer and Charette [1-4] and Charette [5] along BB' (see figure 2.3) and near the hole edge. Nevertheless, the further the fibers were located from BB' , the more the two designs differed. Near the opposite edge to BB' in figure 2.3, for the curvilinear path designed by Cincinnati Milacron, the fiber angles were positive instead of being negative. For this upper part of figure 2.3, the fiber orientation was exactly the opposite to the orientation shown in figure 2.8. Because of the manufacturing limitations, the philosophy used to manufacture the plates was to make the curvilinear design as simple as possible and learn from this case before going to either of the designs analyzed in refs. [1-6]. This step would require either making larger plate specimens, or altering the tow placement head.

The plies shown in figure 2.8 were further trimmed. The plates consisted of 16 plies. The stacking sequence of the curvilinear plate was $(\pm 45/C_2/0/90/C_2)_s$, where C denotes a curvilinear ply. To make straight fiber plates, the curvilinear plies are replaced by 0°

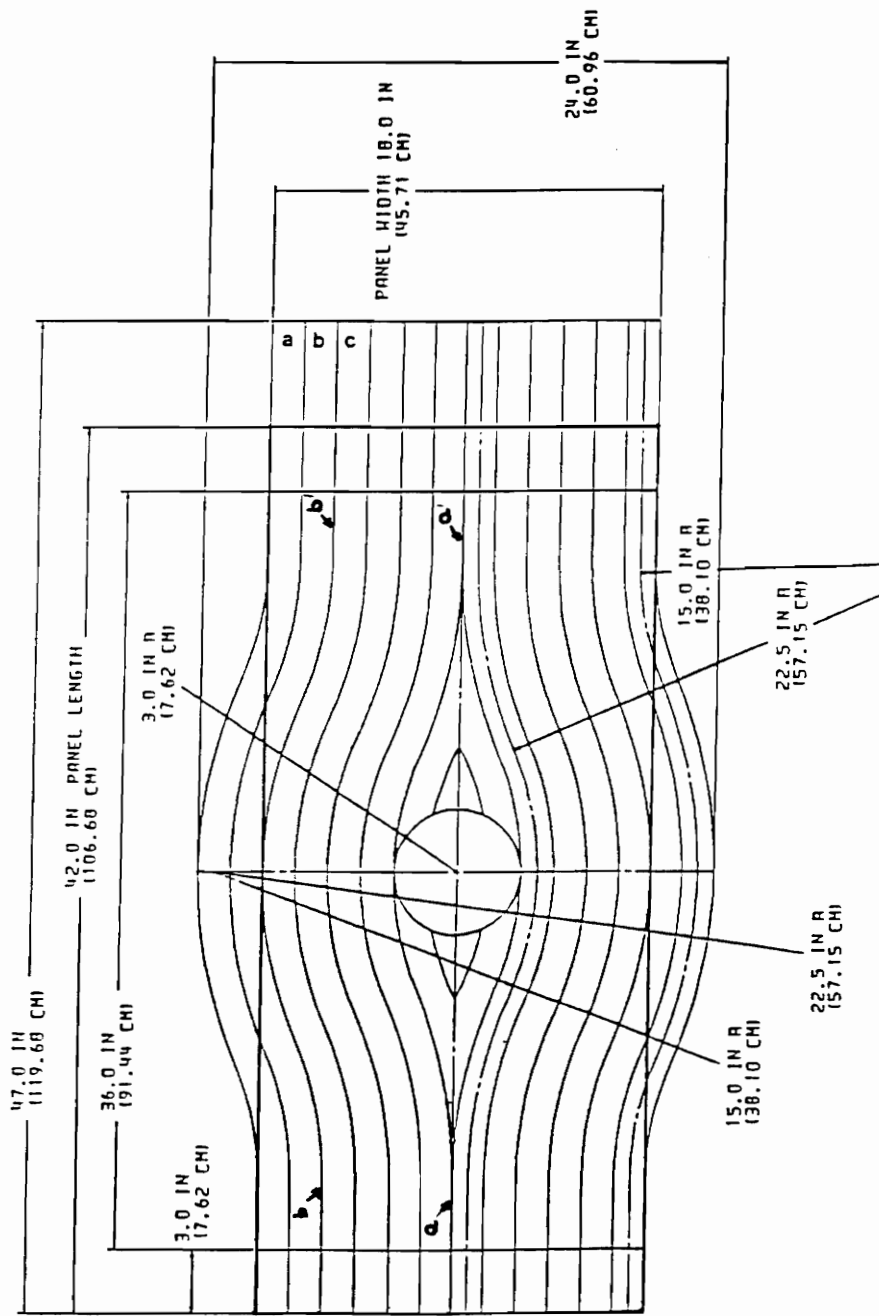


Figure 2.8: Data provided by Cincinnati Milacron for the fiber paths in ref. [7]

plies, resulting a $(\pm 45/0_3/90/0_2)_s$ laminate. The 0° direction is along the longest side of the plate. Non destructive C-scans of the specimens were performed after curing to check that no defect appeared.

Description of the tensile specimens

The two plates for the tensile testing, one using the curvilinear fiber format and the other using the straight fiber format, were trimmed to be rectangular. The length of the plates was 1.067m and the width 0.43m. On each end 0.152m was used for gripping. As shown in figure 2.9, steel grips which held the specimens by bolting them between the two halves of the grips were used to load the plates. Glass-epoxy doublers were bonded in the bolting region. The specimens were placed vertically in a load frame and the lower end was loaded downward, with the upper end being held stationary. Strain gages were placed on the plates. Their locations are shown on figure 2.9. Each gage represented on the figure symbolizes a pair of gages, one on the front side and the other on the backside of the plate (back-to-back gages). For the tension loading, an average strain value was computed for the two gages and that strain was assigned to this location.

Description of the compression specimens

The two plates for compression testing were trimmed to be square, specifically, 0.43m square (see figure 2.9). The location of the back-to-back strain gages for these panels was the same as for the tensile tests. Besides the strain gages, displacement transducers were installed to measure the out-of-plane deflection and the end-shortening of the plate. One surface of each compression specimen was painted white and shadow moire interferometry used to study out-of-plane deflection. The two loaded edges (top and bottom in figure 2.9) were clamped while the two other edges were simply supported. The plates were placed vertically in the load frame. The top clamped edge was displaced downwards and buckling occurred.

A comprehensive discussion of the tensile and the compression testing will be presented

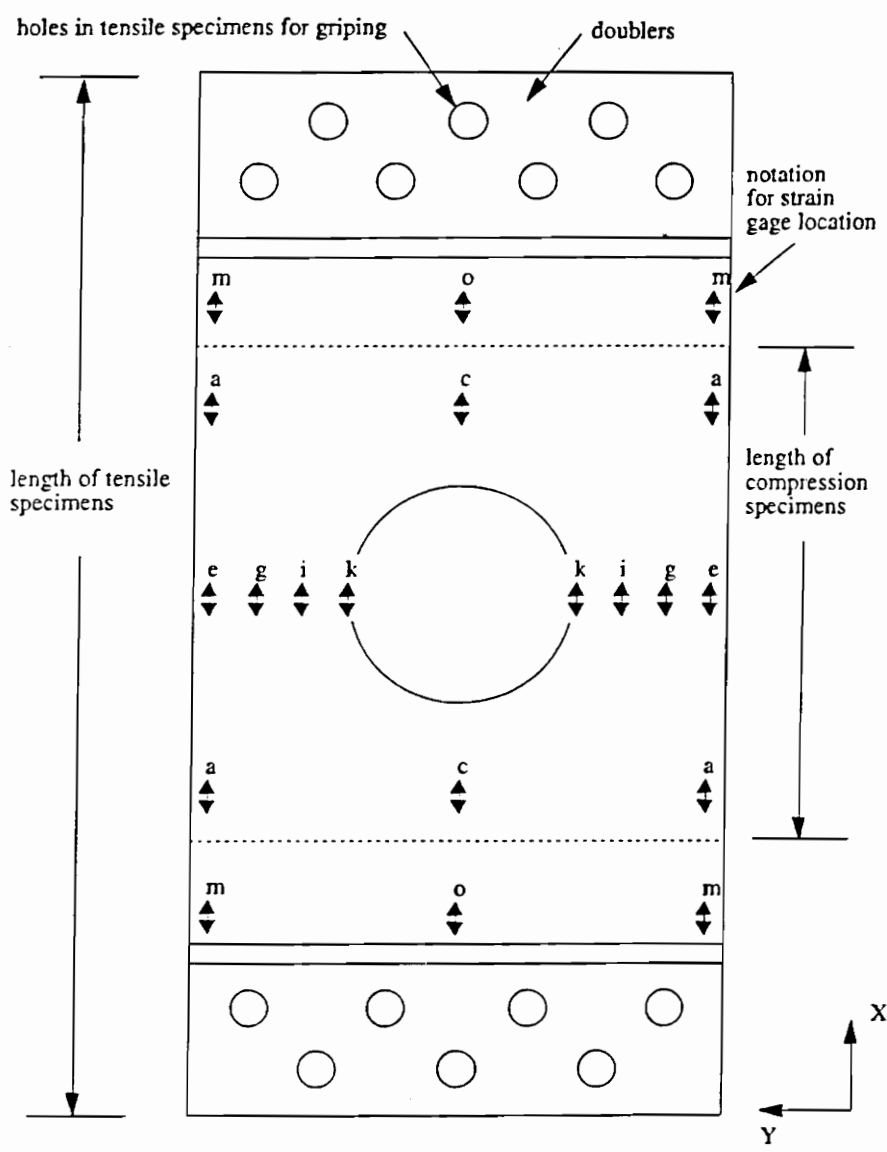


Figure 2.9: Dimensions of test plates in ref. [7]

in later chapters. However, the primary motivation for the current study is the fact that the curvilinear fiber tensile specimens failed at a load 39% *less than* the straight fiber tensile specimen. This was a very surprising result. On the other hand, the buckling load of the curvilinear fiber compression specimen was 12% *greater than* the buckling load of the straight fiber compression specimen. This conformed to the predictions of the earlier studies.

As a summary, this chapter has discussed the fact that in past research several finite element models suggested there may be an advantage to using the curvilinear format. No experiments had previously been conducted to confirm these findings. However, Cincinnati Milacron, in collaboration with the NASA Langley Research Center, manufactured and tested plates using a simplified curvilinear fiber format. The goal of the work presented here is to analyze all the results provided by these experiments and to contribute to the research in the field of curvilinear fiber format construction.

Chapter 3

Representation of fiber trajectories

Since the curvilinear fiber trajectories are so central to this study, this chapter focuses the trajectories in the plates manufactured by Cincinnati Milacron and discusses how these trajectories are represented in the analyses. This information is also needed for a complete understanding of the results from the material property testing discussed in Chapter 4. A brief description of the finite element models used is necessary, but issues like boundary conditions and loadings are addressed in later chapters.

3.1 Finite element approach

The commercially available general purpose program PATRAN, a product of PDA Engineering [8], was used as a finite element pre- and post-processor for all the models created for this investigation. ABAQUS, a product of Hibitt, Karlsson and Sorenson, Inc [9, 10], and a finite element program for plates, FEM2D, developed by Liu [11] were used as processors. Preprocessing includes the creation of the model geometry, the definition of boundary conditions, the definition of the loading, and the assignment of the material properties. Processing takes care of the computational part. Processing calculates the model stress state, its deformations, or other mechanical response requested by the user. All the results, such as the deformed shapes or strain contours, were visualized with PATRAN.

3.1.1 Mesh

The plate had two axes of symmetry, one along the x and one along y axis. The loading, the material properties and the boundary conditions were perfectly symmetric with respect to these axes. Therefore for inplane tensile loading only a quarter of the plate needed to be considered. The model is presented on figure 3.1. The mesh was made up 200 elements.

The presence of the hole at the center of the plate implied a stress concentration. This stress concentration was taken in consideration by refining the finite element mesh around the hole. For compression testing, the specimens were trimmed to be square. Hence the compression specimen was defined by considering the area A of the figure 3.1.

For the model used in tension, the mesh was adjusted in the gripping area such that a node was located at the exact position of each bolt hole (see figure 2.9). The element used was an 8-node rectangular element with nine integration points (also called a serendipity element). The model consisted of 663 nodes. The order of the nodes and the integration points for the element are presented on figure 3.2. ABAQUS offers a large array of element types. The element selected from ABAQUS for the tensile model was a two-dimensional plane stress element. The thickness of the plate was part of the ABAQUS input file. The element in FEM2D was a two-dimensional plane stress element capable of using anisotropic material properties.

3.2 Modeling of the curvilinear fiber path

An important step in developing the finite element model was the determination of the fiber orientation in the curvilinear plies in each element of the mesh. Ideally, having an expression for computing the fiber angle at any given location within the curvilinear ply would be the most convenient. This was accomplished by using the drawing supplied by Cincinnati Milacron, figure 2.8. From figure 2.8, the $x - y$ coordinates of two curvilinear fiber paths, denoted as a-a' and b-b' in figure 2.8, were determined by using a digitizer. The origin point, $x = 0$ and $y = 0$, was considered to be at the center of the hole. The

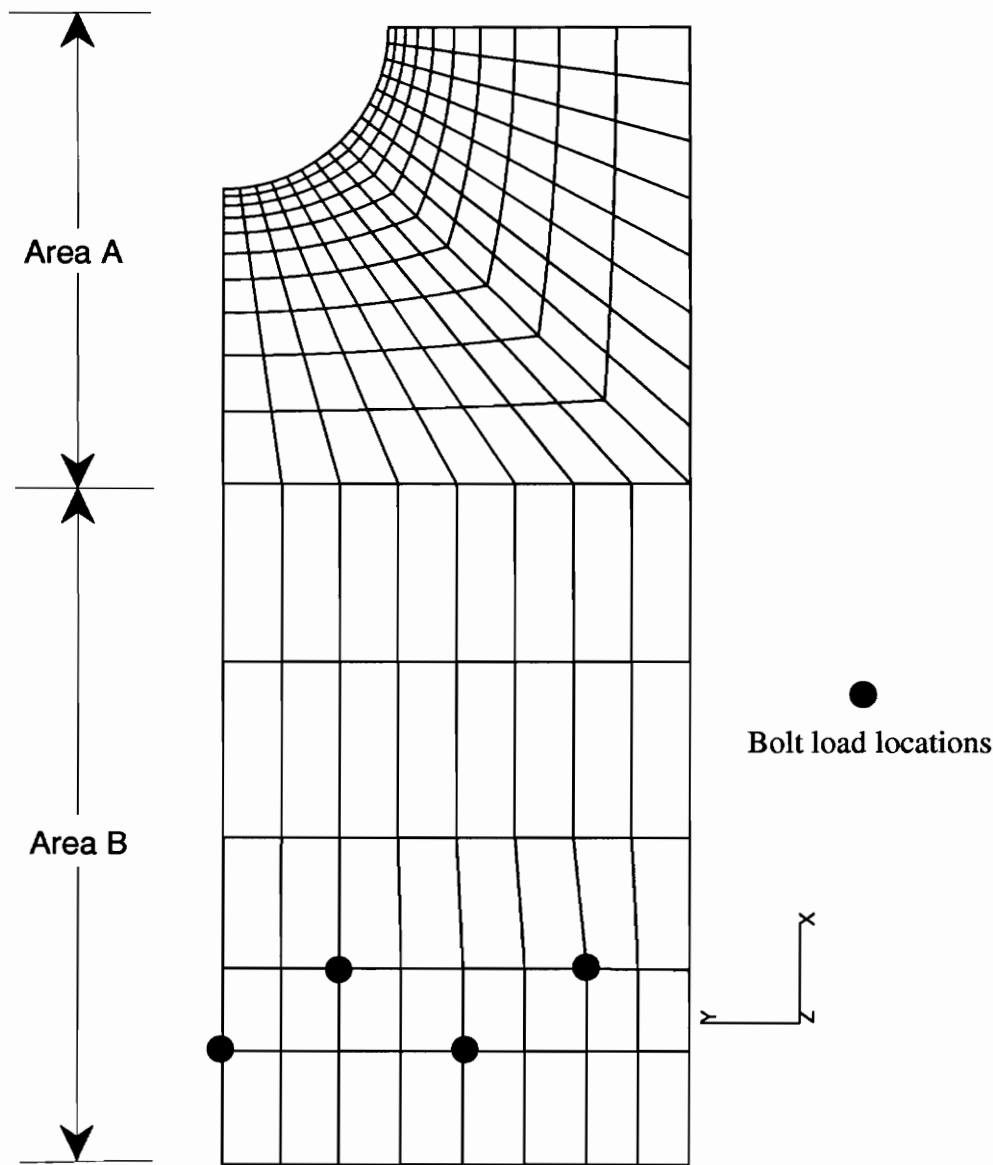


Figure 3.1: Finite element mesh for plates loaded in tension

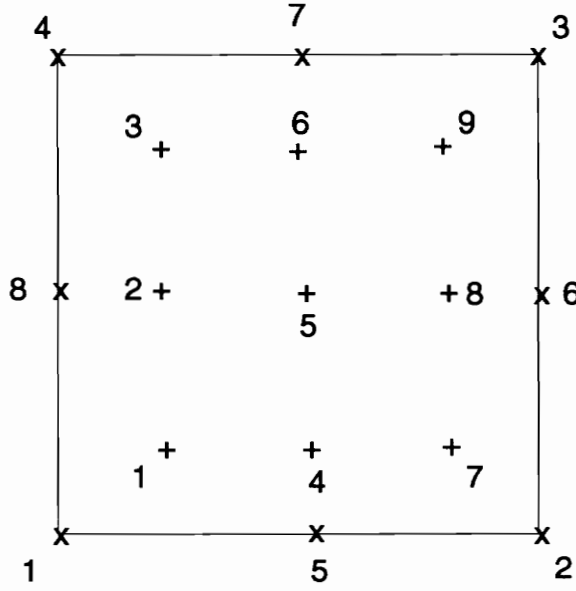


Figure 3.2: Node numbers and integration point numbers for a serendipity element

digitized path consisted of 120 $x - y$ data points. Several functions were used to fit the data so the fiber angle could be determined. Figure 3.3a illustrates the digitized data. Because of its "bell shape", the form of the normal equation was chosen as a prime candidate for the curve fitting. The first equation form considered was

$$y(x) = \text{Exp}[a + b * x^2], \quad (3.1)$$

with a and b to be found. The curve fitting proposed by *Mathematica* [12] is plotted on figure 3.3b. The equation of the curve is

$$y(x) = \text{Exp}[-2.36137 - 35.64x^2]. \quad (3.2)$$

The curve fitting was judged not to be satisfactory. To improve the precision, another term, x^4 , was added to the exponential, i.e.,

$$y(x) = \text{Exp}[a + bx^2 + cx^4]. \quad (3.3)$$

The equation

$$y(x) = \text{Exp}[-2.5744 - 20.46x^2 - 132.88x^4] \quad (3.4)$$

was obtained. The curve is presented on figure 3.3c. The contribution of the term in x^4 was important. The result obtained was close to the path described by the measured points. Nevertheless a third equation was considered by adding x^6 to the exponential. The resulting equation

$$y(x) = \text{Exp}[-2.5744 - 20.4646x^2 - 213.8x^4 + 618.39x^6] \quad (3.5)$$

is plotted on figure 3.3d. The difference with the former result is negligible. Hence, equation 3.4 was considered as the best choice to describe the fiber trajectory. This equation describes the fiber path tangent to the hole edge (b-b'). The other fiber paths can be obtained either by translating the equation in the y direction, or by using symmetry with respect to the x axis for the second half of the plate.

The finite element mesh and the representation of the fiber path were superposed to compute the fiber angle for each element. This superposition is shown in figure 3.4. The fiber trajectory was approximated as a straight line within an element. Two approaches were taken to compute the fiber angle according to the element location. In the area B (see figure 3.1), two sides of the elements are perpendicular to the x axis. Call Δy the distance between the ordinate of a fiber entering particular element and the ordinate of the same fiber exiting the element. In area B, Δy is constant within an element. Call Δx the length of a element in the x direction. The fiber angle in this element is thus

$$\theta = \sin^{-1} \frac{\Delta y}{\Delta x} \quad (3.6)$$

The value of Δy can be easily obtained by considering the equation of the fiber trajectory and the value of Δx depends on the mesh. For area A, the fiber angles were computed by hand. An average angle was estimated per element using a protractor.

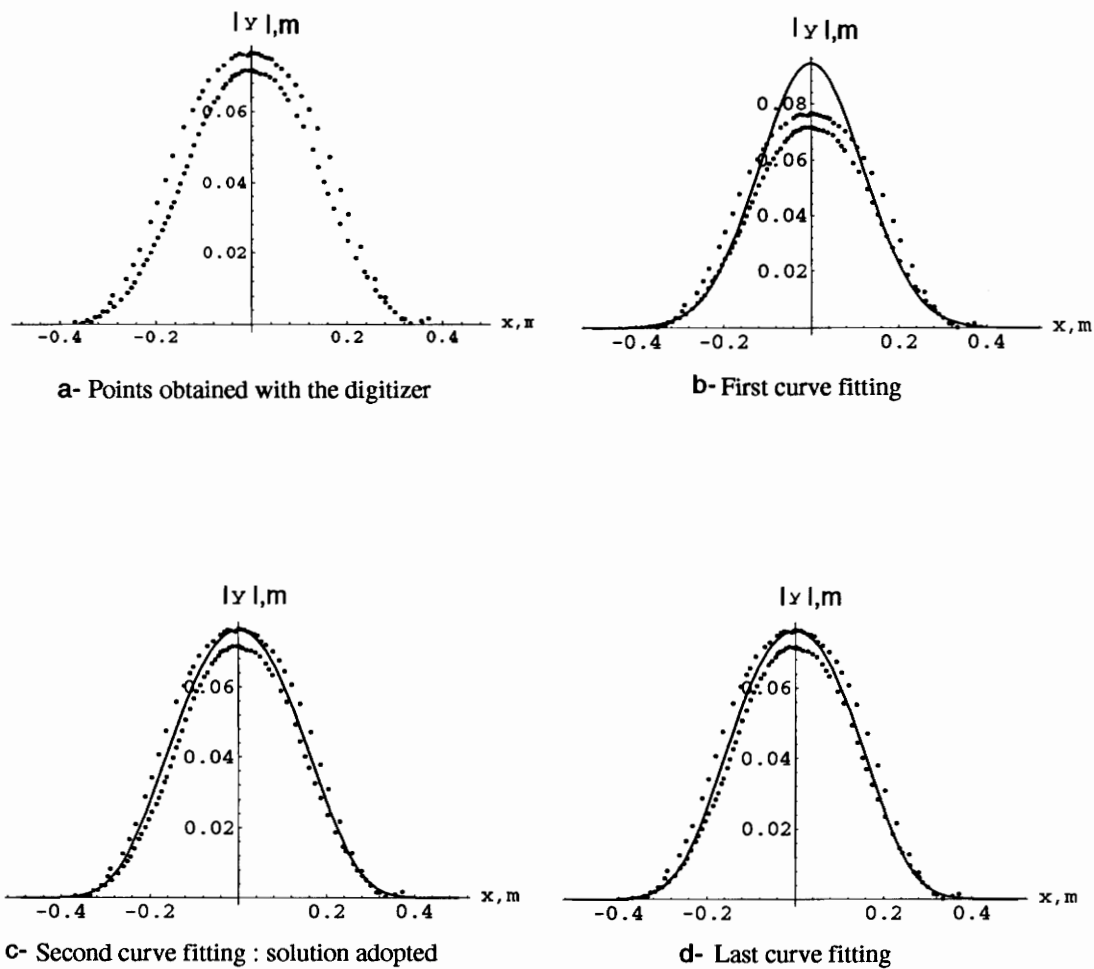
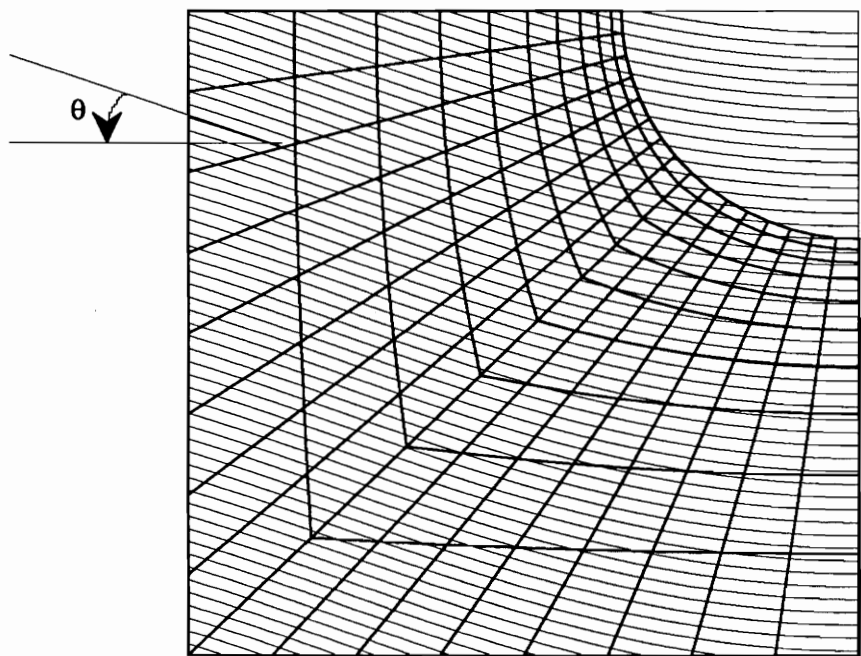
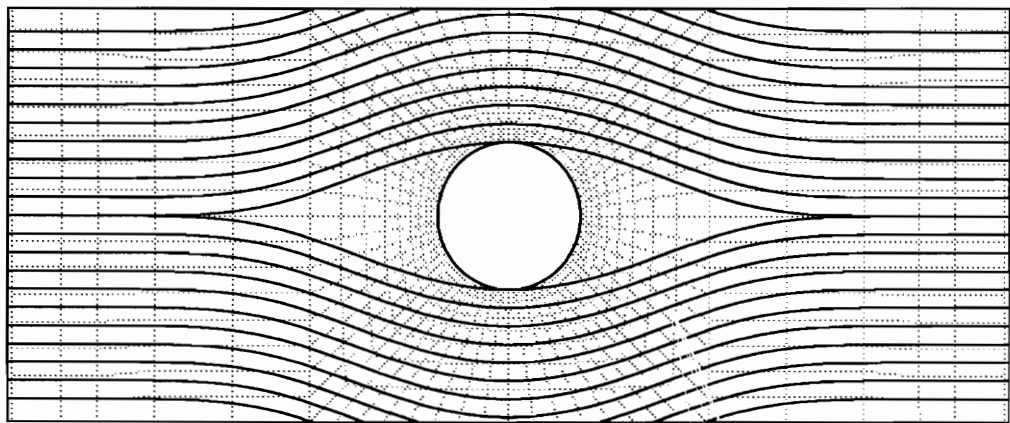


Figure 3.3: Curve fitting for fiber trajectories



a- For area A



b- For the entire plate

Figure 3.4: Superposition of the finite element mesh and curvilinear fiber paths

Chapter 4

EXPERIMENTS WITH PLATE COUPONS

As has been mentioned, the unexpected lower load capacity of the curvilinear tensile specimens prompted an investigation of the properties of both the curvilinear and the straight fiber materials. The investigation was conducted by way of mechanical tests. Two categories of mechanical testing were performed. First, two straight sided-coupons were cut from the remnants of broken plates that were loaded in tension: one from the plate containing curvilinear fibers, the other from its straight fiber counterpart. The purpose of this first set of tests was to calculate elastic properties to be used in the finite element analyses. Second, eight other coupons, four from each fiber format, were cut from the remnants to investigate the strength properties of the plates. These coupons were tapered so as to have a minimum cross-sectional area at midlength. The geometry of the coupons are described in this chapter, as are the tests conditions. The results from the testing are presented and discussed.

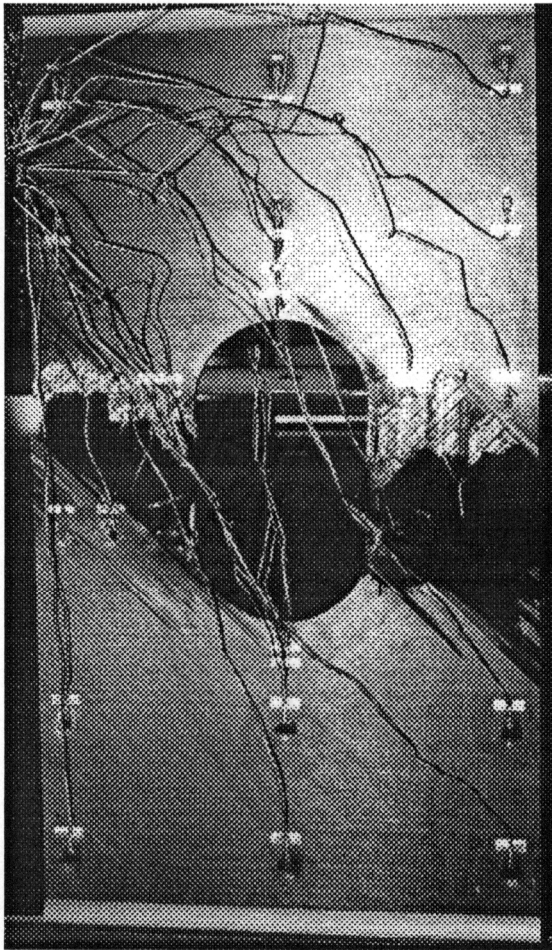
4.1 Plate thickness

Only small areas of the two plates tested in tension were not damaged. Pictures from the broken plates are presented in figure 4.1. As shown in figure 4.2, the coupons were cut from the broken plates as close as possible to the glass-epoxy doublers. Two reasons motivated this choice of location. First, this region of the plate was not damaged by the tests, either for the plate using the curvilinear fiber format, or for the plate using the straight fiber format. Second, it was in this region that the two plates were the most alike. As was seen in the last chapter, the fiber angle in the curvilinear plies varied between 3° and 20.5° in the regions from where the coupons were cut.

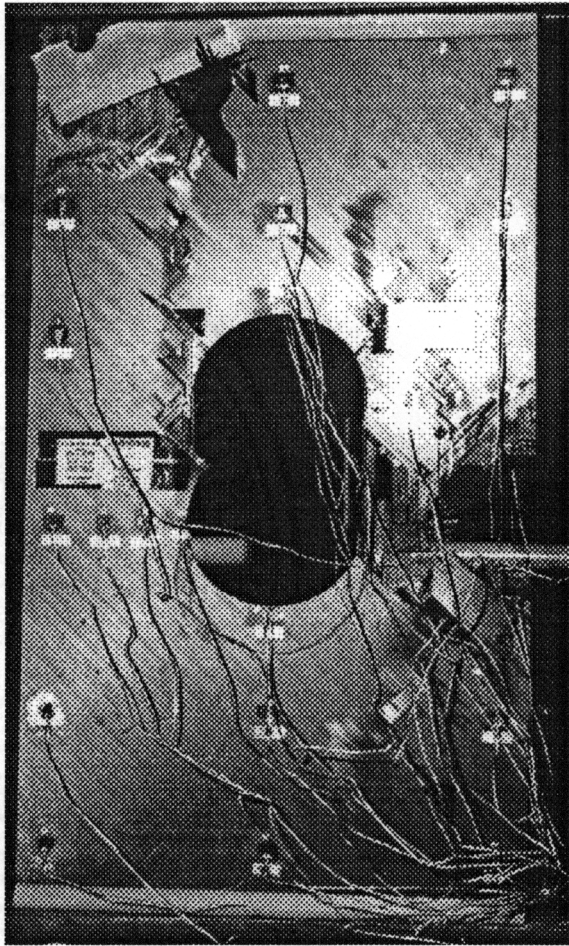
According to ref. [7], the thickness of the tow material used to make the plates was 0.28mm. Hence, with the plate being made of 16 plies, the total plate thickness was originally estimated to be 4.48mm. As will be seen in Chapter 6, the plate thickness is a major parameter for the computation of the buckling load and the postbuckling response of the plate. The ultimate tensile load can also be influenced by thickness variations. Hence, the thickness of the coupons cut from the plates was measured and investigated.

The thickness was measured with a micrometer at three different locations for each coupon. These locations are indicated on the subfigure of the tapered coupon in figure 4.2 as 1, 2, and 3. All the measurements were taken twice to reduce the error. The two values for each location were averaged. An average over all the measurements was computed to determine the ply thickness to use in finite element analyses. Several interesting points can be made from these measurements. First, all the values of the measurements were below the anticipated thickness presented in ref. [7]. The average thickness evaluated over 30 locations (3×10 coupons) was 4.03mm. This represents a 10% difference relative to the expected thickness considering the 0.28 mm tow material of ref. [7].

The second point of interest was the variation of the thickness within a coupon. By measuring the thickness from location 1 to 3 (see figure 4.2), this variation depended upon whether the coupons came from the plate using the curvilinear fiber format, denoted as



(a) Curvilinear fiber plate



(b) Straight fiber plate

Figure 4.1: Pictures of the broken plates tested in tension

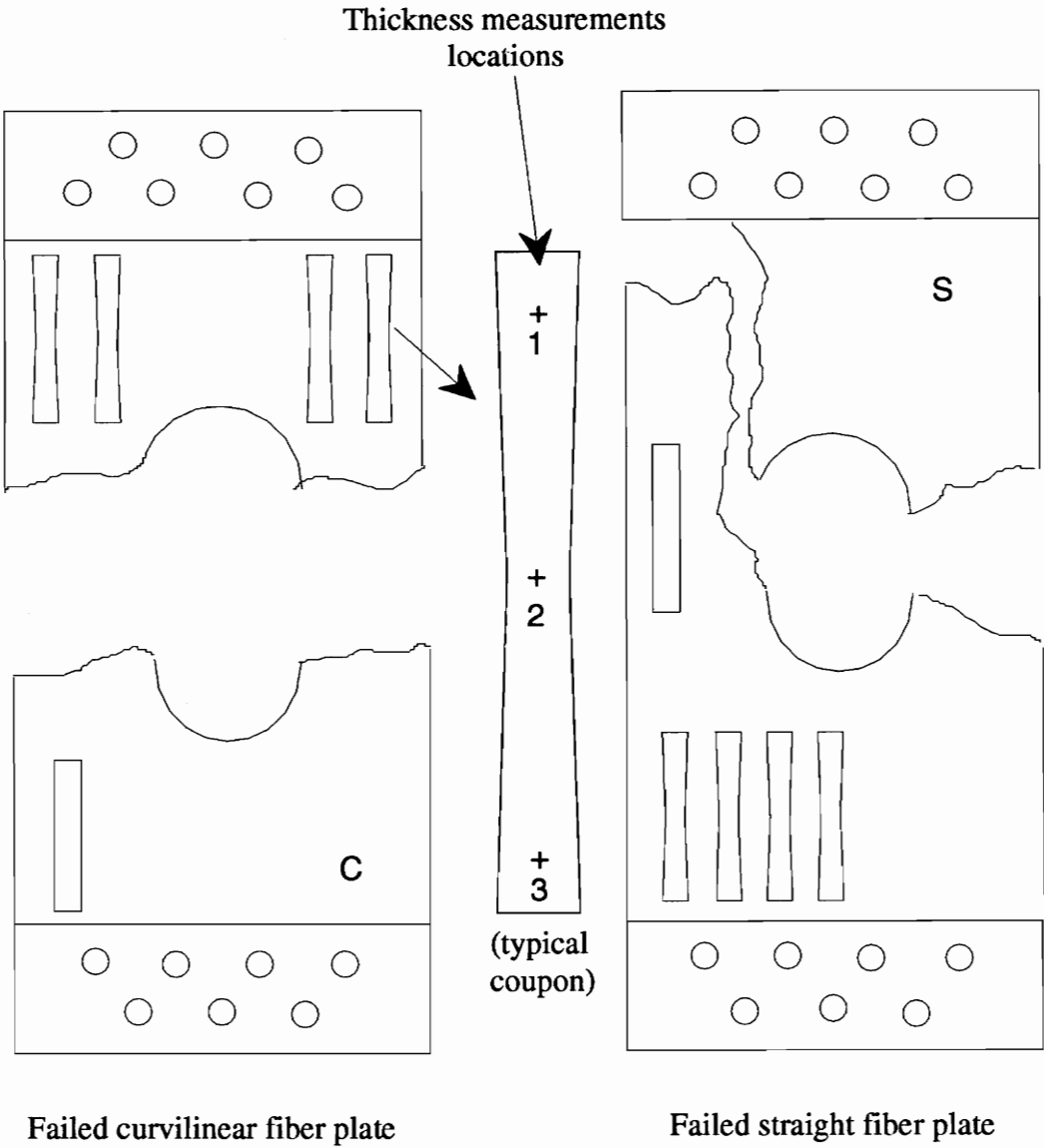


Figure 4.2: Location of the coupons and location of the thickness measurements

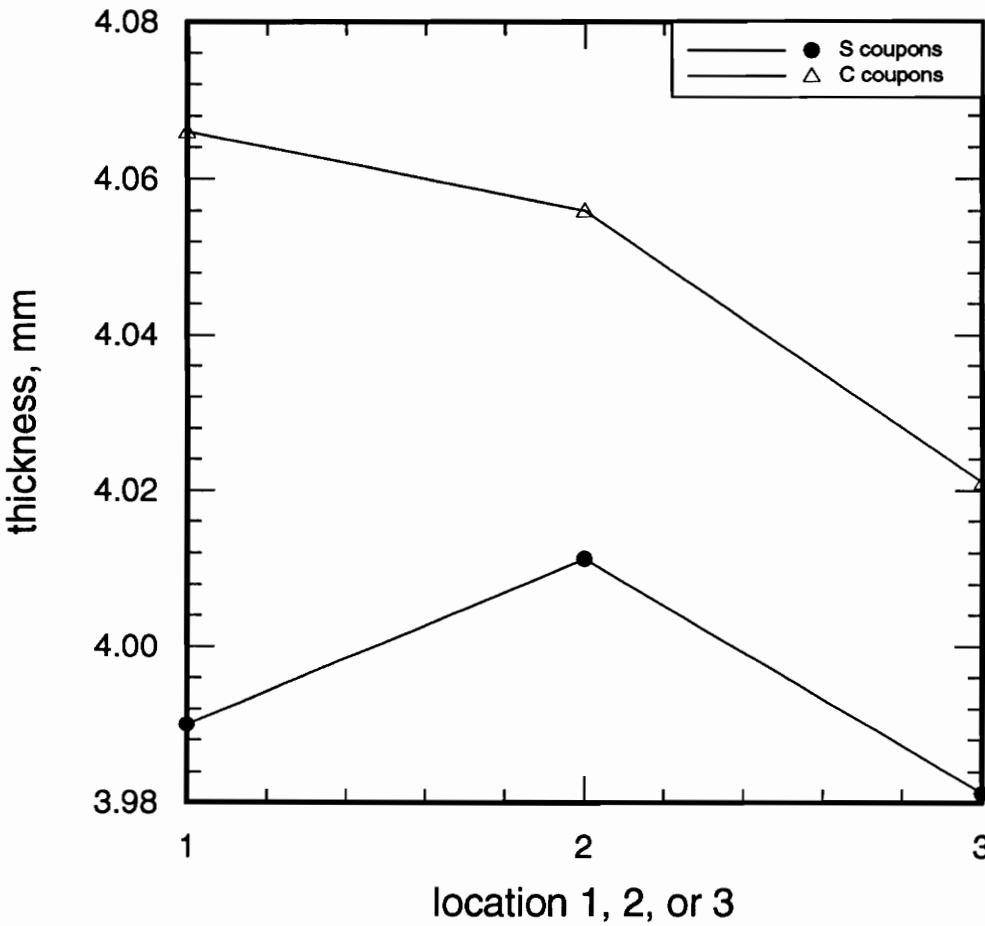


Figure 4.3: Variation of the thickness within a coupon

C, or whether the coupons came from the plate using the straight fiber format, denoted as S. As shown in figure 4.3, the thickness variation in the C coupons was almost twice as large as the variation in the S coupons. Moreover, the thickness of the C coupons tended to decrease linearly going from the location 1 to 3. Because of the damage due to the testing, measurements on the remnants far beyond point 3 were not possible. Nevertheless, as shown in figure 4.2, location 3 was close to the hole edge and so it was subjected to high stress. Hence, the thickness at the failure location within the tensile plate could have been smaller than elsewhere on the plate.

4.2 Material Characterization Testing

This first category of tests were performed to estimate the elastic properties of the curvilinear and straight fiber plates. According to Cincinnati Milacron, the plates using the curvilinear fiber format and the plates using the conventional straight format were made from the same material, and the plates were processed in an identical manner.

4.2.1 Coupon Geometry

Figure 4.4 presents the geometry of the coupon used for the elastic property tests. The coupon was designed to be as long as possible without encountering any damage in the failed plates. For elastic property testing a straight sided coupon was adopted because no stress concentration due to geometrical factors would appear. This geometry was not considered for measuring the strength of the material because of the large variation of the failure location it would induce. The coupons were not loaded to failure to determine the elastic properties. Two pairs of back-to-back strain gages were placed on each side of the coupon (see figure 4.4). The first pair of strain gages was bonded on the coupon in the longitudinal, or loading, direction. These gages were used to compute longitudinal strain ϵ_x . The other pair was placed orthogonally with respect to the first one to determine transverse strain ϵ_y . Knowing the applied load, F , and the cross-section area S of the

coupon, the material properties E_x and ν_{xy} could be computed by applying the formulae:

$$E_x = \frac{F}{S \times \epsilon_x} \quad (4.1)$$

$$\nu_{xy} = \frac{-\epsilon_y}{\epsilon_x} \quad (4.2)$$

where E_x is Young's modulus in the x direction and ν_{xy} is a Poisson's ratio.

Testing conditions

On each end of the coupons 38.1mm of length were used for gripping. The coupons were placed vertically and the upper end was displaced upward with the lower end held stationary. Much care was taken aligning the longitudinal axis of the coupons with the loading axis. The magnitude of the applied load and the strain for each strain gage were sent to a computer in terms of voltages. A FORTRAN program was written to convert these raw voltage data to MPa for the stress and to $\mu\epsilon$ for the strains.

Presentation of the results

For each of the straight-sided coupons two analyses were performed, one by varying the load from 0 to 1000N, and the other by varying the load from 0 to 50 000N. Young's modulus E_x and Poisson's ratio ν_{xy} were computed for each of these load ranges and compared.

Results obtained from the coupon with straight fibers

The results obtained for the coupon using straight fibers are shown in the upper two figures of figure 4.5. Young's modulus could be approximated by computing the slope of the relation

$$\sigma_x = f(\epsilon_x) \leftrightarrow \sigma_x = E_x \times \epsilon_x. \quad (4.3)$$

In the same way, ν_{xy} was equal to the slope of the relation

$$\epsilon_y = f(\epsilon_x) \leftrightarrow \epsilon_y = -\nu_{xy} \times \epsilon_x. \quad (4.4)$$

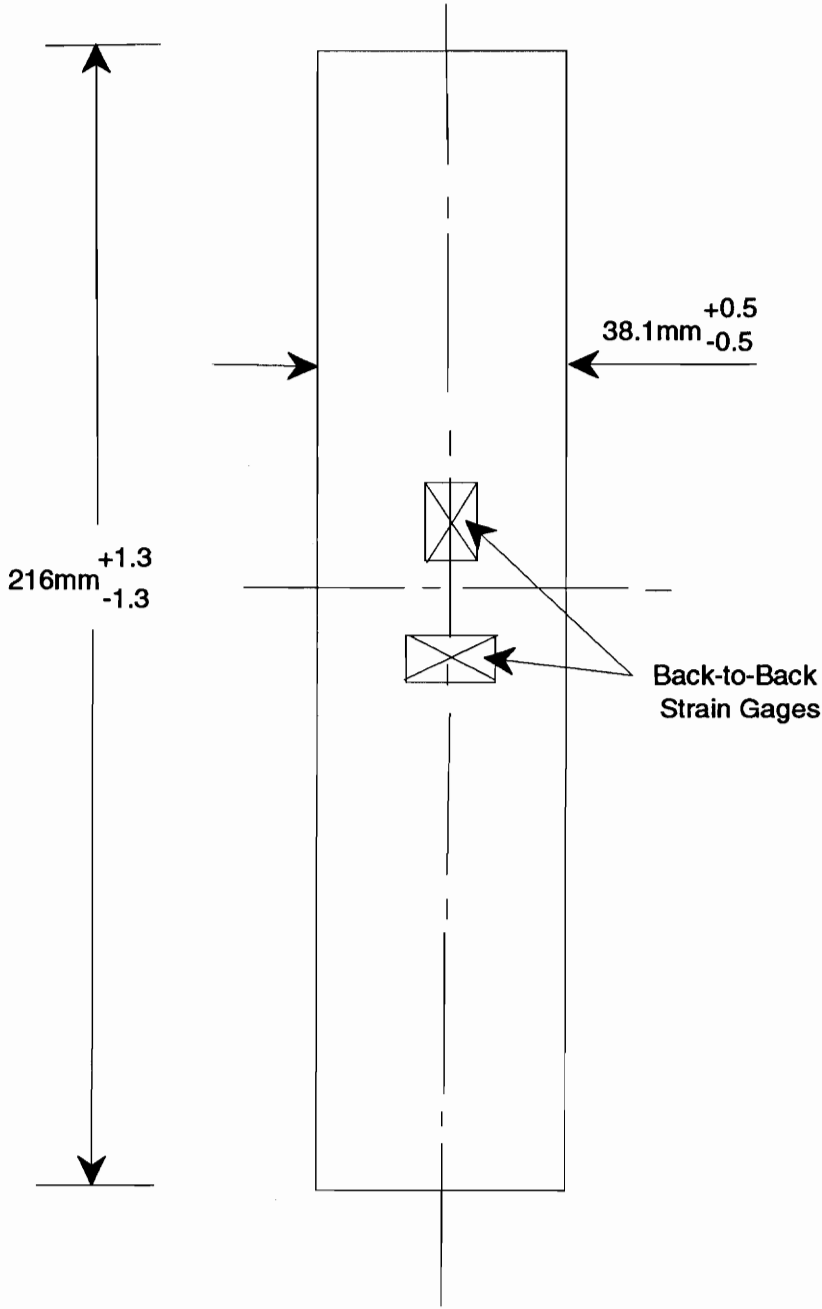


Figure 4.4: Geometry for elastic property characterization coupons

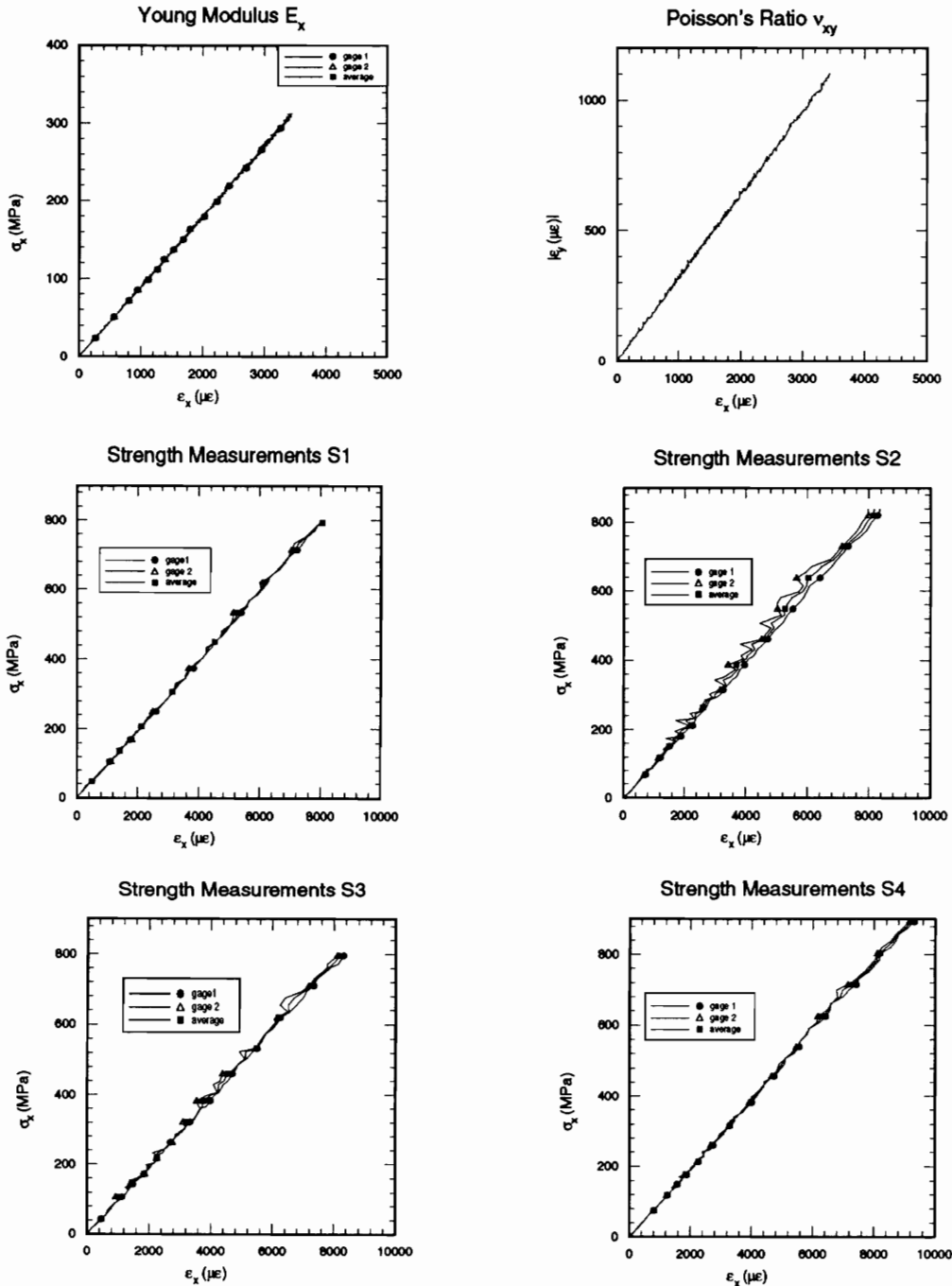


Figure 4.5: Experimental results for the coupon using straight fibers

Table 4.1: Results from elastic property characterization testing of the straight fiber coupon

	0-10000N	0-50000N
$E_x(\text{GPa})$	88.7	90.6
ν_{xy}	0.318	0.319

The mathematical expressions of these two relations have been defined by a linear curve fitting. The results are presented in table 4.1. The curve fitting precision factor was very high and almost equal to 100%. Values of the engineering constants are the same for the two load ranges within a 2% tolerance. The data provided by each gage of the back-to-back pair of strain gages measuring the same strain were very close to each other. As shown in figure 4.5 for the load range 0-50 000N, the strain data for each gage of the back-to-back pairs almost coincided. Thus there was no bending in the coupon. The average value of two strain gages was considered for the computation of E_x and ν_{xy} in table 4.1.

Determination of E_1 , E_2 , ν_{12} and G_{12}

Knowing E_x and ν_{xy} is not sufficient to be able to compute all the elastic properties at the ply level. Two more engineering constants, i.e., E_y and G_{xy} , are required to be able to compute exactly E_1 , E_2 , ν_{12} , and G_{12} . However, since there was interest in the strength of the plates in the loading directions and since strength testing should rely on more than one coupon, the limited amount of remnants of the failed plates were used for multiple strength test coupons oriented in the loading direction, as shown in figure 4.2. To measure E_y and G_{xy} , coupons at other orientations would be required and there simply were not enough remnants for this. Thus the ply level elastic properties were estimated using the value of E_x , ν_{xy} , the ply orientation, the ply thickness, and micromechanics. Table 4.2 presents the engineering properties of a typical graphite-reinforced composite as a function of the fiber volume fraction. The values presented in table 4.2 were taken as a baseline for computing the relative variation of three engineering constants with respect to the remaining one of

Table 4.2: Variation of the material properties with respect to the fiber volume fraction for a typical graphite-epoxy composite

composite property	fiber volume fraction		
	0.2	0.4	0.6
E_1 (GPa)	50.2	96.1	141.7
ν_{12}	0.324	0.289	0.259
E_2 (GPa)	6.69	9.03	12.38
G_{12} (GPa)	2.23	2.97	4.05

them, i.e., for instance

$$\Delta\nu_{12} = f(\Delta E_1) \quad \Delta E_2 = f(\Delta E_1) \quad \Delta G_{12} = f(\Delta E_1). \quad (4.5)$$

These relationships are quite close to being linear. By considering the engineering constants for a 0.6 fiber volume fraction as a 100% basis, it was shown that decreasing E_1 by 10.0% was accompanied by an increase of 1.41% for ν_{12} , and a decrease of 2.2% for the values of E_2 and G_{12} . Hence, successive values of E_1 , E_2 , G_{12} , and ν_{12} , along with the plate stacking sequence and the ply thickness computed in the previous section, were used as input to a FORTRAN program to compute E_x and ν_{xy} . The quantities E_x and ν_{xy} were computed using the following formulas:

$$E_x = \frac{A_{11} \times (1 - \nu_{xy}\nu_{yx})}{N \times h} \quad (4.6)$$

$$\nu_{xy} = \frac{-A_{12}}{A_{11}} \quad (4.7)$$

with N the number of plies and h the ply thickness. The variation of E_x with respect to the fiber volume fraction is presented in figure 4.6. The elastic property characterization tests presented previously for the coupon using the straight fiber design showed that E_x was equal to 90 GPa and ν_{xy} was equal to 0.319 (see Table 4.1). For these values of E_x and ν_{xy} , the micromechanics scheme gave the results presented in table 4.3.

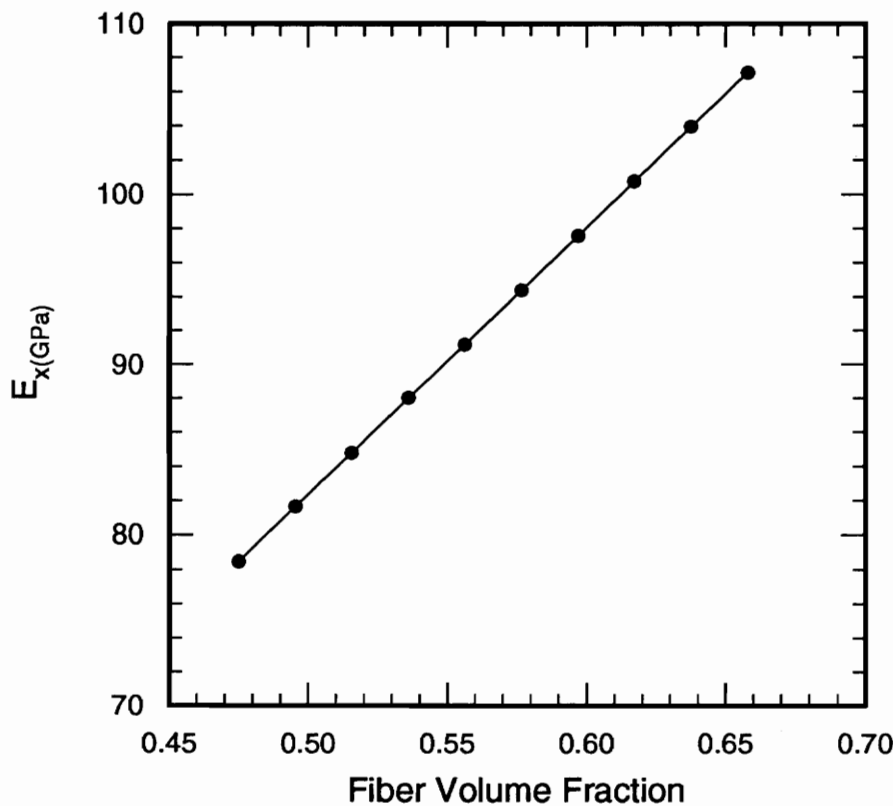


Figure 4.6: Variation of E_x with respect to the fiber volume fraction

Table 4.3: Estimates of the elastic properties at the ply level

E_1 (GPa)	130.0
E_2 (GPa)	10.66
ν_{12}	0.263
G_{12} (GPa)	3.88

Results obtained from the coupon with curvilinear fibers

The interpretation of the results obtained by testing the C coupon was more complex because of the presence of plies containing curvilinear fibers. As stated previously, the coupons were cut as close as possible to the glass-epoxy doublers, so the curvilinear angles were as close to zero as possible. The curvilinear path within the curvilinear ply is shown in fig 4.7. This path, of course, is an approximation. The fiber angle actually varied continuously along the length of the specimen. However, for the finite element analysis, as discussed in chapter 3, fiber angles were assumed to be constant within an element. The fiber angles shown in the coupon in figure 4.7 are consistent with the fiber angles in the finite elements in figure 3.4 which span the coupon. This variation in the fiber orientation within a coupon induced an important variation of the global material properties within the coupon. Assuming that the plates using the curvilinear fibers and the plates using the straight fibers were manufactured with the same material, the engineering constants evaluated previously should be valid for either plate. By considering an orientation variation from 3° to 20.5° , as illustrated in figure 4.7, the engineering constant E_x could be expected to vary from 88.7 GPa to 56.4 GPa within the coupon.

A straight-sided coupon cut from the panel using a curvilinear fiber format was tested following the same testing conditions as used for the straight fiber format coupon. Back-to-back pairs of strain gages were placed at the midlength of the coupon. The results from that testing are shown in the upper portion of figure 4.13. The experimental value of $E_x = 57.3$ GPa was obtained by curve fitting load vs. strain data from this coupon.

To further study the issues associated with the curvilinear fiber coupon, a finite element analysis of the straightside curvilinear fiber coupon was developed. The displacements of the nodes representing the bottom part of the coupon which was held fixed in the grip were restrained in the 3 directions, i.e., x , y , and z . A constraint equation imposed a constant displacement in the loading direction for the nodes representing the part of the coupon held in the upper grip. The longitudinal strain field of the model is presented in figure 4.8

for a load of 100 N. Considering the cross section of the coupon, this load corresponds to a stress of 0.672 MPa. The strain at the strain gage location computed by the finite element analysis was equal to $9.14\mu\epsilon$. By applying Hooke's law, Young modulus at the strain gage location obtained by the finite element analysis was 73 GPa. This value was 20% higher than the value 57.3 GPa found experimentally. This difference could have resulted from approximations made regarding the finite element analysis, or it could be that the curvilinear fiber material was different than the straight fiber material. The point was not investigated further and it was assumed that the elastic properties of the curvilinear fiber plates were the same as the elastic properties of the straightline fiber plates.

4.3 Strength Measurements

Testing strengths is not as simple as testing for elastic properties. The geometry of the coupon strongly influences the results. The strength coupons were again cut as close as possible to the glass-epoxy doublers. Hence, the coupons from the panel using the curvilinear fibers and the ones from its straight fiber counterpart should behaved similarly. This section describes the coupons used for the strengths measurements, the strength measurement results, and an analysis of the results.

4.3.1 Coupon Geometry

Strength property measurements in structural materials can be characterized in terms of three regions in the coupon: 1. the gripping region, 2. the central gage region, 3. the transition region between the gripping and the gage region. The coupon geometry has a significant influence on the quality of the tests results. To neglect one of these three regions in the coupon design could lead to misleading results. The first part of this section describes the different coupon designs presented in the literature [13, 14, 15].

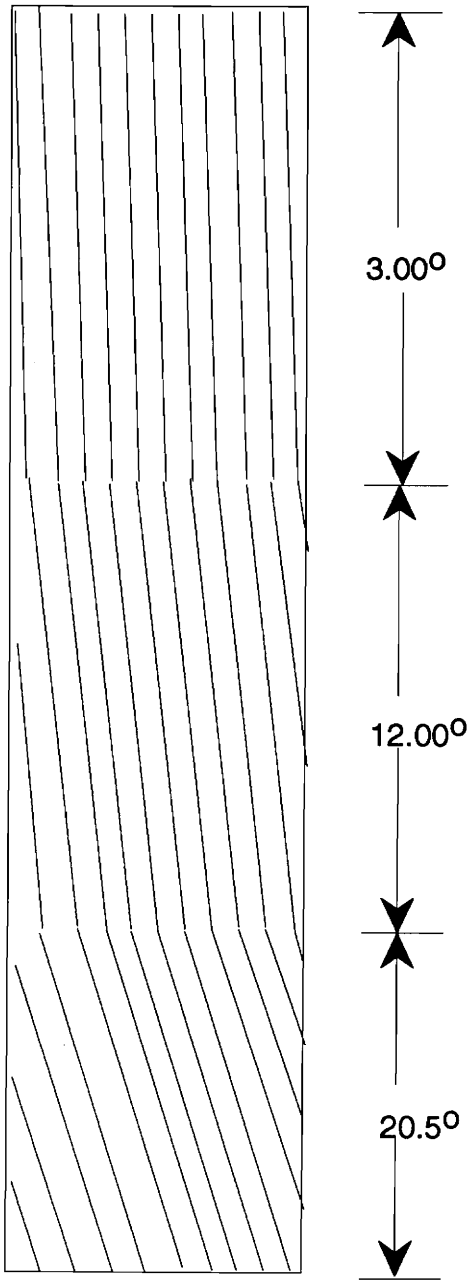


Figure 4.7: Fiber orientation of a curvilinear ply within the coupon

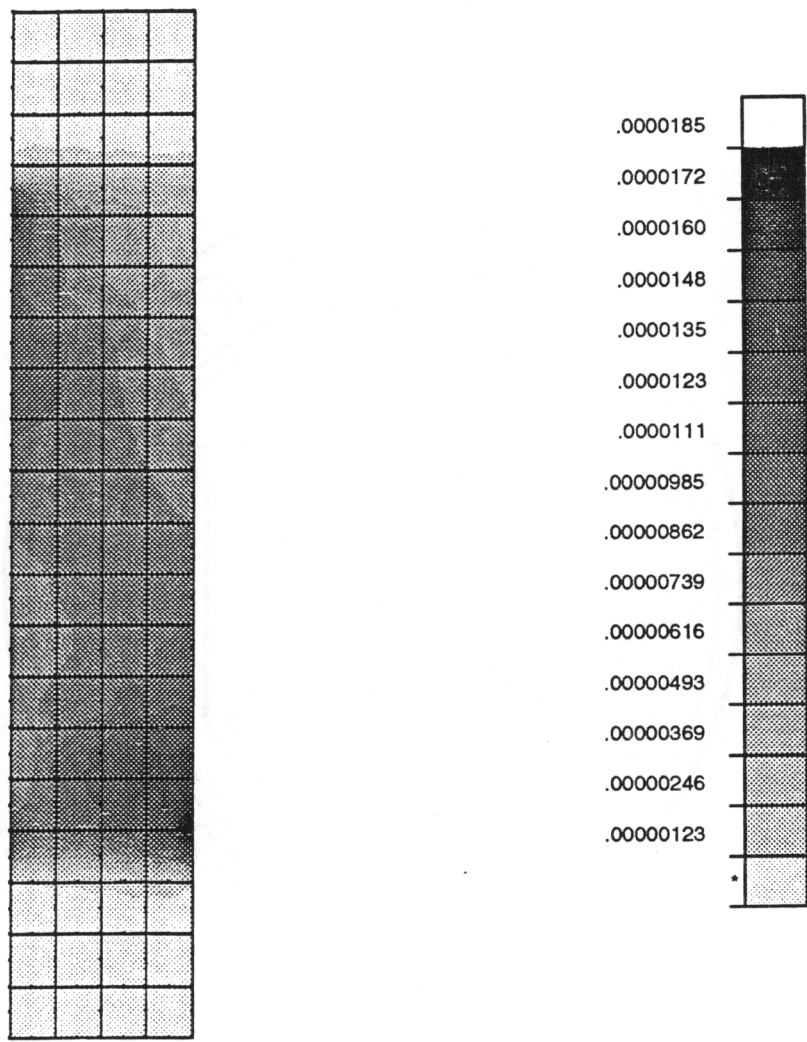


Figure 4.8: Predicted longitudinal strain field in the straight-sided curvilinear fiber coupon during tensile testing

Description of the coupons currently used in the industry

Three popular coupon designs are presented in figure 4.9. These are described below.

The ASTM D638 ("Dogbone") coupon

According to [13], the dogbone coupon, figure 4.9.a, does not provide a satisfactory tension coupon for fiber-dominated materials. The stress distribution is uniform in the gage section but important stress concentrations appear in the transition region. As a result, the strengths of the material are highly underestimated using the dogbone coupon. The analysis presented in [15] judges this coupon unsatisfactory for both unidirectional and laminated composites.

The straight-sided coupons

Results of a survey presented in [13] indicates that straight-sided coupon with bonded doublers, figure 4.9.b, embraced under ASTM test Method D3039, provides test results generally considered acceptable. However the stress field near the tab termination is complex and includes stress concentrations which can sometimes lead to questionable results. A straight-sided coupon was not used for the strength tests here mainly because of the inability to know where along the length failure would occur.

Linear tapered "bowtie" coupon

The bowtie shape, figure 4.9.c, was designed to solve the stress concentration and doublers problems. Reference [15] provided very encouraging results for this design. The failure mode is consistently in the gage area and the results are close to the computed strengths of the material. Its main disadvantage is its length. The length required is large. A coupon of this size could not be cut from the plate remnants.

Streamline coupon

The streamline coupon is theoretically free from stress concentration. It was designed by considering fluid mechanics concepts. Conventional machining techniques cannot be used to cut a coupon with a streamline shape.

Either because of complexity or lack of sufficient material, none of the coupon designs currently used by the testing community were suitable for the present study. Nevertheless the “bowtie” coupon was taken as baseline to create the design used in the present study. A finite element analysis of the specific design was conducted to determine the stress distribution and estimate the stress concentration factor in the gage area.

4.4 Design of coupon used in present study

According to [13], the ideal strength coupon should provide a large effective loaded area in the grip region to compensate for stress concentrations caused by the gripping arrangement. It should also allow the stresses in the gage region to approach a uniform condition of high stress to ensure that failure takes place in that region. The bowtie coupon best fits these criteria and thus served as a reference to design the coupon used.

The coupon design is presented in figure 4.10. As stated earlier, its dimension were limited by the size of the region of the remnants from which to cut coupons. The end regions of the coupon were wider to make gripping easier. The width of the coupon was minimum at midlength. A pair of back-to-back longitudinal strain gages were bonded at this location. The reduction of the width of the coupon induced a stress concentration and insured failure might occur at this location. The strain gages were used to measure load vs. strain.

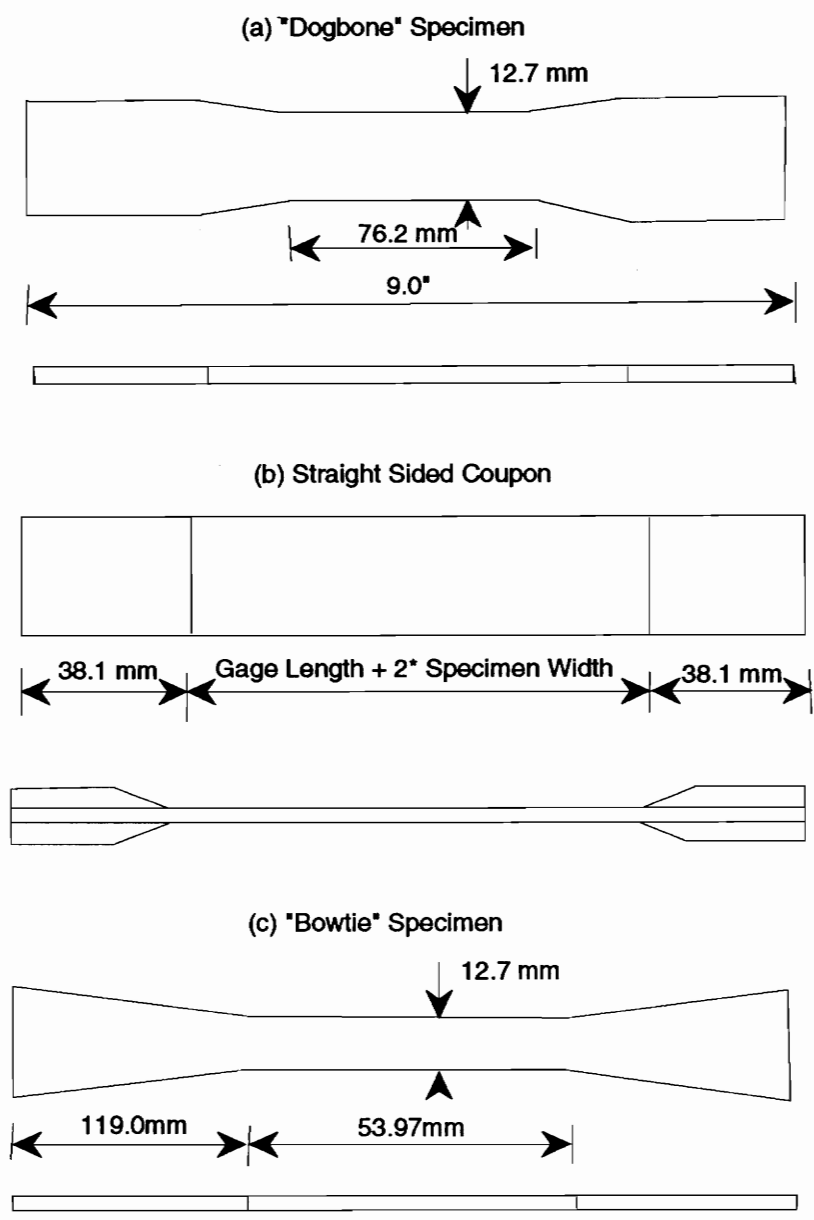


Figure 4.9: Coupons currently used in the industry

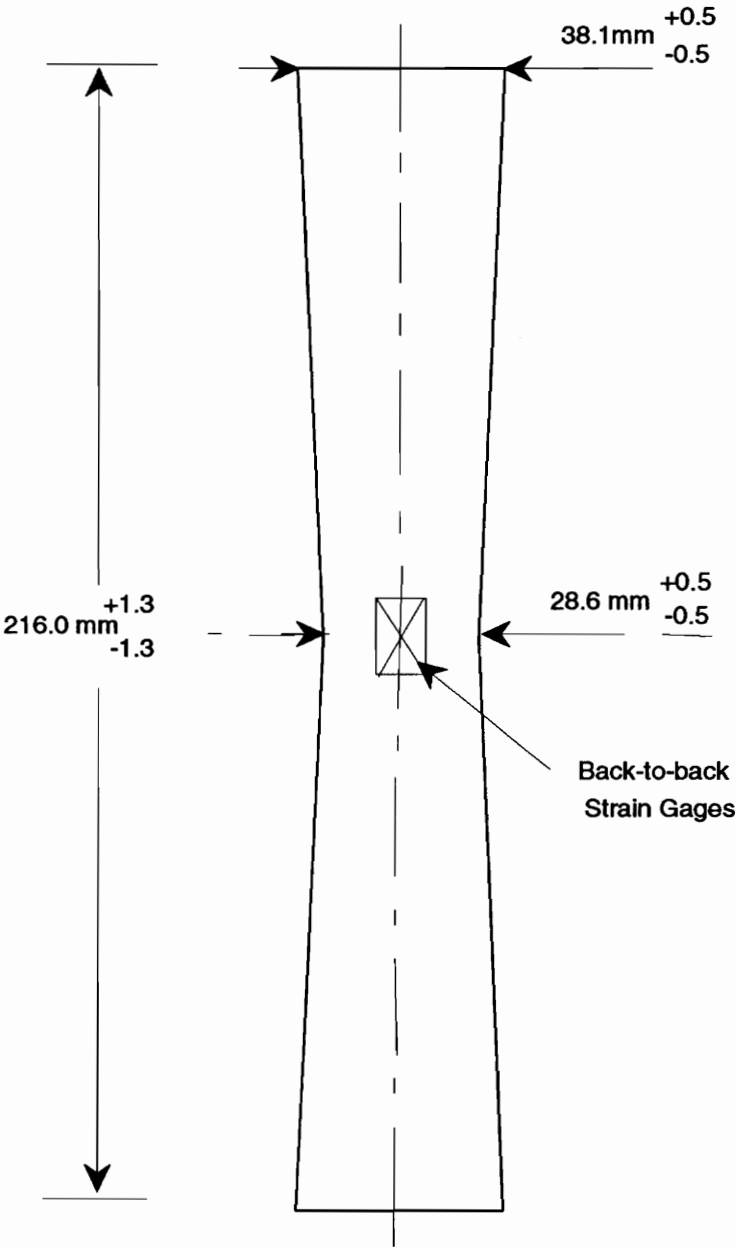


Figure 4.10: Geometry for strength measurement coupons

4.5 Coupons with straight fibers

The testing conditions for strength measurements were the same as the ones used for the elastic property characterization tests. A length of 38.1 mm was used on each end of the specimens to clamp the coupon between steel grips.

4.5.1 Finite-Element analysis - strain concentration factor

A finite element analysis of the strength testing was used to estimate the stress concentration factor due to the reduction in width. The resulting predicted strain distribution in the load direction for a load of 100N is shown in figure 4.11. As foreseen, a strain concentration appeared in the minimum width area. During the test, the strain gages measured the strain at midlength, at the intersection of the two axes of symmetry. A strain concentration factor was computed to predict a actual failure strain for the material. For the 100 N load, the highest strain in the minimum width location was $\epsilon = 11.9\mu\epsilon$. It occurred at the edge of the coupon. For the same load, the strain at the midwidth location but in the center of the coupon away from the edge was $9.45\mu\epsilon$. This translates into a strain concentration factor of 1.26.

4.5.2 Experiments

For strength testing, four coupons, denoted as S1, S2, S3 and S4, were cut from the panel containing the straight fibers. The four coupons were loaded to failure. The raw results to voltages were converted in MPa for the stresses and to $\mu\epsilon$ for the strains. The results are presented in the lower two-thirds of figure 4.5. In each subfigure in figure 4.5, three curves are plotted for each coupon, two represent the results provided by each of the two back-to-back gages, and the third one is an average of the two gages. In general, there was good agreement between the two back-to-back strain gages. Table 4.4 summarizes all the results. The strain ϵ_s is the strain at the minimum width location away from the edge, and ϵ_m is the strain concentration factor (1.26) times this strain. The scatter of the final

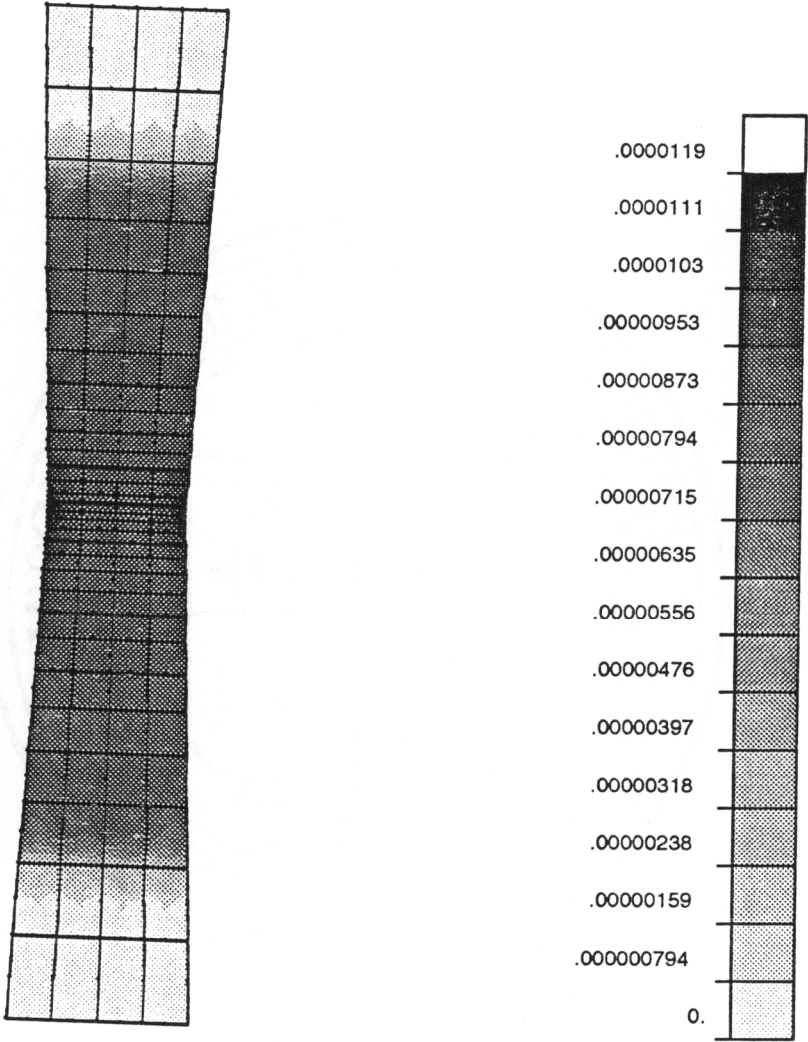


Figure 4.11: Strain in the loading direction in the straight fiber strength coupons

Table 4.4: Straight fiber coupons: Results from the strength measurements

Coupon	Failure load F (N)	Cross-section area at the gage location, S (mm ²)	Final stress $\frac{F}{S}$ MPa	Failure Strain ϵ_s for coupon ($\mu\epsilon$)	Failure strain for material $\epsilon_m = f\epsilon_s$ ($\mu\epsilon$)
S1	92 050	114.4	804.6	8 175	10 300.5
S2	100 500	117.6	854.6	8 175	10 300.5
S3	87 820	108.2	811.64	8 205	10 338.3
S4	106 600	117.6	906.5	9 230	11 629.8
Average	96 742.5	114.45	845.28	8 446.0	10 642.0
Scatter	19%	8.21%	12%	12.5%	12.1%

f: strain factor

stress and the failure strain is 12%. This is reasonable for strength measurements. The failure strain computed from the average over the four coupons was equal to 10 642 $\mu\epsilon$. It is interesting to correlate the experimental results with the finite element analysis. According to the finite element analysis, the strain field in the coupon reached a strain of 10 642 $\mu\epsilon$ in the minimum area region for a load equal to

$$\frac{\epsilon_m}{\epsilon_{fem}} \times Load_{fem} = \frac{10\ 642\mu\epsilon}{11.9\mu\epsilon} \times 50N = 89\ 362N \tag{4.8}$$

with ϵ_{fem} being the highest strain obtained from the finite element analysis (see figure 4.11). This failure load agrees within a 7% tolerance with the failure load determined experimentally, i.e., 96 742.5 N (see Table 4.4). The agreement between the experimental results and the results provided by the finite element analysis gives credit to the value of the engineering constants computed and ply thickness measurements investigated in the previous section.

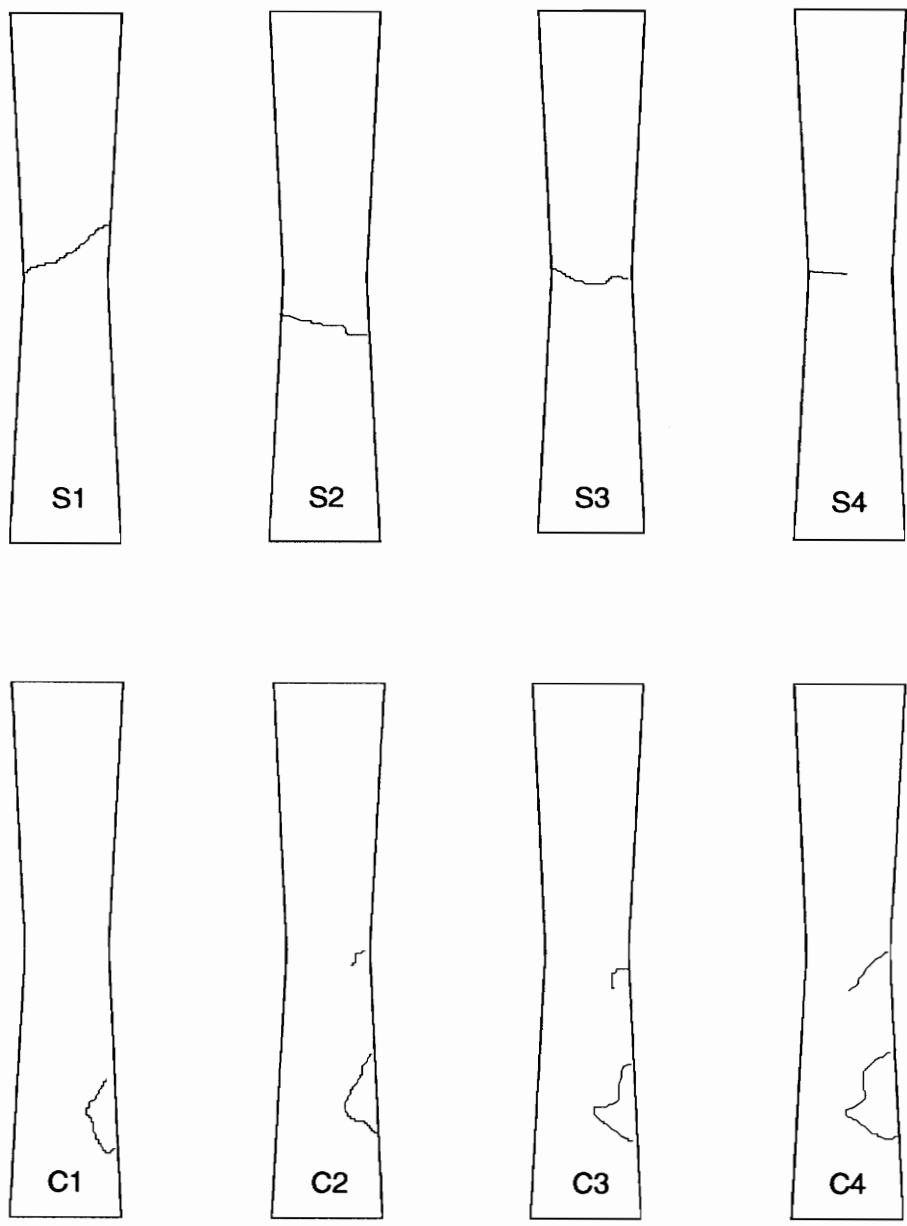


Figure 4.12: Failure location in strength coupons

4.5.3 Failure location

The upper portion of figure 4.12 shows the failure location for the four straight fiber strength measurement coupons. According to the finite element analysis, the coupons should have failed at the cross section with the minimum area. The results presented in figure 4.12 are very satisfactory. Coupons S3 and S4 failed at the cross section. In coupons S1 and S2 the failure was initiated at one side of the coupon and then propagated across the coupon near the minimum area.

4.6 Coupons with curvilinear fibers

4.6.1 Results

The testing conditions for the strength coupons with the curvilinear fibers were the same as the ones used for the strength coupons with straight fibers. Four coupons, denoted as C1, C2, C3 and C4, were loaded to failure. The resulting relations between strain and average stress are presented in the lower portion of figure 4.13 for the four coupons. Again, these figures represent the results provided by each of the two back-to-back strain gages, and their average. As with the S coupons in figure 4.5, the figures demonstrate the lack of bending for coupons C1-C3. Coupon C4 experienced some bending. The values obtained for the peak loads and the strains of the tapered coupons just before failure are summarized in table 4.5.

Compared to the results obtained for the S coupons, the strains at failure were not as consistent. Also, the failure load was much lower for the coupons with curvilinear fiber plies. This difference in the load carrying capacity can be explained by considering the stacking sequence of the laminates. The stacking sequence of the curvilinear panel was $(\pm 45/C_2/0/90/C_2)_s$, where the C denotes layers with the curvilinear trajectories. The fiber orientation within a coupon was shown in figure 4.7. None of the fibers in the curvilinear plies traversed the coupon from one gripped end to the other. Only two 0° plies offered

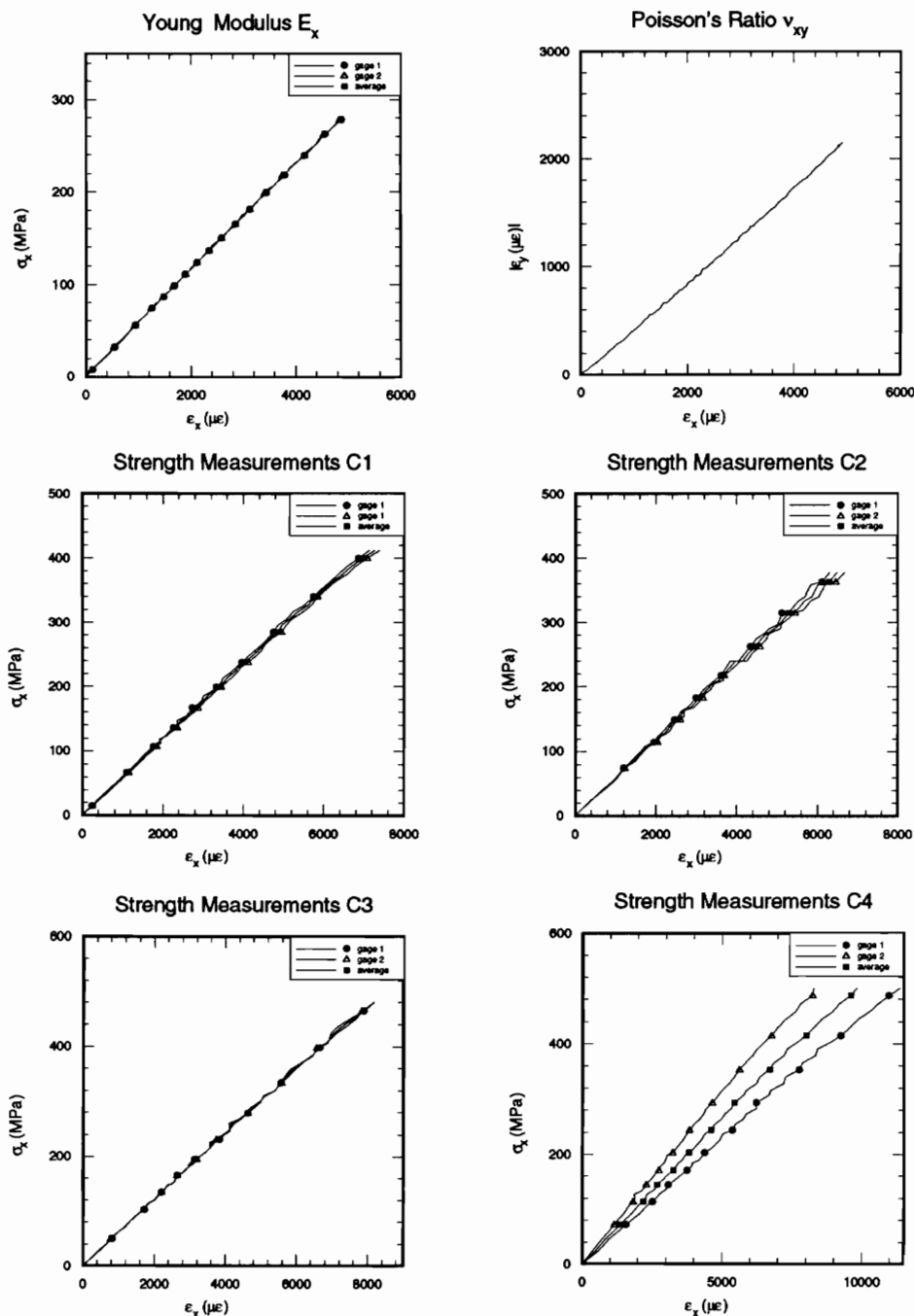


Figure 4.13: Experimental results for the coupons using a curvilinear fiber format

Table 4.5: Curvilinear fiber coupons: Results from the strength measurements

Coupon	Failure load F (N)	Cross section area at gage location, S (mm^2)	Final stress $\frac{F}{S}$ MPa	Failure Strain ϵ_s for coupon ($\mu\epsilon$)
C1	49 770	118.5	420	7 260
C2	42 300	109.9	384.9	6 492
C3	54 400	111.9	486.1	8 179
C4	59 170	118.5	499.3	9 830
Average	51 410	114.7	447.6	7 940
Scatter	32%	7.5%	25%	42%

full fiber resistance in the loading direction. On the other hand, the stacking sequence of the straight fiber panel $(\pm 45/0_2/0/90/0_2)_s$ included 10 0° plies in the loading direction. This is five times more than the number of 0° plies in the sequence with the curvilinear plies. So, assuming that the volume fraction was the same for the two fiber formats, the number of fibers passing from one grip to the other was much more for the S coupons. This can explain the difference in the failure load between the S and C coupons. Nevertheless, assuming that the two plates were made of the same material, the ultimate failure strain in the fiber direction should have been the same. A failure analysis would assume laminate failure when the first fiber breakage occurs in any ply. The 0° fibers, being parallel to the loading direction, would be the first to break.

4.6.2 Finite element analysis

To study the strains in the 0° plies, a finite element analysis was developed to determine the strain field in the C coupons. The fiber angle in the curvilinear plies was considered to be constant within an element and the fiber angles for the curvilinear plies for the coupon were presented in figure 4.7. A 100 N load was applied to one end of the coupon while the other end was held fixed. The strain in the loading direction is shown in figure 4.14. The failure location was not in the notched area, rather it occurred where the fiber angle

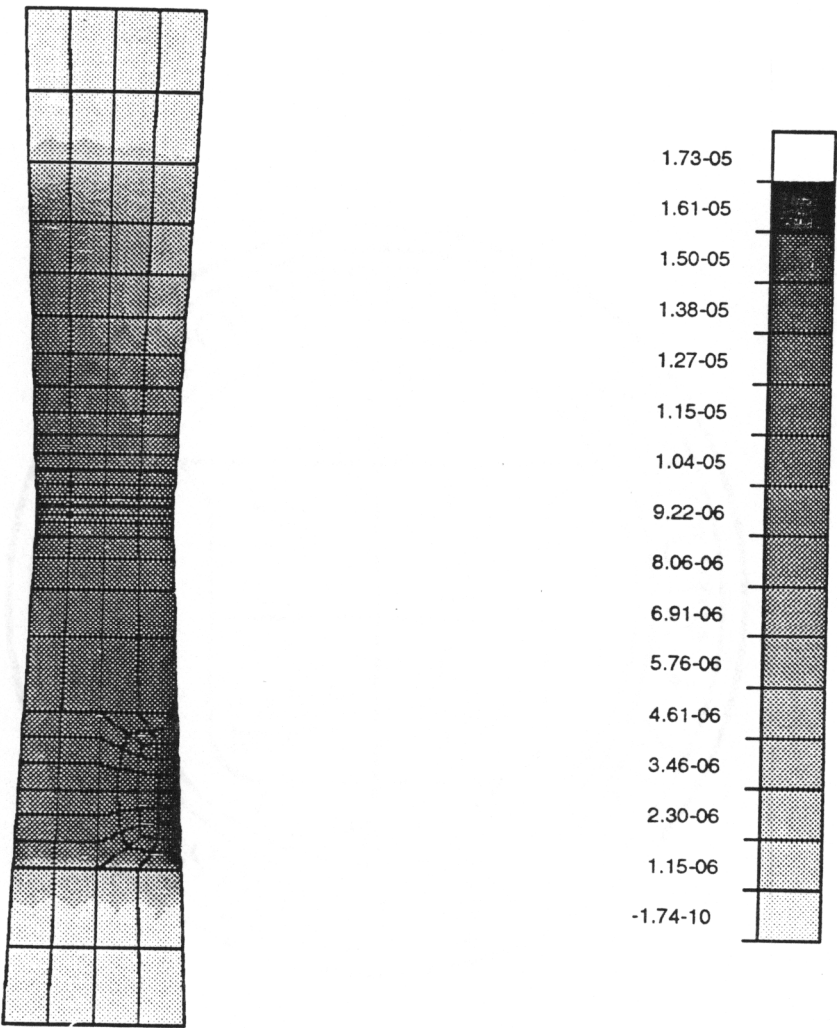


Figure 4.14: Strain in the loading direction of the curvilinear fiber strength coupons

in the curvilinear ply was the highest (i.e., 20.5° , see figure 4.7). For a 100 N load, the maximum strain at this location was equal to $17.74\mu\epsilon$. According to the tests on the S coupons, the maximum strain in the 0° plies just before failure was $10\,642\mu\epsilon$ (see table 4.4). Because of the linearity of the finite element analysis, the load for this strain level for the C coupon was equal to 59 988 N. This failure load computed by the finite element analysis was compared with the values found experimentally in table 4.5. There was a 14% difference between the finite element predictions and the average failure load found experimentally. This difference can find various interpretations. First, the elastic properties of the panels using the curvilinear fibers may have been softer than the elastic properties used for the panels manufactured with straight fibers. Here they are assumed to be the same. A second approach is to say that a 14% difference was reasonable for strength measurements. As shown in table 4.5, the scatter of the final load was 32%. This percentage is somewhat usual for strength measurements. The third explanation, which is the most plausible, is that the 10 0° plies in the straight fiber coupons didn't all fail exactly at the same time. The laminate was capable of bearing load after some of these plies fail. Experimentally, the first failures for the S coupons could be heard when the laminate reached approximately 75% of the failure load. On the other hand, for the C coupons, having only two 0° plies, the final failure coupon followed almost immediately the first audible report from the coupon.

4.6.3 Failure location

The failure locations as they appeared on the broken coupons are sketched in figure 4.12. Comparing figure 4.12 and the finite element predictions illustrated in figure 4.14, there was almost perfect agreement as regards failure location.

4.7 Closure

With a reasonable estimate of the elastic and strength properties, attention turned to the prediction of the response of the straight and curvilinear fiber tensile and compression

plates. That is the subject of the next several chapters.

Chapter 5

TENSION TESTS

This chapter presents the finite element model used to analyze the tension tests. The finite element mesh was shown in figure 3.1. Issues like the boundary conditions, loading, and the type of finite elements chosen are addressed. The results obtained by the finite element analysis are systematically compared with the experimental results. The ultimate failure load was computed with FORTRAN programs using various failure criteria. The fiber path in the curvilinear plies was optimized with an improved scheme based on earlier work of Hyer and Charette [1-4] and Charette [5].

5.1 The Finite Element Approach

5.1.1 Preprocessing

Boundary Conditions

The boundary conditions were the result of two characteristics of the model: the choice of an inplane finite element and the two axes of symmetry of the plate. The analysis consisted of an inplane problem, so the third degree of freedom (i.e., the displacement in the z direction) was not active in the model and could not be restrained. Second, modeling a quarter of the plate was sufficient because of symmetries involving geometry,

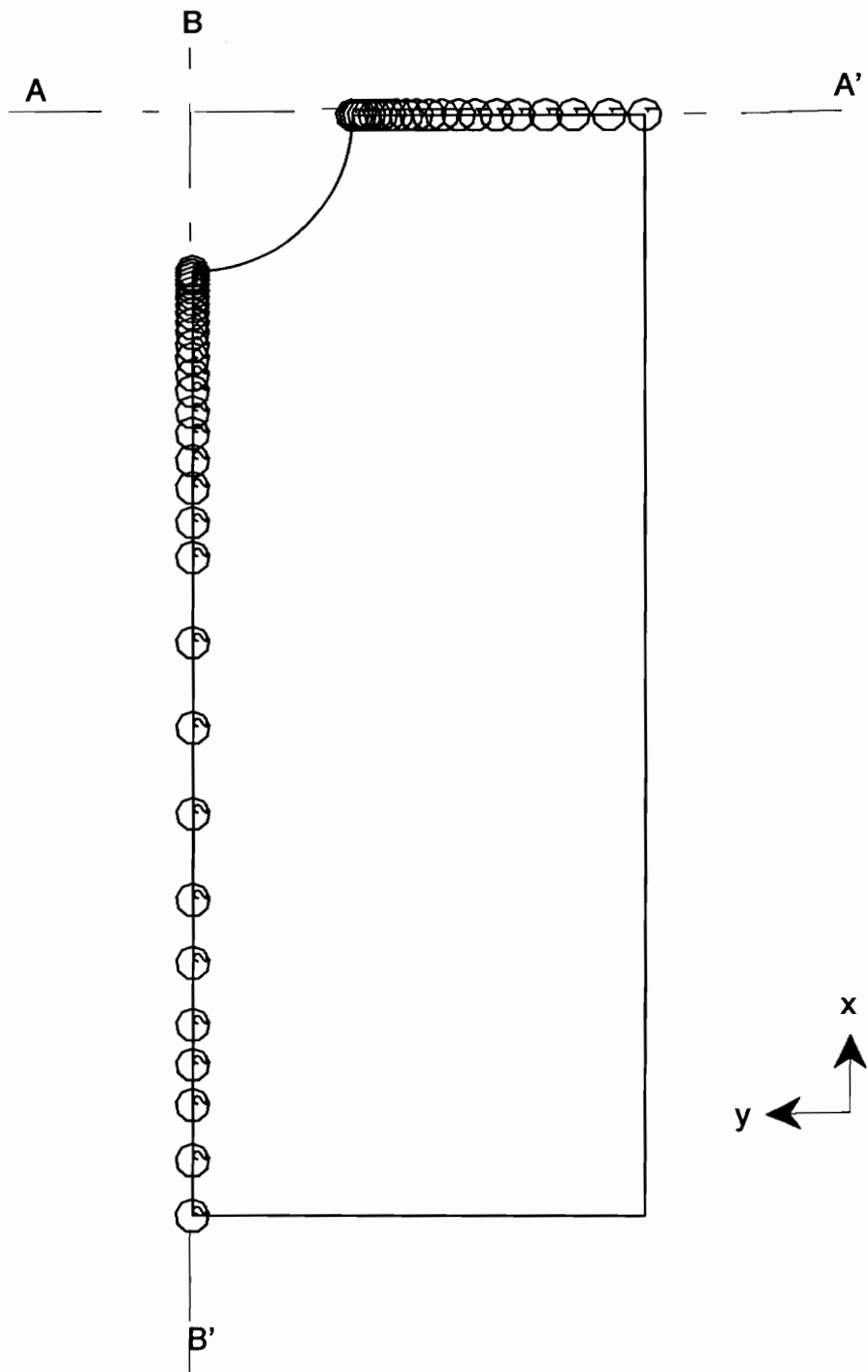


Figure 5.1: Boundary conditions for analysis of tensile plates

loading, material properties, and boundary conditions with respect to the x and y axes. As shown in figure 5.1, the symmetry of the plate was represented by two classic roller type boundary condition. Formally, the boundary conditions applied along AA' and BB' can be summarized as :

$$u = 0 \text{ along AA'}$$

$$v = 0 \text{ along BB'},$$

where u and v represent the displacement field in the x and y directions.

Loading

Steel grips, with serated surfaces, held each end of the tensile plates by bolting through the thickness of the specimen. The serated surface of the grips bore against the glass-epoxy doublers used in the bolting region. The glass-epoxy doublers were shown in figure 2.9. These loading features were complex and difficult to model. The glass-epoxy doublers and the end of the plate were compressed between the steel grips, and pulled by concentrated loads at the location of the bolts. The serated surface of the grip also exerted a force on the plates, hopefully greater than the concentrated loads. As seen earlier, the mesh was arranged so that a node was situated at the exact location of each bolt. In the first loading case of the finite element analyses, the model was loaded by concentrated loads applied at these nodes (see figure 3.1). In the second loading case, a uniform load was applied downward along bottom edge of the plate (see figures 3.1 and 5.1). A uniform load would be realistic if the steel grips and the doublers were perfectly coupled through the serated surface. In this case, there would be no stress concentration due to the bolts.

All the model characteristics discussed so far were defined in PATRAN. This preliminary PATRAN model was converted into a preliminary ABAQUS input file through the PATABA translator.

5.2 Processing

A whole section devoted to composites materials has been developed by ABAQUS several years ago. Through the keywords COMPOSITES and ORIENTATION, the material characteristics of the model can be defined at the ply level within the *MATERIAL card. This card has to refer to elements. The first finite element analyses were made with this arrangement. The results revealed a mesh instability. Instabilities arose because of shortcomings in the element formulation process, such as the use of low-order Gauss quadrature rules. All the shell elements in the ABAQUS element library are defined with a reduced integration and are rather unduly susceptible to inplane load patterns. For the current configuration, computed displacement were excessive [16]. Therefore, using shell elements combined with the COMPOSITE option could not be considered for this problem. The analysis of the plate using the curvilinear fibers could not be proceed in ABAQUS unless the ANISOTROPIC option was used to define the material properties. This option required the input of an eight by eight stiffness matrix for each element of the mesh. This alternative was judged to be too laborious and thus FEM2D was used.

No preprocessor was available for FEM2D. Hence, the preprocessing was created using PATRAN and PATABA. A program in FORTRAN was created to translate the ABAQUS input file into a file readable by FEM2D. The nodal coordinates, boundary conditions, and connectivity matrix were read from the ABAQUS input file, reformatted, and then placed in the appropriate order in a file for FEM2D. The material characteristics for the composite layup were defined by providing the $[A]$ matrix for each element. The $[A]$ matrix is sufficient to characterize composite material behavior due to inplane loads. Ordinarily, the resultant forces and moments are written in terms of the middle surface extensional strains and curvatures as

$$\begin{pmatrix} N \\ M \end{pmatrix} = \begin{bmatrix} A & B \\ B & D \end{bmatrix} \times \begin{pmatrix} \epsilon^o \\ \kappa \end{pmatrix}. \quad (5.1)$$

In the current case, there are no moments. Moreover, the symmetry of the stacking sequence implies that the matrix [B] is equal to zero. Hence the former relation can be reduced to

$$(N) = [A] \times (\epsilon^o). \quad (5.2)$$

The program written to create the input file for FEM2D computed for each element the [A] matrix according to the element material properties, stacking sequence, and curvilinear fiber trajectories. The [A] matrices computed in the gripping area took into consideration the influence of the glass-epoxy doublers. The input file contained all the information necessary to analyze the problem. The results provided by the program (i.e., displacements, stresses, strains...) were computed at the integration points of the elements. Several post-processing programs were written. One program transformed the results into a neutral file readable by PATRAN. All the results computed by FEM2D could be visualized, e.g. the deformed shape or the stress resultants. A second post-processor included several failure criteria to predict the ultimate load of the plates.

For the straight fiber plate the lay-up was a balanced $(\pm 45/0_3/90/0_2)_s$ arrangement. ABAQUS could be used and the option LAMINATE was used to define the material properties, i.e., E_x , E_y , ν_{xy} , G_{xy} , G_{yz} , and G_{xz} , in the global coordinate system at the ply level. For a balanced laminate, the terms A_{16} and A_{26} are equal to zero so the A matrix could fully be defined just by considering E_x , E_y , ν_{xy} , G_{xy} . That is,

$$\begin{aligned} A_{11} &= \frac{E_x \times N \times h}{1 - \nu_{xy} \times \nu_{yx}} & A_{22} &= \frac{E_y \times N \times h}{1 - \nu_{xy} \times \nu_{yx}} \\ A_{12} &= \frac{\nu_{xy} \times E_y \times N \times h}{1 - \nu_{xy} \times \nu_{yx}} & A_{66} &= N \times h \times G_{xy}. \end{aligned} \quad (5.3)$$

The values E_x , E_y , ν_{xy} and G_{xy} , in the global coordinate system were calculated using a standard approach based on classical laminated theory [17].

Two sets of material properties had to be defined. The presence of the glass-epoxy doublers in the gripping area at the ends of the plate had to be taken in consideration.

Hence two different `*SOLID SECTION` inputs (see table 5.1 for the keywords meaning) were defined to differentiate the gripping area from the rest of the plate.

In ABAQUS, the output results could either be presented for each node, each element, or at each integration points. The PATABA interface gave the user the flexibility to choose the response quantities to be calculated. Practically, almost all the quantities were computed at the integration points and then extrapolated to the requested locations. The type of results (i.e., displacement, strains, stresses...) requested by the user in the interface PATABA appeared at the bottom of the input file. All the results were translated by a second interface called ABAPAT in a file readable by PATRAN to visualize the results. It includes most of the keywords described in the table 5.1.

5.2.1 Material Properties

The material properties used in the analysis were experimentally determined and discussed in Chapter 4. Specifically, the ply properties used were given in Table 4.3. A ply thickness was taken to be 0.25mm. A tensile failure strain in the fiber direction of $10\,642\mu\epsilon$ was used.

5.2.2 Validity of the finite element programs

Many checks were conducted to confirm the validity of the finite element results. The model using straight fibers was investigated using both ABAQUS and FEM2D. For the ABAQUS analysis, an 8-node thin solid element was used. The results provided by ABAQUS and FEM2D were compared. Stresses, strains, and displacements were compared at various locations of the plate and always showed a perfect agreement between the two programs. As an example, figure 5.2 shows the strains computed along the bottom edge (see figure 5.1) of the plate for a specific load level for the case of a uniform loading.

Table 5.1: ABAQUS keyword definition for tension test

KEYWORDS	MEANING
*NODE	Nodal coordinates definition
*NSET	Node set creation
*EQUATION	Multipoint constraint
*ELEMENT,TYPE=CPS8,ELSET=PID0	Element set creation, Element type, Identification
*SOLID SECTION,ELSET=PID0,MAT=1	Element property assignment, Element set named PID0, Identification of the material used for this element set
*MATERIAL,NAME=1	Material definition, Name of the material
*ELASTIC,TYPE=LAMINA	Elastic material properties, type of the material
*STATIC	Implies a linear analysis
*CLOAD	Loading definition
*BOUNDARY	Definition of the boundary conditions
*NODE FILE, *NODE PRINT	specify calculated quantities

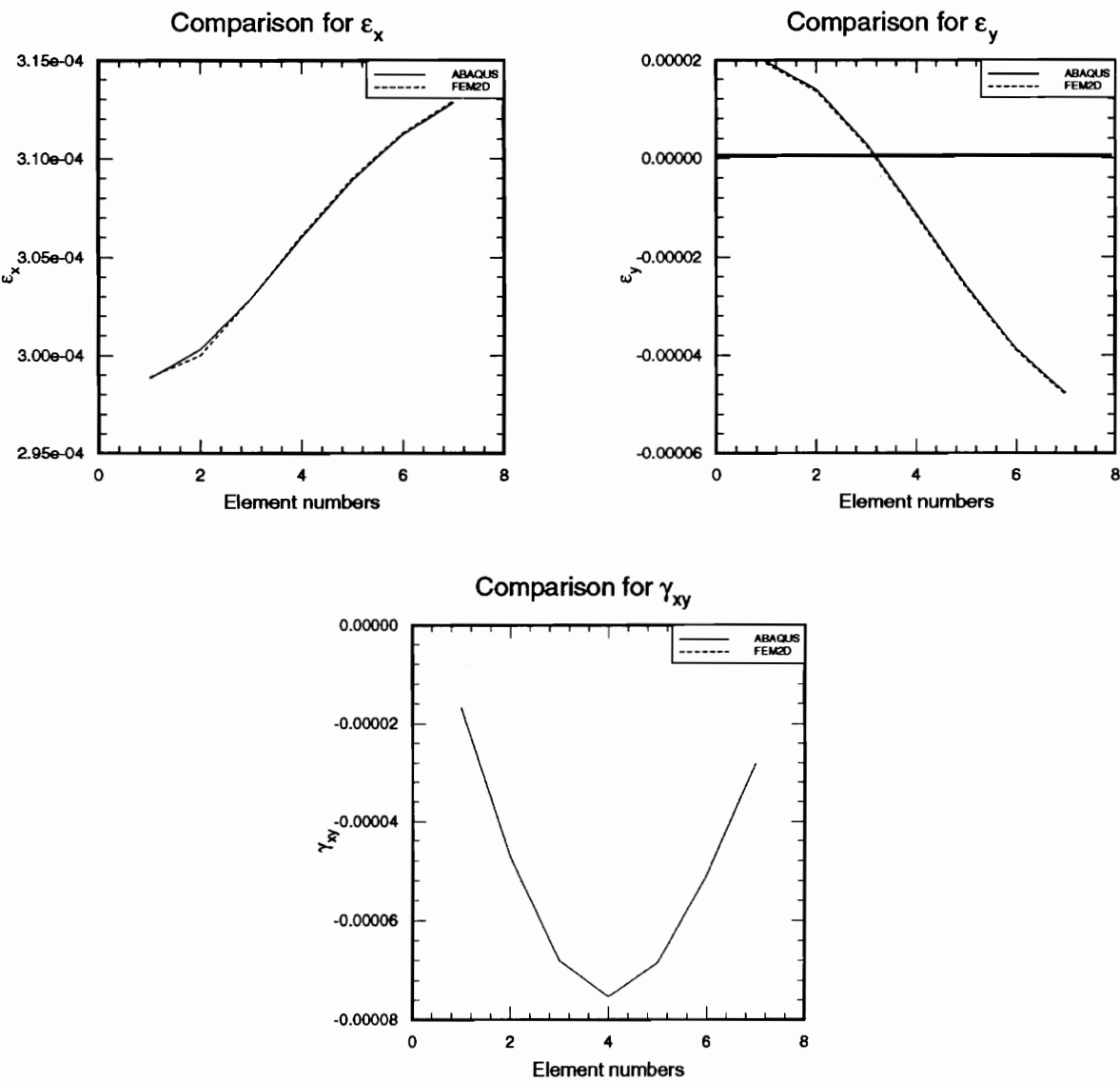


Figure 5.2: Comparison between the results provided by ABAQUS and FEM2D

5.3 Strain gages

As was seen in figure 2.9, back-to-back strain gages at different locations monitored the response of the plate during the tensile test. The strain response indicated that the loading was symmetric across the width of the plate, and along the top and bottom edges. The strains measured by the gages at various location on the two specimens are compared in figure 5.3 and in figure 5.4 with the finite element predictions. Figure 5.3 compares the experimental results with the results obtained by the finite element analysis considering a uniform loading case. Figure 5.4 compares the experimental results with the results obtained by the finite element analysis considering concentrated loads.

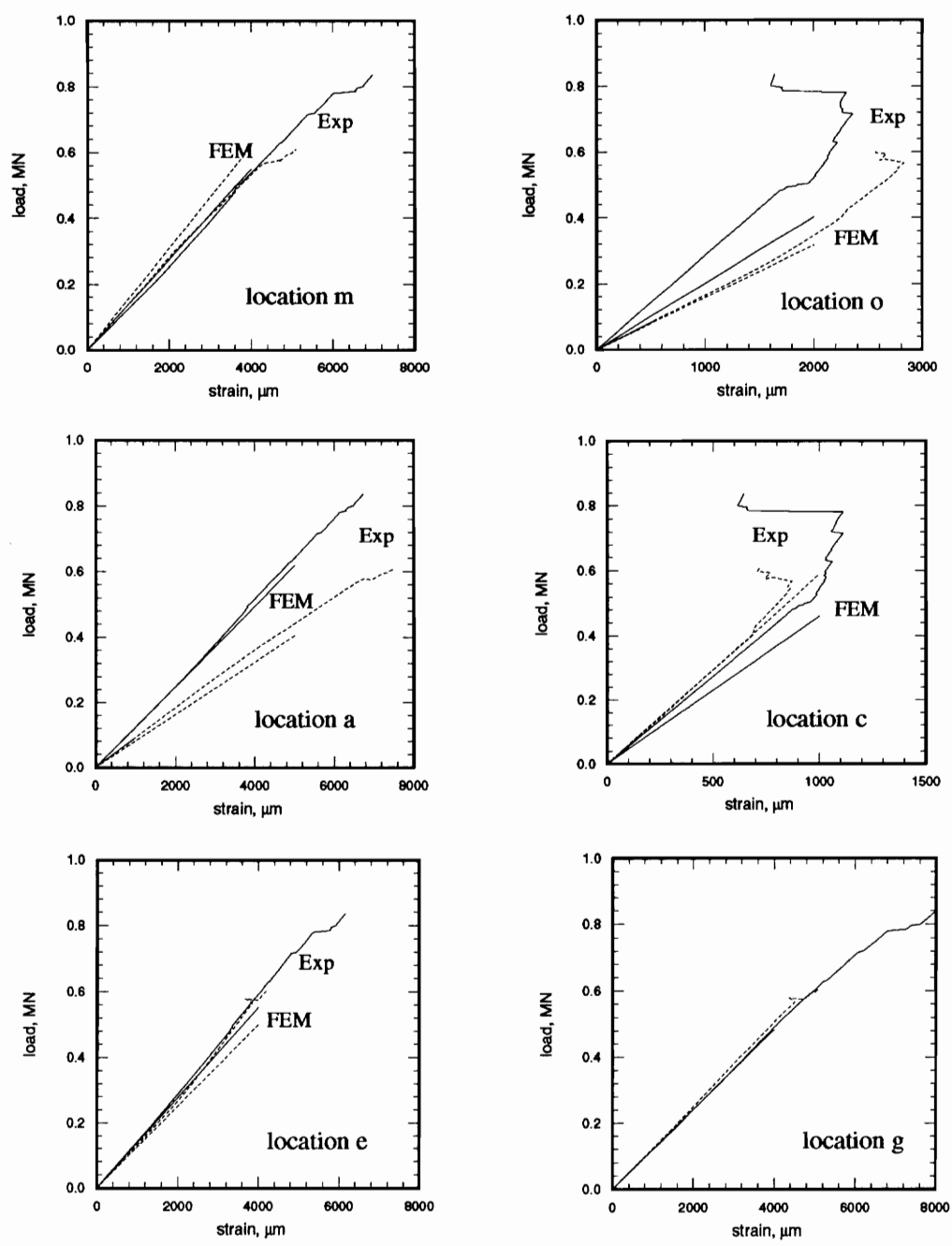
5.3.1 Summary of experimental results

During the experiments, until failure, the strains at location ‘m’, ‘c’, ‘e’, ‘g’, and ‘i’ were practically the same for the curvilinear fiber specimen as they were for the straight fiber specimen. At locations ‘a’ and ‘o’ the curvilinear fiber specimen was more highly strained than the straight fiber specimen. The strain field between ‘a’ and ‘m’ seemed to be more uniform for the plate using straight fibers than for the plate using the curvilinear fibers. At the location ‘k’, where failure should occur, the strains for the curvilinear specimen were slightly higher in the linear range.

5.3.2 Analysis of figures 5.3 and 5.4

General comments

By studying figures 5.3 and 5.4, it is seen that the boundary conditions in the gripping area didn’t strongly influence the strain fields at the gage locations. For the finite element analyses, the strains predicted at the net section were the same considering either concentrated loads or a uniform load. For the straight fiber plate, the finite element analysis and the experimental data coincided almost perfectly at the locations ‘a’, ‘e’, ‘g’, and ‘i’.



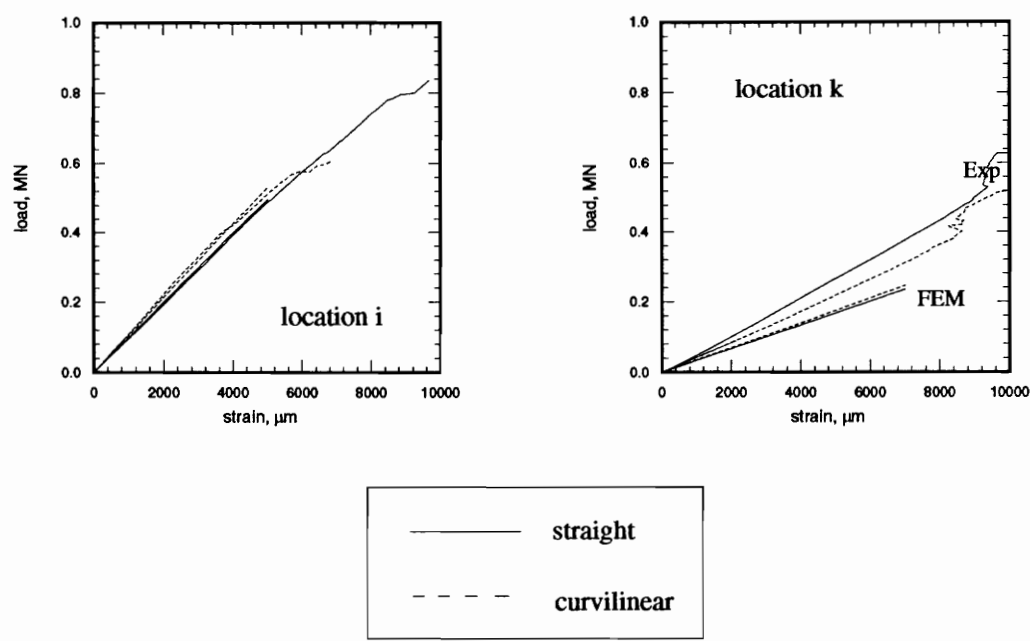
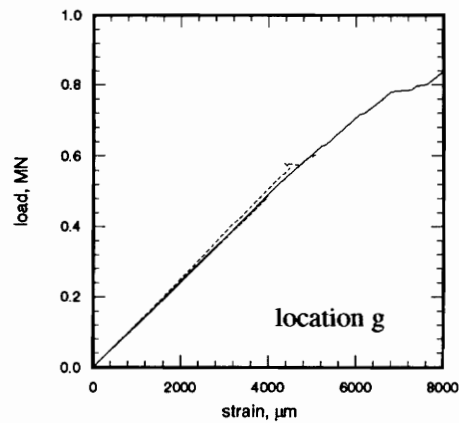
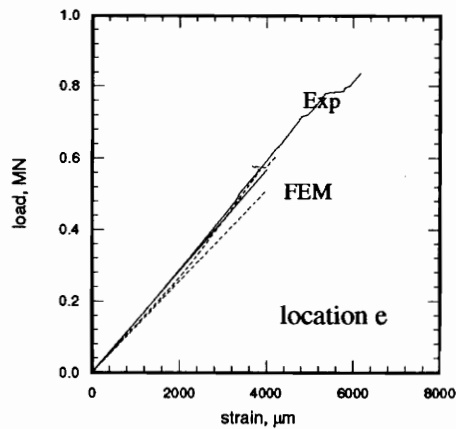
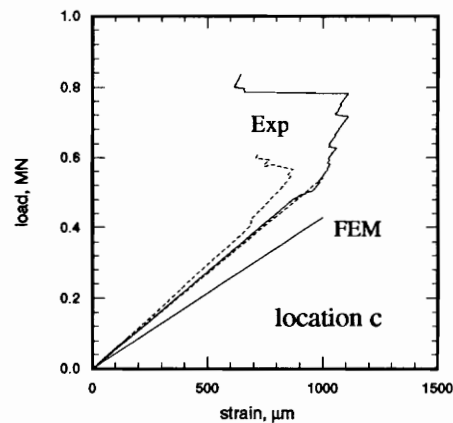
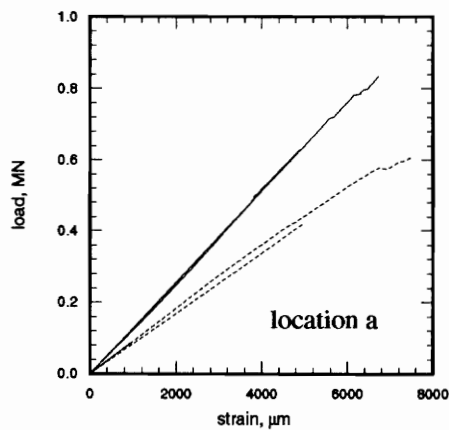
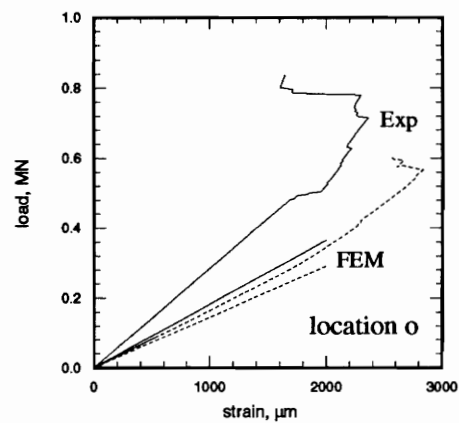
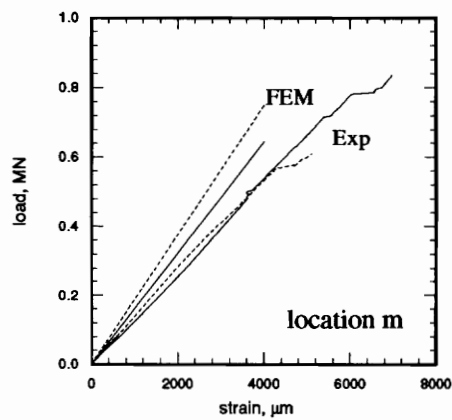


Figure 5.3: Results obtained at strain gage locations considering a uniform load



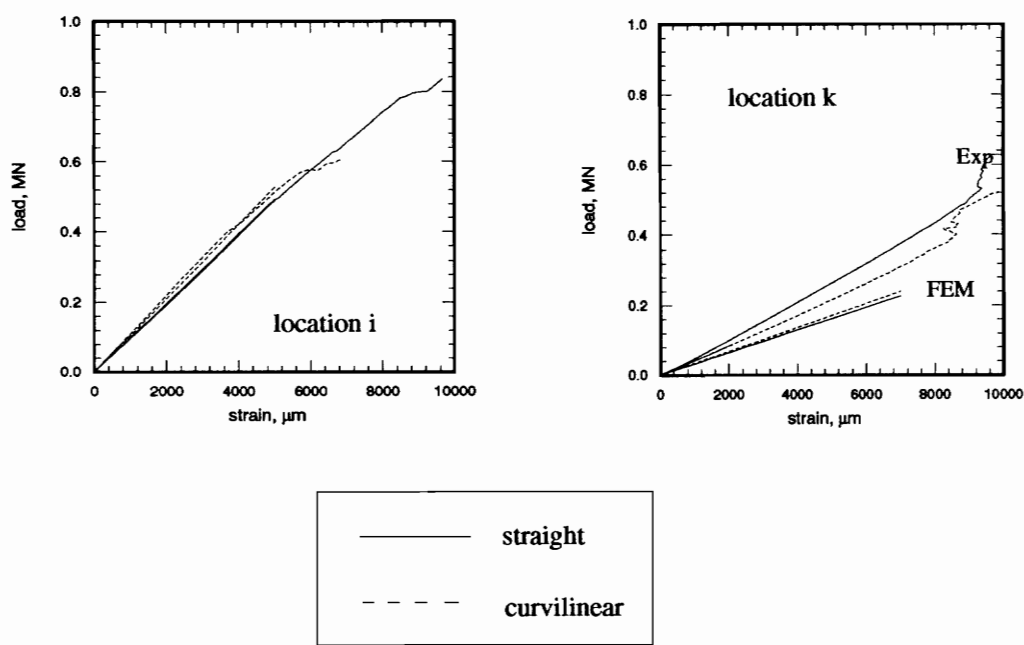


Figure 5.4: Results obtained at the strain gage locations considering concentrated loads

Upper part of the plate: gages ‘m’, ‘o’, ‘a’, and ‘c’

For the upper part of the plate, the results obtained by considering a uniform load seemed to match somewhat better the experimental data. For both the loading cases, the strains obtained from the straight fiber plate at location ‘c’ and ‘o’ were less than the finite element predictions, while they corresponded fairly well for the curvilinear fiber plate. For the straight fiber plate there was a maximum of 43% difference in the slope between the experimental data and the finite element predictions at location ‘o’ with concentrated loads. At location ‘m’ the experimental data corresponded fairly well for the uniform load case. On the other hand, for concentrated loads, the experimental strains were higher than the finite element predictions at location ‘m’, i.e., there was a 21% difference in slope for the straight fiber plate and a 35% difference in slope for the curvilinear fiber plate. At the location ‘a’, for both loading cases the finite element analyses agreed almost perfectly with the experimental data for the straight fiber plate, and are fairly close for the curvilinear plate.

Net-section: gages ‘e’, ‘g’, ‘i’ and ‘k’

In general, the strains measured during testing and the strains computed with the finite element analyses agreed within a 3% tolerance at the net section for gages ‘e’, ‘g’, and ‘i’. On the other hand there was a noticeable difference between the finite element predictions and the experimental results at location ‘k’. Location ‘k’ was at the hole edge and slight misalignment of the gages, or imperfections in the edge of the laminate from cutting the hole, could impact gage response.

Closure

In general, the strains measured during the testing agreed reasonably well with the strains computed from the finite element analyses. The loading mode (concentrated loads or uniform load) did not seem to have an important effect on the strain field.

5.4 Failure analysis of tensile specimens

The straight fiber plate failed at a load of 0.836 MN and the curvilinear fiber plate failed at 0.609 MN. This represents a 37% difference. The failed specimens are shown in ref. [7] and in figure 4.1. The plate using the curvilinear fiber format failed at the net section. During the loading, very sharp noises emanated from this specimen. The straight fiber plate also failed at the net section, but only on the right side. On the left side, there was failure at the doublers or within the doublers. The goal of this section is to study the failure modes of the two plates based on the finite element results. These failure modes are compared with the experimental failure modes.

Many failure criteria for fiber-reinforced composites have been developed within the last ten years. The most frequently used ones are the maximum stress, maximum strain, Tsai-Hill, Tsai-Wu, and Hashin-Rotem criteria. All these criteria use quantities computed at the ply level.

The program FEM2D computed all the strains at the integration points in the global coordinate system. However, only the value computed at the fifth integration point, the center one, was considered for this failure analysis. A FORTRAN program was developed to estimate the ultimate failure load of the plates manufactured by Cincinnati Milacron. This program had three main objectives: first, to compute the stresses at the ply level; second, to apply different failure criteria, and finally; to classify the failures by ranking the load level required to produce them.

5.4.1 Stress Computation

The middle surface strains were obtained from FEM2D. Because the middle surface curvatures were equal to zero for the test in tension, the middle surface strains at the plate level were equal to the strains in each ply in the global coordinate system. Let σ_x , σ_y , τ_{xy} , ϵ_x , ϵ_y , and γ_{xy} be the values of the stress and strain fields within an element. The quantities σ_1 , σ_2 , τ_{12} , ϵ_1 , ϵ_2 , and γ_{12} denote the stresses and strains at the ply level in the

principal material coordinate system. The ply angle is denoted by θ . The transformation matrix is T and R is an intermediate matrix to pass from the tensor shear strain to the engineering shear strain. In order to compute the stresses or the strains in the principal material coordinate system, the following transformations have to be carried out:

$$\begin{bmatrix} T \end{bmatrix} = \begin{bmatrix} \cos^2 \theta & \sin^2 \theta & -2 \sin \theta \cos \theta \\ \sin^2 \theta & \cos^2 \theta & 2 \sin \theta \cos \theta \\ \sin \theta \cos \theta & -\sin \theta \cos \theta & \cos^2 \theta - \sin^2 \theta \end{bmatrix} \quad (5.4)$$

$$\begin{bmatrix} R \end{bmatrix} = \begin{bmatrix} 1 & 0 & 0 \\ 0 & 1 & 0 \\ 0 & 0 & 2 \end{bmatrix} \quad (5.5)$$

$$\begin{pmatrix} \epsilon_x \\ \epsilon_y \\ \epsilon_{xy} \end{pmatrix} = \begin{bmatrix} 1 & 0 & 0 \\ 0 & 1 & 0 \\ 0 & 0 & 0.5 \end{bmatrix} \times \begin{pmatrix} \epsilon_x \\ \epsilon_y \\ \gamma_{xy} \end{pmatrix} \quad (5.6)$$

$$\begin{pmatrix} \epsilon_1 \\ \epsilon_2 \\ \epsilon_{12} \end{pmatrix} = \begin{bmatrix} T \end{bmatrix} \times \begin{pmatrix} \epsilon_x \\ \epsilon_y \\ \epsilon_{xy} \end{pmatrix} \quad (5.7)$$

$$\begin{pmatrix} \epsilon_1 \\ \epsilon_2 \\ \gamma_{12} \end{pmatrix} = \begin{bmatrix} R \end{bmatrix} \times \begin{pmatrix} \epsilon_1 \\ \epsilon_2 \\ \epsilon_{12} \end{pmatrix} \quad (5.8)$$

$$\begin{pmatrix} \sigma_1 \\ \sigma_2 \\ \tau_{12} \end{pmatrix} = \begin{bmatrix} Q_{11} & Q_{12} & 0 \\ Q_{12} & Q_{22} & 0 \\ 0 & 0 & Q_{66} \end{bmatrix} \times \begin{pmatrix} \epsilon_1 \\ \epsilon_2 \\ \gamma_{12} \end{pmatrix}, \quad (5.9)$$

where Q denotes the reduced stiffness matrix.

5.4.2 Failure criteria

The usual failure criteria either assume no stress interaction (maximum stress, maximum strain) or full stress interaction (Tsai-Hill, Tsai-Wu, Hashin-Rotem) [18, 19]. The following section presents briefly the different failure criteria used in this study. The criteria selected were the maximum stress and the maximum strain criteria from the no interaction criteria group, and the Tsai-Hill criterion from the interactive criteria group. According to the literature, they are the most generalized and representative from their group.

As was seen in Chapter 4, the mechanical characteristics of the material used to manufacture the plates were not well known. All the failure criteria defined in this section use strengths at the ply level, i.e., in the fiber and matrix directions. In the present case, the strengths were defined considering values for usual graphite-epoxy material and extrapolating these data in the context of the experimental results obtained in Chapter 4. Because of the lack of precise data for the strengths, the goal of the following paragraphs is not to precisely predict the failure loads of the specimens, but rather to compare the performances in tension of the curvilinear plate with the performances in tension of its straight fiber counterpart. All the failure loads are compared to the load for which the first fiber failure occurs in the straight fiber plate. This investigation was achieved by considering both a uniform load at the end of the plate and then considering concentrated loads. No important difference between the two cases were detected. Hence, only the results computed with a uniform load will be presented.

Maximum stress criterion

According to the maximum stress criterion, failure occurred when the stresses in the principal material directions reached their individual failure levels. That is, when either

$$\frac{\sigma_1}{X} = 1 \Rightarrow \text{fiber failure}$$

or

$$\frac{\sigma_2}{Y} = 1 \Rightarrow \text{matrix failure}$$

or

$\frac{\tau_{12}}{S} = 1 \Rightarrow$ shear failure.

The tensile and compressive strengths, X, Y, and S, have to be chosen based on the sign of the local stresses. It is usual to consider that the structure failed at the first fiber failure. Call F_1 the load when the first fiber failure occurred in the straight fiber plate and express other results in terms of F1. The failure scenario based on the maximum stress criterion is shown in Tables 5.2-5.5.

Table 5.2: Fiber failure for the straight fiber plate: maximum stress criterion

Rank	Location (see fig. 5.5)	Ply	Failure load
1	16	0°	F_1
2	13	−45°	$1.076 F_1$
3	14	−45°	$1.097 F_1$

Table 5.3: Matrix failure for the straight fiber plate: maximum stress criterion

Rank	Location (see fig. 5.5)	Ply	Failure load
1	16	90°	$0.433 F_1$
2	15	90°	$0.472 F_1$
3	14	0°	$0.480 F_1$

Table 5.4: Fiber failure for the curvilinear fiber plate: maximum stress criterion

Rank	Location (see fig. 5.5)	Ply	Failure load
1	16	0°	$1.055 F_1$
2	16	C	$1.055 F_1$
3	15	C	$1.143 F_1$

Table 5.5: Matrix failure for the curvilinear fiber plate: maximum stress criterion

Rank	Location (see fig. 5.5)	Ply	Failure load
1	16	90°	0.457 F_1
2	15	90°	0.503 F_1
3	14	0°	0.563 F_1

Maximum strain criterion

According to the maximum strain criterion, failure occurred when the strains in the principal material directions reached their individual failure levels. That is, when either

$$\frac{\epsilon_1}{X_c} = 1 \Rightarrow \text{fiber failure}$$

or

$$\frac{\epsilon_2}{Y_c} = 1 \Rightarrow \text{matrix failure}$$

or

$$\frac{\gamma_{12}}{S_c} = 1 \Rightarrow \text{shear failure.}$$

Tensile or compressive maximum strains, X_c , Y_c , and S_c , have to be chosen on the basis of the sign of the local strains. Call F_2 the load when the first fiber failure occurred in the straight fiber plate and express other results in terms of F_2 . The failure scenario based on the maximum strain criterion is shown in Tables 5.6-5.9.

Table 5.6: Fiber failure for the straight fiber plate: maximum strain criterion

Rank	Location (see fig. 5.5)	Ply	Failure load
1	16	0°	F_2
2	13	-45°	1.069 F_2
3	14	-45°	1.095 F_2

Table 5.7: Matrix failure for the straight fiber plate: maximum strain criterion

Rank	Location (see fig. 5.5)	Ply	Failure load
1	16	90°	$0.560 F_2$
2	13	0°	$0.618 F_2$
3	14	0°	$0.636 F_2$

Table 5.8: Fiber failure for the curvilinear fiber plate: maximum strain criterion

Rank	Location (see fig. 5.5)	Ply	Failure load
1	16	0°	$1.051 F_2$
2	16	C	$1.051 F_2$
3	15	C	$1.076 F_2$

Discussion

As can be seen by an examination of Tables 5.2-5.9, in general, application of the maximum stress and maximum strain criteria gave similar results. In both cases, the first fiber breakage was predicted to occur at the net section in the 0° , and the 0° and curvilinear plies for plates with straight and curvilinear fibers, respectively. The ranking of the failures was the same for both the failure criteria. For the straight fiber plate, first fiber failure was predicted to occur in element 16 at the net section. It was followed by a failure in the -45° plies in elements 13 and 14. For the curvilinear fiber plate, the first fiber failure appeared at the element 16 in the 0° and C plies. This was followed by a fiber failure in the element directly next to it, element 15, in the same plies.

For both the straight and curvilinear fiber plates, matrix failure initiated at about half the failure load and at the net section, i.e., for the elements 16 and 15 in the 90° plies, and for elements 14 and 13 in the -45° plies.

By considering that failure occurs at the first fiber breakage, both the maximum stress

Table 5.9: Matrix failure for the curvilinear fiber plate: maximum strain criterion

Rank	Location (see fig. 5.5)	Ply	Failure load
1	16	90°	0.601 F_2
2	15	90°	0.680 F_2
3	14	0°	0.691 F_2

and the maximum strain criteria showed that the failure load of the curvilinear fiber plate should have been 5 to 6% higher than the failure load of its straight fiber counterpart. The predictions contradicted the experimental results presented in [7].

Tsai-Hill criterion

The various interactive criteria predict failure should have occurred when a polynomial function involving stresses (or strains) and strengths (or maximum strains) was satisfied [17]. The Tsai-Hill criterion can be derived from considering the von Mises criterion for metals. The Tsai-Hill criterion polynomial is as follows:

$$\left(\frac{\sigma_1}{X}\right)^2 + \left(\frac{\sigma_2}{Y}\right)^2 + \left(\frac{\sigma_1}{X}\right) \times \left(\frac{\sigma_2}{X}\right) + \left(\frac{\tau_{12}}{S}\right)^2 = 1. \quad (5.10)$$

Because of the interaction between X, Y, S, the Tsai-Hill criteria can give results close to experiments. Nevertheless, for several layups, it was shown [18] that the criterion not only can underestimate the ultimate laminate failure, but it may not correctly predict the trend of the data. Tables 5.10 and 5.11 present the results from the failure analysis using the Tsai-Hill criterion. The failure load for the straight fiber is case denoted as F. All other failure results are interpreted in terms of F.

Table 5.10: Failure of the straight fiber plate using Tsai-Hill failure criterion

Rank	Location (see fig. 5.5)	Ply	Failure load
1	14	0°	F
2	13	0°	1.010 F
3	17	0°	1.105 F

Table 5.11: Failure of the curvilinear fiber plate using Tsai-Hill failure criterion

Rank	Location (see fig. 5.5)	Ply	Failure load
1	14	0°	1.130 F
2	13	C	1.138 F
3	17	C	1.201 F

Discussion

As can be seen by inspection of Tables 5.10 and 5.11, the failure locations were predicted to be the same for both the curvilinear and the straight fiber plates. Both the plates failed at the element 14 in the 0° plies. Nevertheless, the failure load of the curvilinear plate was 13% higher than the failure load of the straight fiber plate. The difference between the Tsai-Hill criterion predictions and the experimental results are very important. Possible explanations are provided in the next sections.

5.5 Investigation into failure resulting from possible manufacturing features

The failure analysis presented in the previous section predicted that the failure load for the curvilinear fiber plate should have been slightly higher than the failure load of its straight fiber counterpart. According to [7], the curvilinear plate failed at a load 37% lower than the

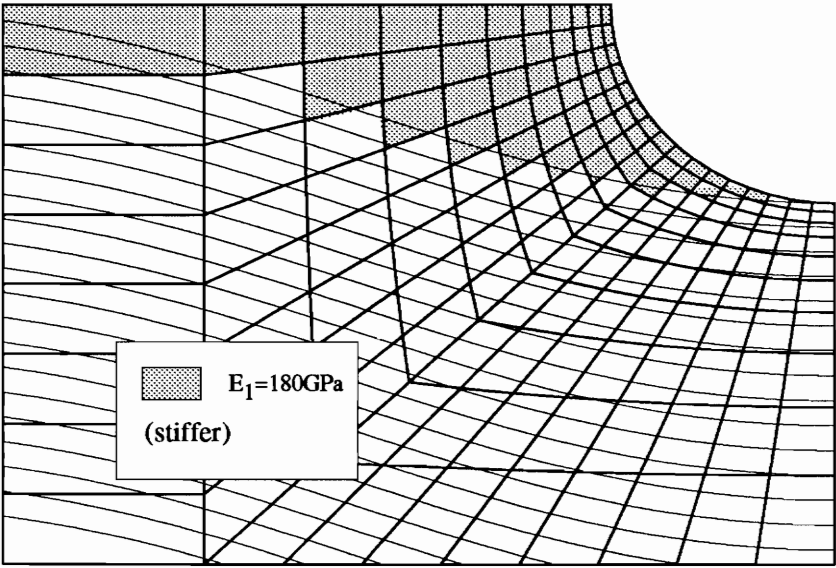
failure load of the straight fiber plate. This difference motivated an investigation regarding possible geometric and/or material characteristics in some regions of the curvilinear plate.

Cincinnati Milacron used a special-purpose path generation program to steer the tows in curvilinear trajectories. Limitations of this special-purpose program allowed only courses that extended from one end of the plate to the other to be laid by machine. The curvilinear courses that did not extend the entire length of the plate were filled in by hand. Laying down the fibers by hand may have affected the material characteristics the curvilinear plies. This is discussed below.

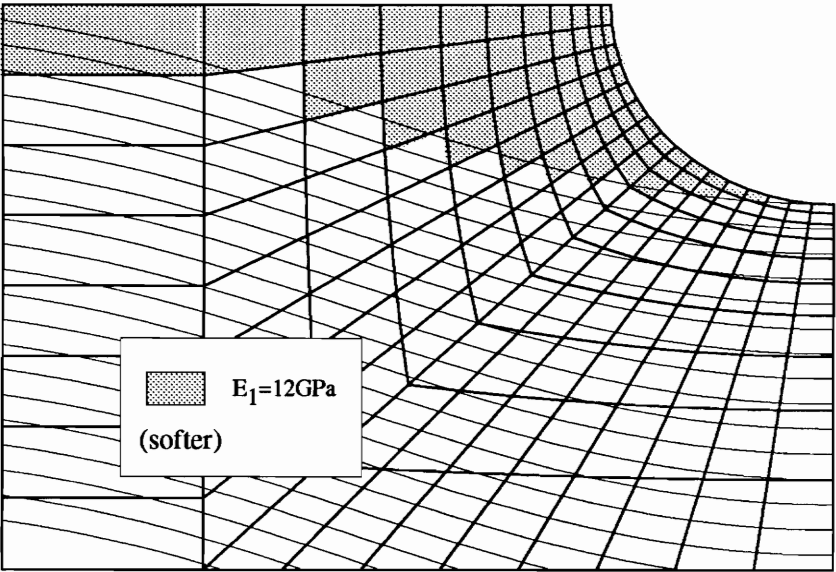
Four different test cases were analyzed by either softening or stiffening the material in the region laid down by hand. The material properties were changed for the elements highlighted in figs. 5.6 and 5.7. The remaining part of the plate retained the material properties defined in Chapter 4, and only the curvilinear plies were affected by these changes. In all four cases, a uniform load was considered at the end of the plate. This assumption seemed to be reasonable in light of the results provided by the strain gages in section 5.3. The failure loads for these modified curvilinear fiber plates were compared to the failure loads for the baseline curvilinear fiber plate.

Case 1: Results obtained by stiffening the material

The material laid down by hand might have had a fiber volume fraction higher than the material laid down using the fiber placement machine. To represent this, Young's modulus in the fiber direction of $E_1 = 180\text{GPa}$ was assigned to the elements highlighted in figure 5.6(a). The other engineering constants in the highlighted area, E_2 , ν_{12} and G_{12} , were not changed. According to the maximum stress and maximum strain criteria, this design would have failed at element 16 (see figure 5.5) in the 0° and C plies. The fiber angle in the C plies was equal to 0° for this element. The failure load for case 1 was only 2% lower than the failure load of the straight fiber plate and 7% lower than the failure load of the curvilinear plate with no material property changes. Thus having a stiffer material in the region laid down by hand would not have seriously influence the failure loads.



(a)



(b)

Figure 5.6: Possible manufacturing features: Cases 1 and 2

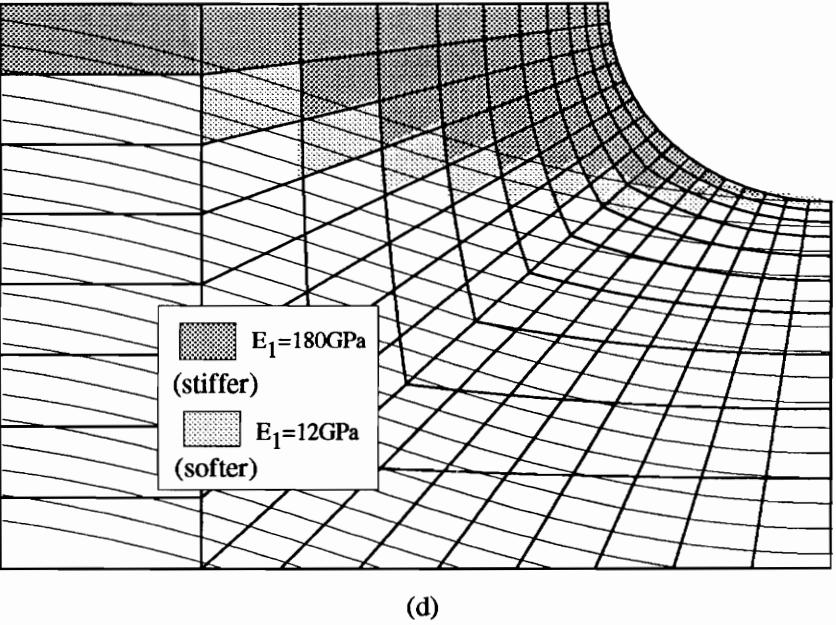
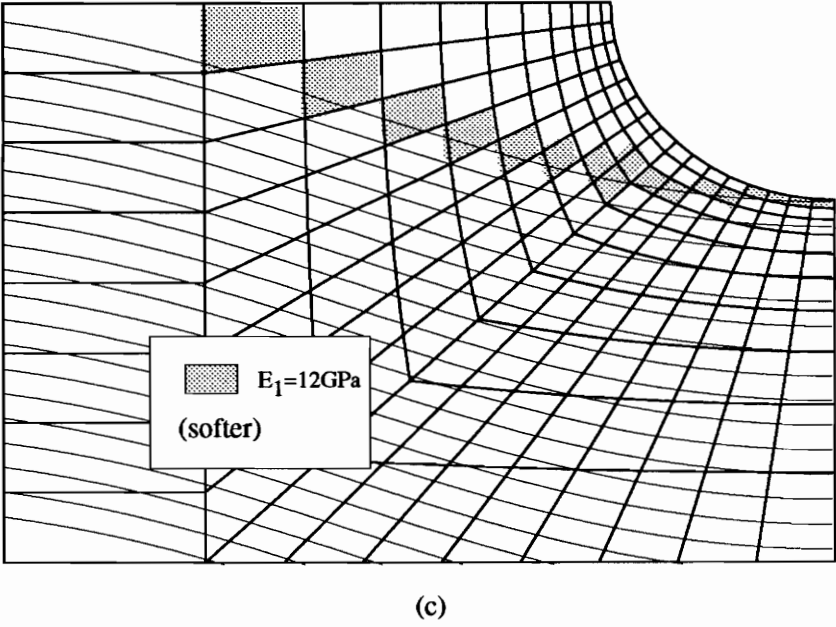


Figure 5.7: Possible manufacturing features: Cases 3 and 4

Case 2: Results obtained by softening the material

An extreme case was considered by setting the Young's modulus in the fiber direction equal to the Young's modulus in the matrix direction, i.e., $E_1 = E_2$, for all the elements highlighted in figure 5.6(b). The maximum stress and maximum strain criteria both predicted the first fiber failure to have occurred at element 14 (see figure 5.5) in the 0° plies. This failure mode was predictable. Element 14 was the element closest to the net section in which the material properties were changed. The fiber angle in the C plies in this element was close to 0° . By weakening the C plies in the element, more load had to be carried by the 0° plies. According to the maximum stress and maximum strain criteria, this design should have failed at the same failure load as the plate using the straight fibers. Lowering the fiber modulus in the area where material was laid down by hand decreased the strength in tension of the curvilinear plate by 5%.

Case 3: Gap between the material laid down by hand and the material placed with the fiber placement machine

This third case studies the effect of a bad transition between the curvilinear plies laid down by hand and the curvilinear plies laid down with the fiber placement machine. During manufacturing resin would possibly fill any gap between these two areas. Therefore, the material properties of the elements highlighted in figure 5.7(c) were changed. Young's modulus in the fiber direction was set up equal to 12GPa. This change didn't appreciably influence the predicted failure load of the plate. According to the maximum stress and maximum strain criteria, such a plate would fail exactly at the net section at element 16 in the 0° and C plies. The failure load of this design would have been slightly higher than the predicted failure load of the straight fiber plate and 3% lower than the predicted failure load of the baseline curvilinear fiber plate.

Case 4: Combination of cases 3 and 1

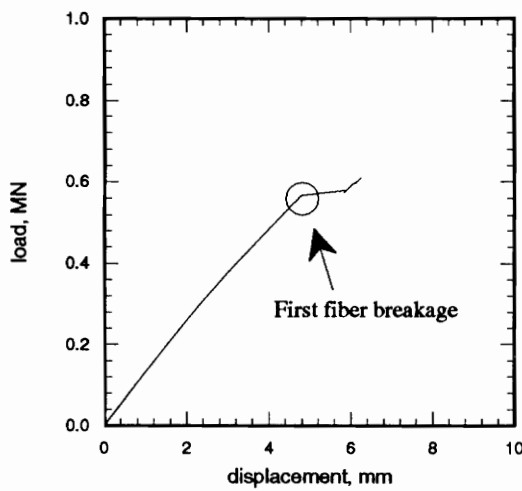
The design presented in figure 5.7(d) was a combination of figures 5.7(a) and 5.7(c). Young's modulus in the fiber direction was increased in the area where material was laid down by hand, and decreased for the elements situated at the transition between the two areas. According to the maximum stress and maximum strain criteria, this design was predicted to fail at the net section in the softer elements in the 0° plies. The failure load was estimated to be 8% lower than the failure load of the straight fiber plate and 13% lower than the failure load of the baseline curvilinear fiber plate. Thus, this last design seemed to be the most critical. However, the 13% reduced load is a factor of three less than the observed 37% reduced load.

Closure

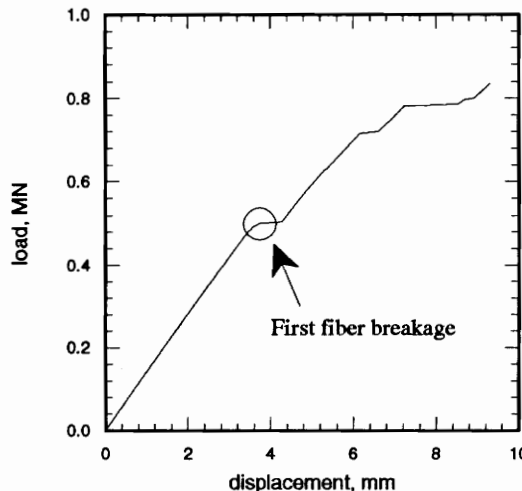
None of the four cases considered could reasonably be a candidate to explain the 37% difference between the experimental failure load of the straight fiber plate and the failure load of the curvilinear fiber plate. Other possibilities had to be sought.

5.6 Validity of the failure analysis: Another interpretation of results

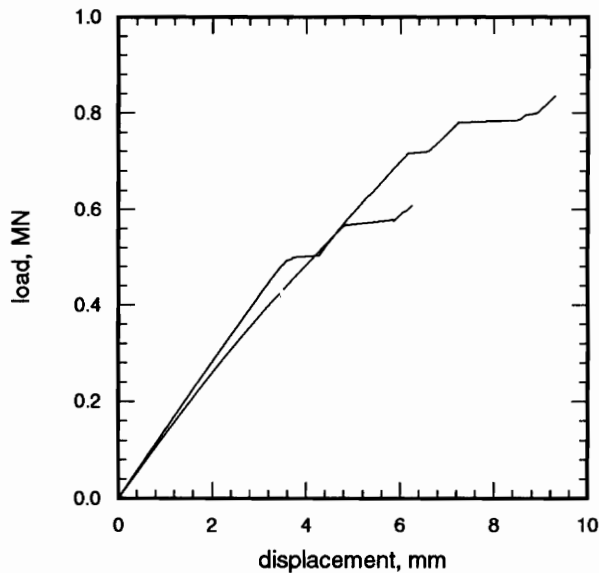
The failure analyses presented in the previous section which showed that the strengths in tension should have been 5% to 13% higher for the curvilinear fiber specimen than the straight fiber specimen contradicts the 37% lower value observed in the experiments. In addition, the various possible manufacturing features did not explain the difference. The difference may be explained by considering the experimental load vs. axial displacement characteristics for the two specimens shown in figure 5.8. It must be noted that the displacement shown in figure 5.8 was the motion between the upper and the lower heads of the load frame. The order of the two curves were inverted by mistake in [7]. Actually the straight fiber specimen



(a)- Curvilinear fiber plate



(b)- Straight fiber plate



(c)- Both plates

Figure 5.8: Load vs. axial displacement characteristic during tensile testing of curvilinear and straight fiber plates

was slightly stiffer than the curvilinear fiber specimen. This remark confirm the conclusions drawn in Chapter 3.

As can be seen in figure 5.8(a), the load vs. axial displacement relation for the curvilinear fiber plate followed a linear path until reaching the first fiber breakage. This occurred at a load of 0.56 MN. Final failure almost immediately followed the first fiber breakage. The final load of the curvilinear fiber plate was estimated to be 0.609 MN in [7]. The first part of the relation presented in figure 5.8(b) looks very much like the load vs. axial displacement relation of the curvilinear fiber plate. It begins with a linear part until it reaches what is probably the first fiber breakage, occurring at 0.51 MN. Contrary to what happened to the curvilinear fiber plate, this first fiber breakage wasn't followed immediately by a total failure. The straight fiber plate kept on sustaining more load. Several hypotheses can be given. First, all the 10 0° plies may not have failed at the same time at the net section. Second, the propagation of the failure or crack may have been more difficult in the straight fiber plate than in the curvilinear plate. More plausible, an unexpected parameter appeared during the testing. The straight fiber plate didn't fail in a classic failure mode. As can be seen in figure 4.1, the straight fiber plate failed at the net section but only at the right side. On the left side there was failure at the doublers. Thus, it may be assumed that the boundary conditions in the gripping area changed during the testing.

By considering a first fiber breakage at a load of 0.51 MN for the straight fiber plate, the experimental results and the failure predictions presented in section 5.4 coincide. Indeed, with this assumption, the first fiber breakage load of the curvilinear plate was 11% higher than the first fiber breakage load of the straight fiber plate during the testing. This difference is close to the predictions given by maximum stress, maximum strain, and Tsai-Hill criteria.

5.7 Improved plate

Neither Hyer and Charette [1-4] nor Charette [5] studied a plate with exactly the same geometry and stacking sequence as the plate manufactured for testing. The goal of this

section is to estimate the ultimate tension load from plates designed by using a scheme similar to the one developed in refs. [1-5] and compare the improved design with the plates manufactured by Cincinnati Milacron. The FORTRAN program written to compute the fiber path was based on FEM2D but with several modifications and added subroutines.

As stated in the literature review, the basic idea developed by Hyer and Charette [1-4] and Charette [5] was to orient the curvilinear fibers in the principal stress directions. In the case of an isotropic material, the material properties, geometry, and the load features determine the principal stress directions. In a laminate the principal stress directions will vary from ply to ply. An iteration process was developed to compute the principal stresses within the group of plies containing curvilinear fibers and to align the fiber trajectory of the plies with the principal stress directions. The plies which used the straight fibers with a constant fiber angle were not subject to any fiber realignment. As mentioned previously, the 0° direction was fixed along the x axis.

Due to the use of a finite element analysis, two approximations were made. As mentioned previously, the fiber path within an element was approximated as a straight line rotated by an angle θ with respect to the x axis. Second, the midplane strains used to determine the principal stresses and principal stress directions were computed at the centroid of the element, i.e., the fifth integration point of the element (see figure 3.2). This location represents an average value within the element. The program FEM2D was modified and used as a subroutine such that only this centroidal value was computed. The entire program used to compute the new fiber angle is shown in Appendix A.

The iteration scheme can be described following a number of steps contained in a loop:

1. A data file was needed to initiate the first iteration. This file was part of an ABAQUS input file created after pre-processing. It contained the nodal coordinates for the mesh, the loading features, and the connectivity matrix. In the main program, an initial value for the fiber angle in the curvilinear plies was assigned to each element. The values of the initial

angle had a slight influence the final plate design. Specifically, the number of iterations necessary to align the fibers with the principal stresses within a certain tolerance was affected.

2. At this point, the main program called the subroutine PRG. This subroutine created an input file readable by FEM2D using the above mentioned data files. The main part of this subroutine was devoted to the computation of the $[A]$ matrix of each element. All the subroutines called by PRG were computational subroutines.

3. The iteration process continued by calling the subroutine containing the finite element processor. This subroutine was actually FEM2D. The data file created by PRG constitutes its input file. The finite element program computed the midplane strains

$$\begin{pmatrix} \epsilon_x^0 \\ \epsilon_y^0 \\ \gamma_{xy}^0 \end{pmatrix}$$

for each element of the mesh at the fifth integration point. Since, the midplane curvatures are equal to zero, the relation for each ply was

$$\begin{pmatrix} \epsilon_x \\ \epsilon_y \\ \gamma_{xy} \end{pmatrix} = \begin{pmatrix} \epsilon_x^0 \\ \epsilon_y^0 \\ \gamma_{xy}^0 \end{pmatrix} + z \times \begin{pmatrix} \kappa_x \\ \kappa_y \\ \kappa_{xy} \end{pmatrix} \quad (5.11)$$

$$\begin{pmatrix} \epsilon_x \\ \epsilon_y \\ \gamma_{xy} \end{pmatrix} = \begin{pmatrix} \epsilon_x^0 \\ \epsilon_y^0 \\ \gamma_{xy}^0 \end{pmatrix}. \quad (5.12)$$

4. Having the values of the laminate strains from the previous step for the fifth Gauss point of each element, the stresses in each ply would be obtained by multiplying the strain vector by the reduced stiffness matrix. These computations were performed only for the curvilinear plies. The plies using the straight fibers were not involved. The principal stress

direction for the curvilinear plies in each element were computed using the equation :

$$\theta = \frac{1}{2} \tan^{-1} \left(\frac{2\tau_{xy}}{\sigma_x - \sigma_y} \right), \quad (5.13)$$

where the principal direction is denoted by θ , and σ_x , σ_y , and τ_{xy} are the stresses within the ply in the $x - y$ coordinate system.

5. At this stage the first iteration was finished. For each element the principal stress direction was compared to the fiber angle. The process was considered to have converged when 190 elements out of 200 exhibited a difference of less than 0.5° between the principal stress direction and the fiber angle. If this requirement was not fulfilled, the element fiber angle was replaced by the principal stress direction. A new cycle of the iteration procedure then began by computing new $[A]$ matrices taking in consideration the new fiber angles in the curvilinear plies. Once 190 elements converged to within the tolerance, the iteration scheme stopped and created an output file containing the final angles and the number of iterations required to reach this results. Figure 5.9, summarizes the main stages of the iteration scheme.

5.7.1 Results

In practice, convergence was realized in 6 to 10 iterations. The fiber angles obtained for each element are presented in figures 5.10 and 5.11. It is interesting to compare the design presented in figures 5.10 and 5.11 with the design proposed by Hyer and Charette [1-4] and Charette [5] shown in figure 2.3. As mentioned in Chapter 2, Hyer and Charette [1-5] and Charette [5] never studied a plate with the exact same geometry and stacking sequence, i.e., $(\pm 45/C_2/0/90/C_2)_s$, as the plates tested. Nevertheless the fiber trajectories presented in figures 5.10 and 5.11 and the fiber trajectories presented in figure 2.3 are similar. The fiber trajectory of the improved plate presented in figures 5.10 and 5.11 and the fiber trajectory considered by Cincinatti Milacron in figure 2.8 differ mainly in the area denoted as 'A' in figures 5.10 and 5.11. Instead of having a negative angle and going away from the hole, the

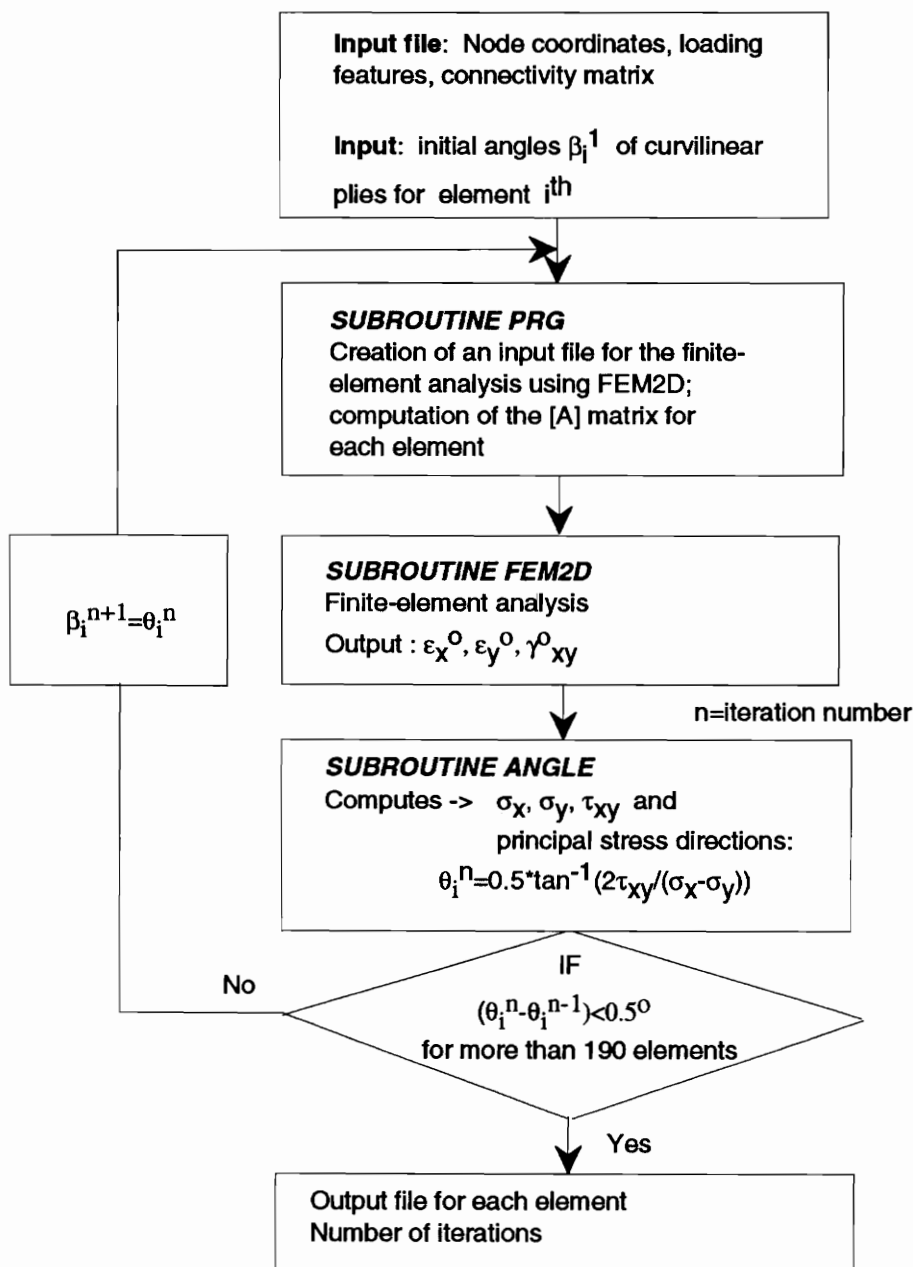


Figure 5.9: Iteration algorithm for improved plate design

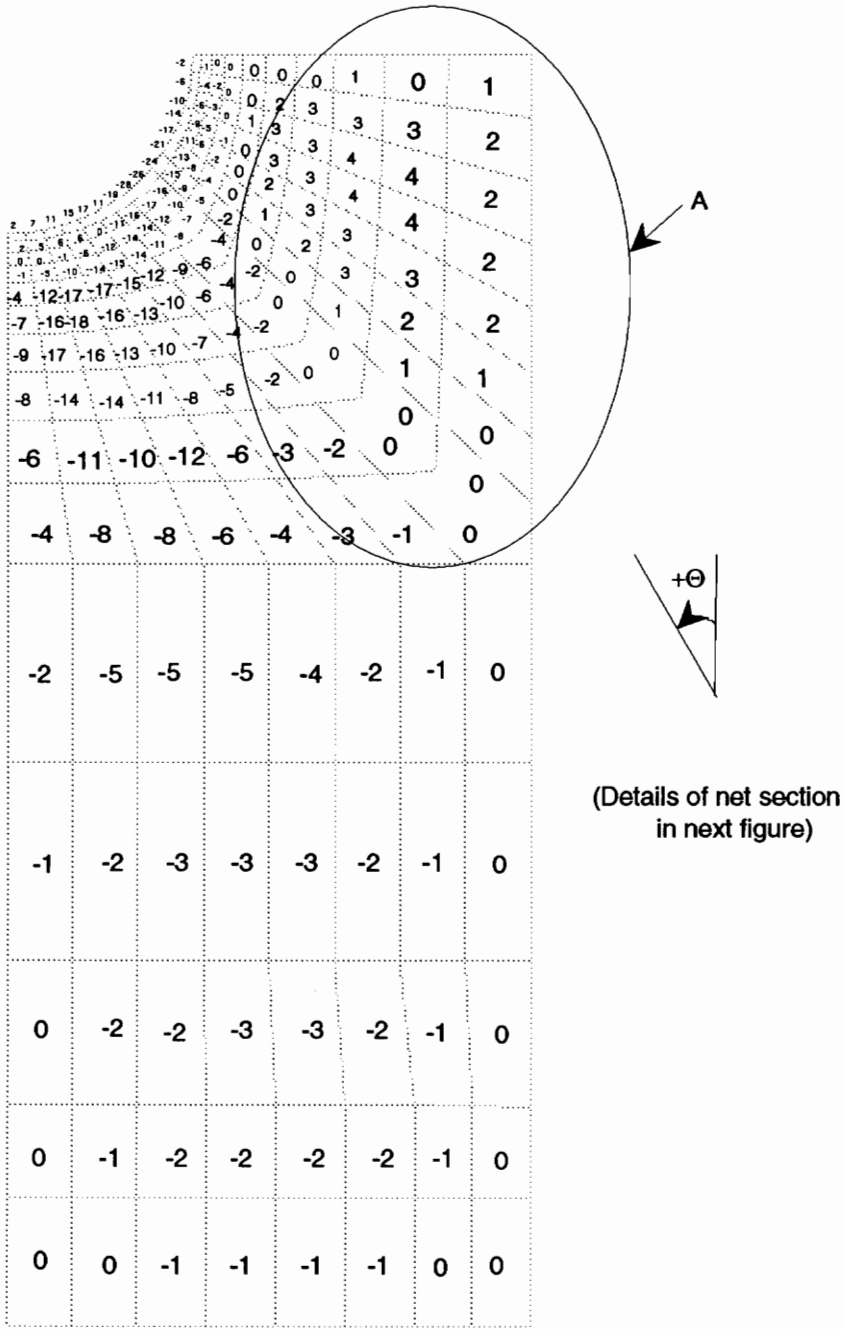


Figure 5.10: Fiber angles for improved plate design

Table 5.12: Failure load of the improved plate

	Failure load max. stress	Failure load max. strain
Straightline fiber ($\pm 45/0_3/90/0_2$) _s	1.00	1.00
Improved plate ($\pm 45/C_2/0/90/C_2$) _s	1.17	1.16

fibers in the upper part ‘A’ have a positive fiber angle and tend to go towards the hole. The fiber trajectories in the gripping area, and near to it, are very similar to the design used to manufacture the plates. By comparing the trajectories in figures 2.3 and 5.11, the conclusion can be drawn that the fiber path computed with the iteration scheme described previously does not strongly depend on the plate geometry and the stacking sequence.

References [4] and [5] showed that when considering a plate with a hole and curvilinear fiber trajectories loaded in tension, the stacking sequence is one of the most important parameters for the strength of the plate. To evaluate the strength of this improved plate design, two failure criteria were considered: the maximum stress criterion and the maximum strain criterion. To provide a basis for comparison, the failure load computed for the improved plate presented in figures 5.10 and 5.11 was normalized by the failure load obtained in the previous section for the plate using straight fibers, i.e., ($\pm 45/0_3/90/0_2$)_s. The results of the comparison are presented in Table 5.12. The failure load of the improved plate was 1.16 times higher than the failure load of its straight fiber counterpart. The results provided by the maximum stress criterion and the maximum strain criterion coincide. The contribution of the curvilinear fiber format may seem less important than expected compared to some designs presented in Chapter 2 which showed a 200% improvement with respect to their quasi-isotropic baseline. However, cases presented in [1-5] with stacking sequences having the same proportions of curvilinear plies as the manufactured plates, i.e., 50%, had results very similar to Table 5.12.

5.7.2 Closure

The scheme considered to improve the fiber trajectory by aligning the curvilinear fibers with the principal stress directions within a finite element treated individual element level angles as design variables. The difficulties of that approach included dependency of the number of design variables on mesh density and most of all, the lack of fiber continuity across the finite elements interfaces. Because of the lack of fiber continuity, the design presented in figures 5.10 and 5.11 would have to be modified to be manufacturable. These modifications would most probably lower performance in tension, performance which is already only 16% better than its straight fiber counterpart. Therefore the most efficient designs manufacturable with a fiber placement utilizing the stacking sequence used by Cincinnati Milacron should have performances very similar to plates using the straight fiber format.

The next chapter focuses on the compression test of the plates. As the plates were loaded past their buckling load, postbuckling response dominated.

Chapter 6

Compression tests

Buckling and postbuckling analyses were performed to compare the results obtained during the experiments and the results provided by finite element modeling. In a manner similar to the analyses for the tension tests, these analyses can be broken down into preprocessing, processing and post-processing steps. Preprocessing again includes definition of geometry, loading, boundary conditions, and material property considerations. The latter involves definition of the fiber paths. Processing involves the computation of the buckling load and the study of the postbuckling behavior for the curvilinear and the straight fiber plates. Postbuckling includes the visualization of the results using PATRAN, and a comparison with the experimental data.

6.1 Preprocessing

As for the tension test, PATRAN [8] was used as a pre- and postprocessor for the finite element analysis. ABAQUS [9, 10] was used as a processor.

6.1.1 Geometry of the plate used in compression

Buckling analyses were performed on both the plate using curvilinear fibers and on its straight fiber counterpart. For compression testing, the specimens were trimmed to be

square, specifically 0.43 meter square. The length of these shorter compression specimens are shown by the dashed lines in figure 2.9. The mesh used for the finite element analyses is presented in figure 6.1 . Because of symmetry, only a quarter of the plate was modeled. As for the model tested in tension, the mesh was refined in the hole area to take into consideration the stress concentration due to the hole. The model contains 160 elements. The element used is a 8-node shell element with reduced integration.

6.1.2 Fiber angles

The stacking sequence of the curvilinear plate was $(\pm 45/C_2/0/90/C_2)_s$, where the C denotes plies with the curvilinear trajectories. The 0° direction was along the x axis. The stacking sequence of the baseline straight fiber plate was $(\pm 45/0_3/90/0_2)_s$. The fiber path presented in figure 2.8 was also valid for the curvilinear plate tested in compression. Hence all the computations performed in chapter 3 in the hole area for the plates tested in tension were applied the compression problem.

6.1.3 Loading

During the tests performed at the NASA Langley Research Center, the compression specimens were loaded by placing the specimen vertically in the load frame and displacing the top edge downward a known amount with the upper head of the load frame. The opposite edge rested on the lower stationary head of the load frame. These loading features were imposed in ABAQUS by mean of constraint equations [9, 10]. A node set was created which contained all the nodes located along the loaded edge. A multipoint constraint equation was defined which imposed the same displacement in the loading direction (i.e., x direction) to all the nodes contained in this node set. Then a concentrated load was applied to one of these nodes. Because of the constraint equation, this concentrated load was equivalent to a uniform displacement of the loaded edge.

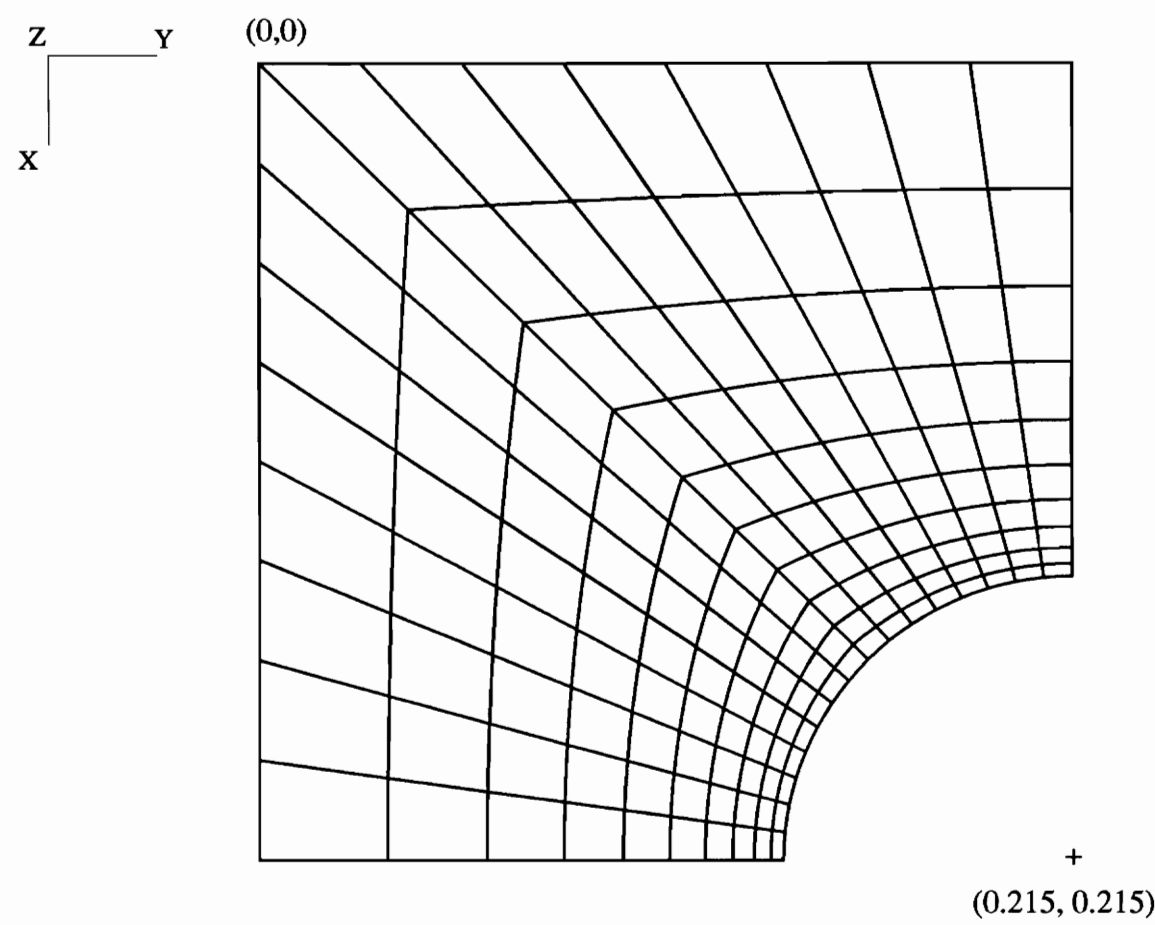


Figure 6.1: Finite element mesh used to model the compression test

6.1.4 Boundary conditions

The top and bottom edges (see figure 2.9) where the load was applied were clamped. The left and right vertical edges of the specimens were simply supported with knife edges running parallel to the loading direction. Note: The origin of the global coordinate system was located at the upper left corner of the model (see figures 6.1 and 6.2). The coordinates of the center of the hole were (0.215m, 0.215m).

The boundary conditions imposed in PATRAN were :

1. Symmetry about $x=0.215\text{m}$. This required $u_x = \Phi_y = \Phi_z = 0$ on that edge of the mesh.
2. Symmetry about $y=0.215\text{m}$. This required $u_y = \Phi_x = \Phi_z = 0$ on that edge of the mesh.
3. Simple supports on the edge $y=0$. This required $u_z = \Phi_y = 0$ on that edge of the mesh.
4. Clamped supports on the edge $x=0$. This required $u_z = \Phi_x = \Phi_y = 0$ on that edge of the mesh.

In the above Φ_x , Φ_y , and Φ_z represents the rotations around the x axis, y axis, and z axis, respectively. Some of the above boundary conditions are irrelevant if one is seeking an analytical solution of this problem. Because of the discretization of the model into finite elements and nodes, a finite element analysis required additional conditions. The lack of one of these conditions could result in obtaining an unstable solution. The boundary conditions are presented in figure 6.2.

6.1.5 Material properties

According to the data provided by Cincinnati Milacron, the plates tested in tension and the plates tested in compression were made of the same material. Hence, the material properties determined in the Chapter 3 were used.

6.2 Processing

The options COMPOSITE and ORIENTATION in ABAQUS were used to define the laminate lay-up. Each ply of the laminate was defined individually by specifying its thickness

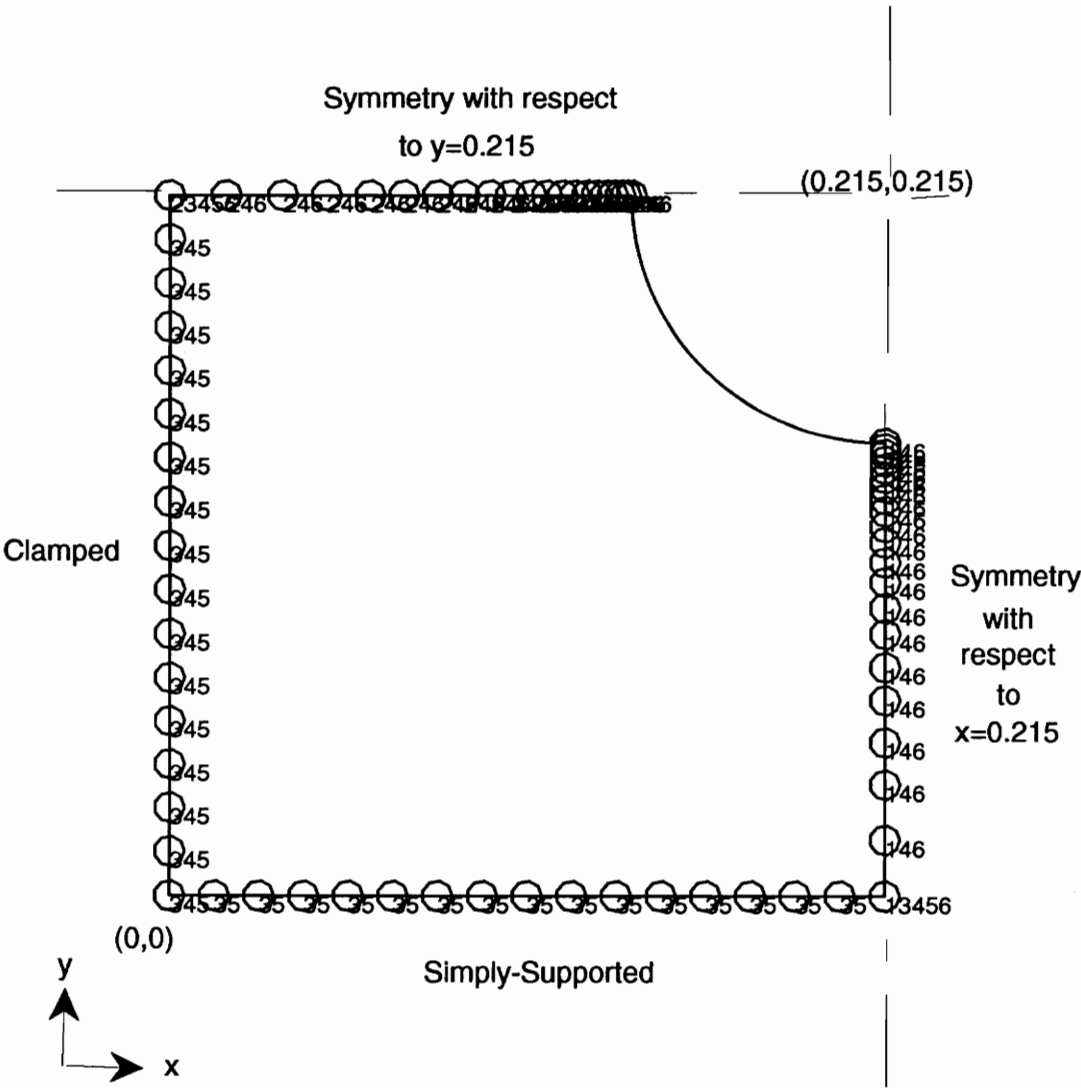


Figure 6.2: Boundary conditions of the model for compression

and fiber orientation. The option ORIENTATION created a local coordinate system for each ply. The local x axis was oriented in the fiber direction. The material properties were prescribed through the option LAMINATE by defining E_1 , E_2 , ν_{12} , and G_{12} . These values had to be defined in the local coordinate system, i.e., E_1 represented Young's modulus in the fiber direction, E_2 Young's modulus in the matrix direction, etc...

6.2.1 Eigenvalue Buckling Prediction

During the tests performed at the NASA Langley Research Center, the specimens were loaded in compression to failure. Failure occurred in the postbuckling range. Hence, the finite element analysis was developed for the postbuckling range. However, collapse studies are typically begun with eigenvalue buckling estimates. Buckling loads were estimated from the experiments by the intersection of the least-square straight lines fit to the load vs. endshortening data just before buckling and just after buckling. With this approach, the buckling load of the straight fiber plate was estimated to be 49 800 N and the buckling load of the curvilinear panel was estimated to be 56 500 N. The prebuckling responses were essentially linear. To compute the buckling eigenvalue is not computationally very costly for ABAQUS. Eigenvalue buckling estimates are obtained by using the *STATIC procedure to specify that the calculation is linear. Finally a *BUCKLE procedure predicts the buckling modes and the corresponding eigenvalues. Since the lowest buckling load is the only one of interest, only the first eigenvalue is required to converge. However, here the first two converged eigenvalues were computed.

To check that no mistake was made in using ABAQUS, a simpler check case was analyzed. This check case was that of a square thin elastic plate simply supported on all four edges and compressed in one direction. All the ABAQUS input described previously was used. However, all the plies in the stacking sequence were aluminum. Therefore E_1 was set equal to E_2 . The purpose of this check case was that an analytical solution could be computed. The solution was presented in by Timoshenko and Gere in 1961 ([10] section

9.2) as

$$N^{crit} = \frac{4\pi^2 D}{b^2}, \quad (6.1)$$

where N^{crit} is the critical value of the edge load per unit length of the edge, b the length of each edge of the plate, and $D = \frac{Et^3}{12(1-\nu^2)}$ is the elastic bending stiffness of the plate having Young's Modulus E , Poisson's ratio ν , and thickness t . The numerical results of these computations do not present a direct interest for this study and therefore they won't be detailed herein. Nevertheless, the buckling load computed by ABAQUS and the one computed using equation 6.1 show a agreement within 3%.

With this check having given satisfactory results, ABAQUS was used to compute the critical buckling load of the finite element models representing the straight fiber and curvilinear fiber plates. Table 6.1 summarizes the results obtained during the experiments and the results computed by ABAQUS. With the finite element analyses, there was a 5% difference between the buckling load of the two plates, the straight fiber case being larger. On the contrary, according the the experiments, the buckling load of the curvilinear fiber plate was 12% higher than the buckling load of the straight fiber plate. Though the magnitudes of the predictions and observations were similar, it was troubling that the finite element analyses predicted a higher buckling load for the straight fiber plate, yet the experiments indicated the curvilinear fiber plate had a higher buckling load. However, the buckling load depends on the 3rd power of the plate thickness. A small difference in the plate thickness can induce an important variation in the buckling load. An 8% difference of the curvilinear fiber plate thickness (i.e., 0.3mm) would bring its buckling load to the value found experimentally. As was seen in chapter 3, 8% was a reasonable variation of thickness to expect. Thus, considering the error factor of the experiments and the importance of the plate thickness, the results presented in table 6.1 were judged to be reasonable.

Cases with nonperfectly clamped boundary conditions were investigated. It is possible that, due to fixture compliance, the clamped boundary conditions were not really clamped. That is, there was a rotation at the clamped boundary due to fixture elasticity. To model this possibility, spring elements were placed at all the nodes associated with the clamped

Table 6.1: Comparison between the experimental and analytical buckling loads

	Experimental buckling load, N	Buckling load computed by ABAQUS, N	Difference
Curvilinear	56 500	48 900	+16%
Straight	49 800	51 500	-3.3%
Difference	+12%	-5%	

loaded edges. The selected spring element had to be placed between a node and "ground". The element used in this investigation was a torsional spring constraining the rotation about the y axis (see figure 6.3). A spring stiffness k ($N - m/rad$) was assigned to the spring elements such that $M = k\Theta$, where M was the restraining moment and Θ the rotation of the supposedly clamped end. The edge of the plate was clamped for $k \rightarrow \infty$ and simply supported for k equal to zero. For any value of k between 0 and ∞ , the boundary conditions for the two loaded edges were an intermediate case between simply supported and clamped. Figure 6.3 presents the deformed shape in the out-of-plane direction for three different type of boundary conditions: simply supported; intermediate case involving spring elements; and clamped. The edge where these boundary conditions were applied is indicated by an arrow. As can be seen the shape of the deformed plate depended strongly on the degree of support of the boundary. The buckling loads were computed as a function of the stiffness coefficient k both for the plate using curvilinear fibers and the plate using straight fibers. These relationships between the buckling load and k are presented in figure 6.4.

Several conclusions can be drawn from figure 6.4. For $0 \leq k \leq 200$ the buckling load was sensitive to the variation of the stiffness coefficient. At the beginning of this interval, the buckling load of the plate using the curvilinear fibers was higher than the buckling load of its straight fiber counterpart. At approximately a stiffness coefficient equal to $170 N - m/rad$ the two fiber formats reached the same buckling load. For $k > 170$, the buckling load of the straight fiber plate was greater than the buckling load of the curvilinear fiber plate. For even higher values of k , the buckling loads both reached plateaus. Nevertheless, in the

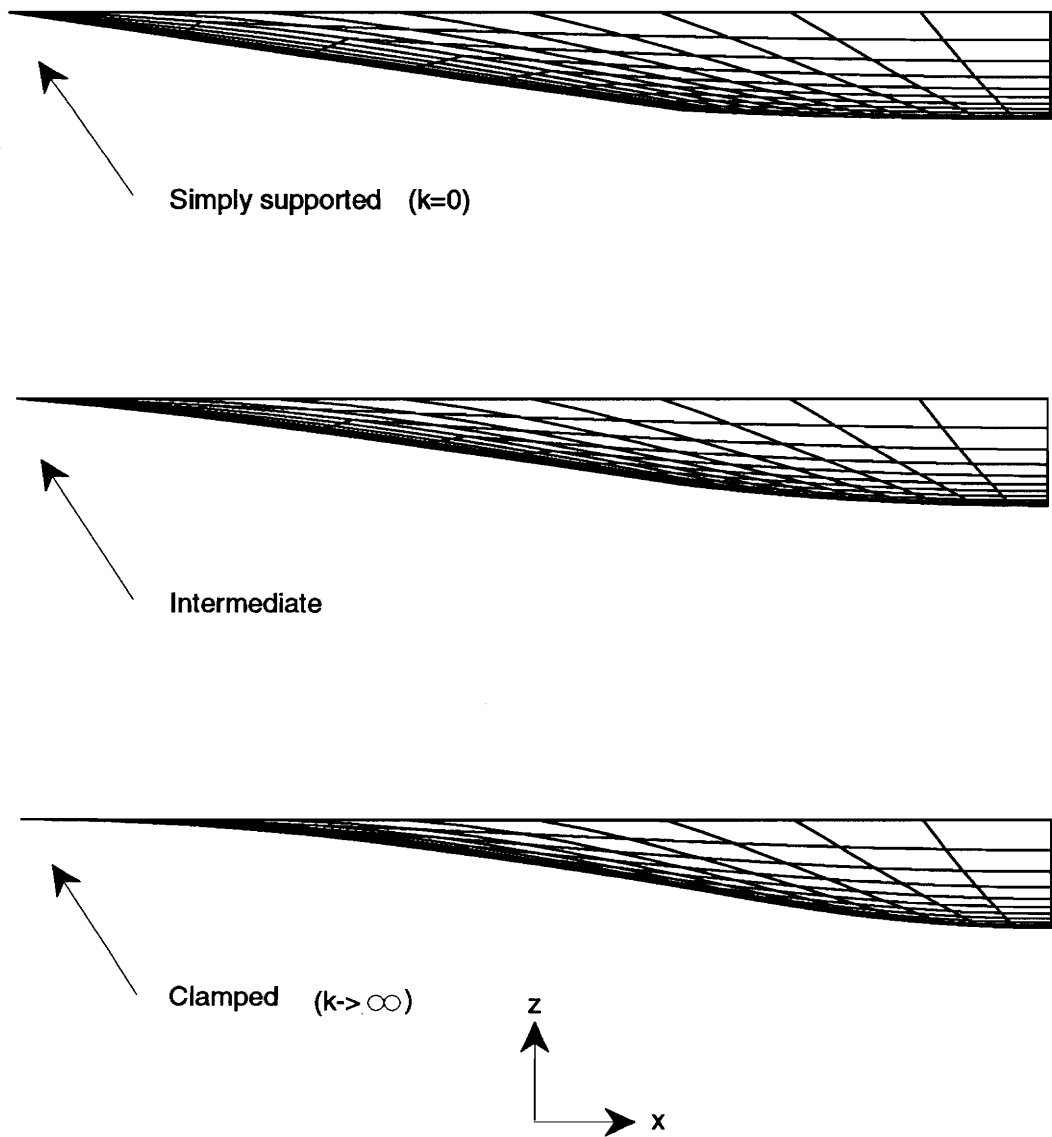


Figure 6.3: Difference in the deformed shape of plate according the boundary conditions

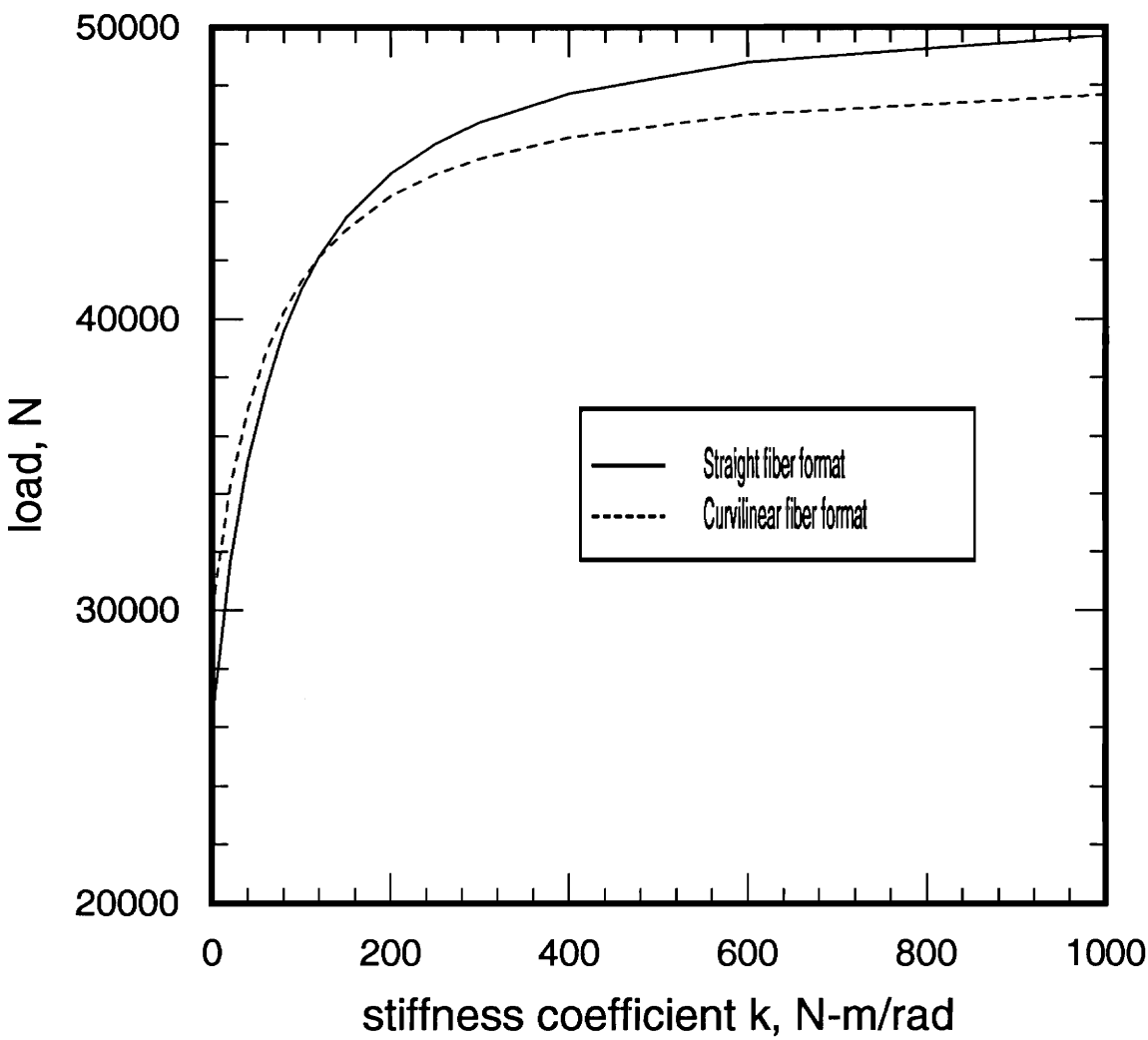


Figure 6.4: Variation of the buckling load of the curvilinear fiber and straight fiber plates as a function of the boundary conditions

range $0 \leq k \leq 1000$ the difference between the two buckling loads never exceeded 10%. In addition, the buckling load obtained by considering the two edges clamped matched the experimental results within a 16% tolerance. Hence the boundary conditions during the experiments were considered clamped.

6.3 Postbuckling

The next phase of the finite element analysis was to study the postbuckling behavior of the plates. This investigation usually included a load-displacement analysis to ensure that the eigenvalue buckling prediction already obtained was accurate. The experiments performed at the NASA Langley Research Center did measure the load vs. end-shortening and the load vs. the out-of-plane displacement for the straight fiber and the curvilinear fiber plates. In this section, all the experimental data were compared with the finite element analyses.

6.3.1 Imperfection

For a postbuckling analysis, the perfect geometry must be "seeded" [9, 10] with an imperfection to force it into a postbuckling state. Theoretically, a plate under compression having a perfect geometry may never buckle because the perfect plate has no prebuckled out-of plane displacement in the postbuckled mode, and thus no ability to switch to that mode. However, the existence of an imperfection in the form of an out-of-plane displacement couples the prebuckled and postbuckled states. The larger the magnitude of the out-of-plane imperfection, the more dominant is the coupling and the more dominant is the out-of-plane response in the prebuckling state. For large coupling, the transition to the postbuckling state is smooth with an ever-increasing out-of-plane deflection. On the other hand, for small initial out-of-plane imperfections, there is little out-of-plane deflection in the prebuckling state. Transition to the postbuckling state is marked by a sudden increase in out-of-plane deflection. In either case, the out-of-plane deflections lead to a loss of inplane stiffness. The magnitude of the initial imperfection can be estimated by examining the load

vs. end-shortening and load vs. out-of-plane displacement relations.

Obviously, imperfections occur naturally in experiments, whereas in analyses they have to be artificially included. An imperfection can be artificially included in a finite element analysis in different ways. One or several nodes can be displaced by a small amount in the out-of-plane direction. In practice, an initial out-of-plane displacement varies usually between 1 to 5% of the plate thickness [9, 10]. Another way to create an irregularity in the plate geometry is to apply a small load at one node of the plate in the out-of-plane direction. This load creates an initial deflection which will provide the necessary perturbation of the solution so that the plate deforms into the postbuckling state. This second alternative was chosen for the current analysis. A transverse load was applied in the out-of-plane direction at a node situated in the center of the plate. The magnitude of this load was small, i.e., 5 N. For smaller load levels, the solution failed to switch from the linear buckling mode to the nonlinear postbuckling behavior. The finite element analysis using the smallest imperfection presented a very sharp loss of stiffness at an applied load close to the critical buckling load computed through the buckling analysis. As the initial imperfection magnitude was increased, the transition from prebuckling to postbuckling became smoother.

6.3.2 Nonlinearity and ABAQUS

All the finite element analyses presented so far in the current work were geometrically linear. To investigate the postbuckling response of the plates manufactured by Cincinnati Milacron required a geometrically nonlinear analysis. The finite element approach used by ABAQUS was rather different from the ones presented in the previous pages. At this stage, the buckling load was known. It was computed by a linear eigenvalue buckling prediction. For the postbuckling analysis, the edge load was applied by requesting that the load be increased monotonically up to 1.5 times the value of the buckling load. This was done by suggesting five equal increments, using the automatic loading capability. ABAQUS subdivided the five equal increments into smaller increments as buckling occurred and the response became more severely nonlinear. A maximum of eight iterations per increment was allowed. The

analysis stopped when too many increments were needed, or when ABAQUS reached the maximum load specified by the user. An ABAQUS input file is shown in Appendix B.

6.3.3 Results of the postbuckling analysis

The compression tests achieved at the NASA Langley Research Center provided several sources of data. Strain gages were bonded at specific location on the compression test specimens. These locations were illustrated in figure 2.9. Displacement transducers measured the out-of-plane deflection and overall inplane shortening. In these section all the experimental data are compared to the results found though the finite element analyses. The load vs. end-shortening relation and the out-of-plane deflection are presented with the results of the finite element analyses in figure 6.5 for the curvilinear fiber specimen and in figure 6.6 for the straight fiber specimen. Overall, the prebuckling slopes of the two specimens and their finite element models were approximately the same.

Load vs. End-shortening relations

As can be seen in figure 6.5 for the load vs. end-shortening relation, the measured postbuckling slope of the curvilinear fiber plate and the postbuckling slope obtained by the finite element analysis were very close. The measured postbuckling slope of the straight fiber plate, figure 6.6, was less than the finite element predictions. The predicted postbuckling slope of the straight fiber plate was greater than the predicted postbuckling slope of the curvilinear fiber plate. This was expected because the postbuckling slope is determined to a large extend by the elements of the D_{ij} matrix, specifically D_{11} . The overall value of D_{11} was greater for the straight fiber case than for the curvilinear fiber case. However, experimentally, the straight fiber case exhibited less slope than the curvilinear fiber case. This difference may be explained by experimental problems which occurred during the tests. Problems with deformations of the simple support fixtures probably masked the actual postbuckling response of the straight fiber plate (see Ref. [7]).

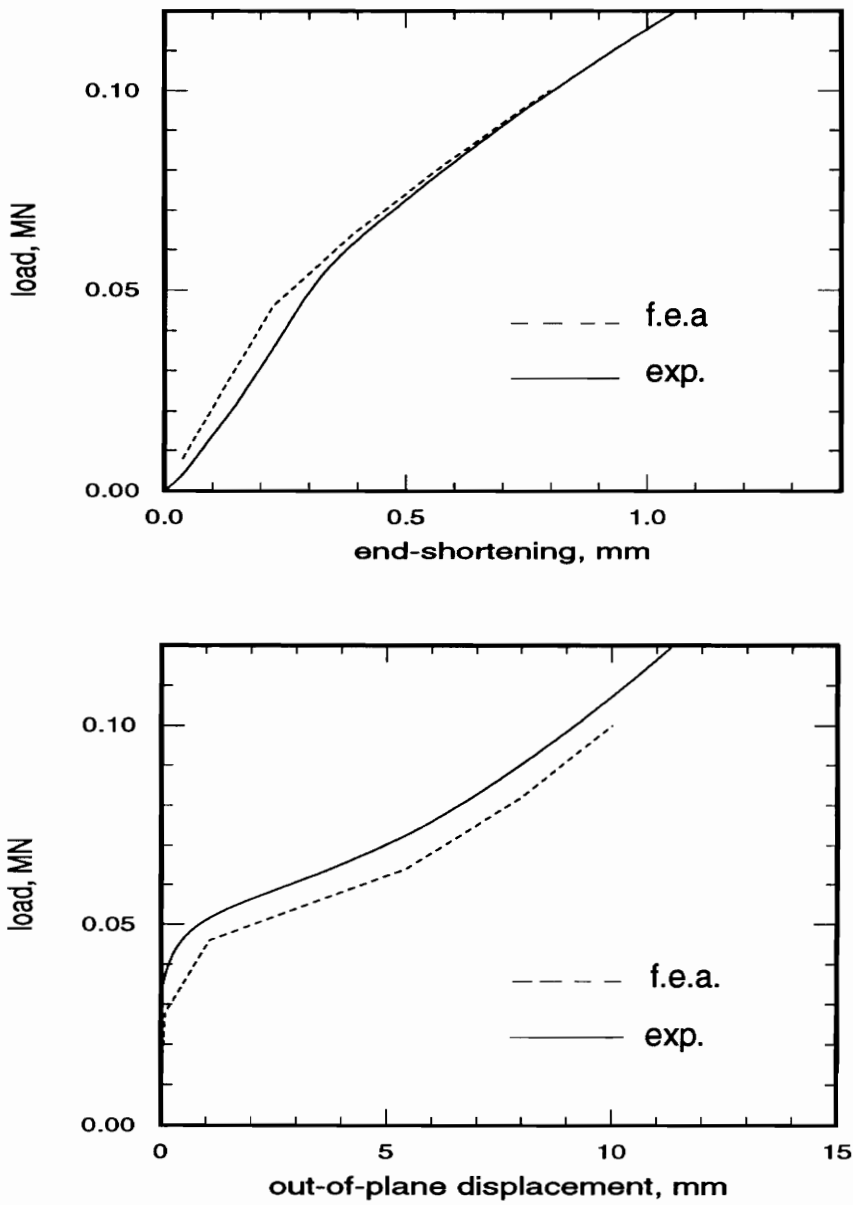


Figure 6.5: End-shortening and out-of-plane deflection relations for the curvilinear fiber plate

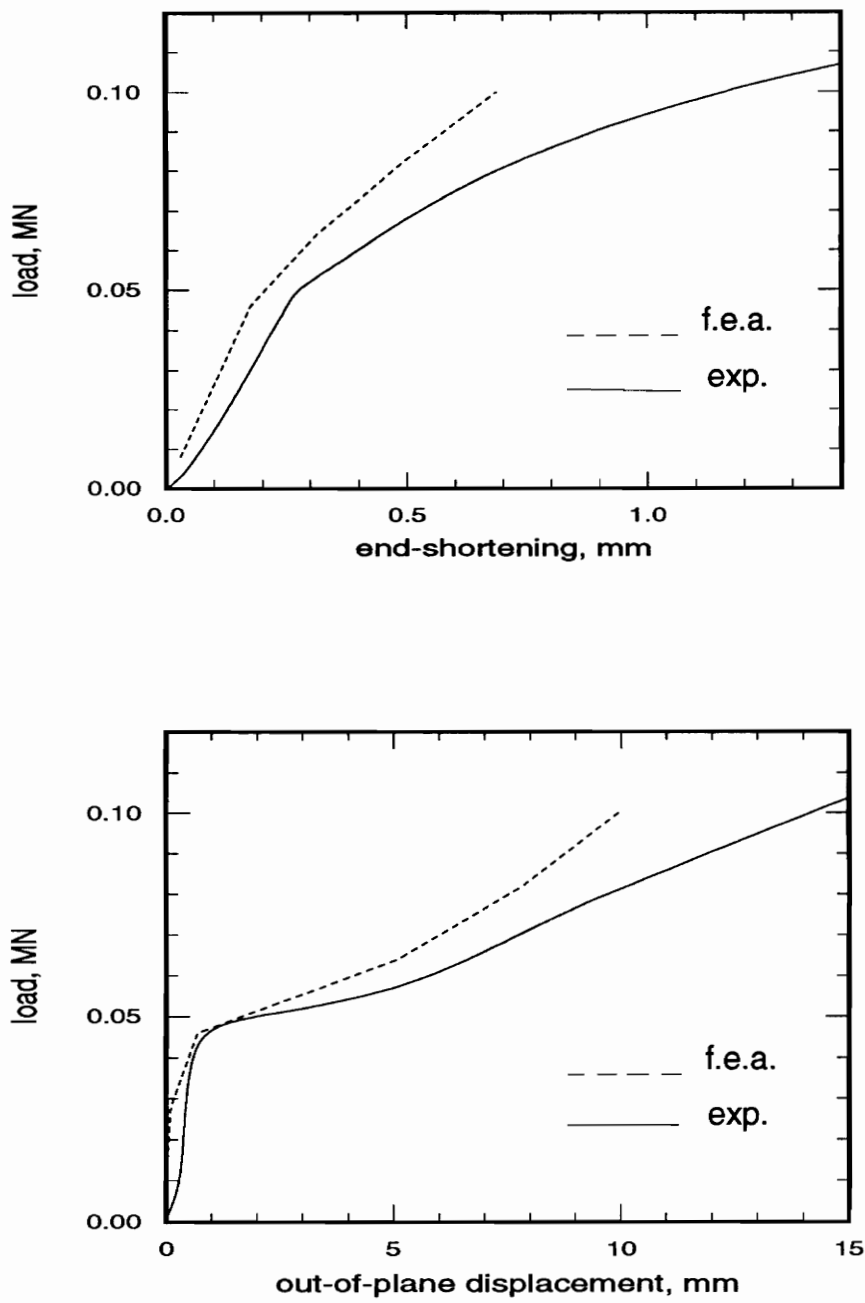


Figure 6.6: End-shortening and out-of-plane deflection relations for the straight fiber plate

Load vs. Out-of-plane deflection relations

The out-of plane deflections of the curvilinear fiber plate shown in figure 6.5 for the experiments and the finite element analysis are similar. The load difference (vertical shift) between the two relationships corresponded almost exactly to the difference between the buckling load found experimentally and the buckling load computed by the finite element analysis (see Table 5.1). The pre- and postbuckling slopes obtained by considering experimental data and the finite element model were almost identical. The out-of-plane deflection from the straight fiber plate is presented in figure 6.6. The prebuckling relation and the beginning of the postbuckling curve for the finite element analysis and the experiments were close. For large deformations, the difference between the two relations was large. Again, this difference may partly be explained by the problems encountered with support fixtures in the experiments.

Results provided by the strain gages

The strains from the back-to-back gage pairs at location ‘a’ though ‘k’ in figure 2.9 were measured during the compression experiments. These data are compared to the strains obtained by the finite element analyses in figure 6.7 for the straight fiber plate, and in figure 6.8 for the curvilinear fiber plate. In these figures, compressive load is considered positive, as is compressive strain.

General comments for both the curvilinear and the straight fiber plates

The back-to-back pairs near the simply supported edge, location ‘a’ and ‘e’, reflected the fact that both gages of the back-to-back pair were always in compression. The simply supports held the plate flat in that region so the response was strictly planar and compressive. Away from the simply supported edges, where the plate was not constrained to remain planar, the strains generally started compressive, and as the plate buckled the strains on one side of the plate became tensile, while the strains on the other side remained compressive. The

strains at location 'c' showed that the loading was symmetric.

Straight fiber plate

As seen in figure 6.7, the agreement between the finite element analysis and the experiment was quite good for the gage 'a', 'g', 'i' and 'k'. For the gage location 'e', the results provided by the strain gage which sustained the largest compression strain coincided well with the finite element model. On the other hand, the second branch of the load vs. strain relation did not compare well. This difference may have been due to edge effects along the sides of the plate. The strains at location 'c' were small. Thus, in absolute value, the difference between the experimental results and the finite element results at location 'c' was acceptable.

Curvilinear fiber plate

From figure 6.8, general comments can be made regarding all the six strain gages. Except, for location 'a', for a given strain the corresponding load computed by the finite element analysis was generally about 10% lower than the load found experimentally. Thus by increasing the computed buckling load by 10%, the measured postbuckling response of the plate using the curvilinear fiber format would coincide almost exactly with the postbuckling response computed by the finite element approach. The comments made previously for the straight fiber plate regarding strains at locations 'e' and 'c' can be repeated here.

Closure

The finite element analyses and the experimental measurements showed a fairly good agreement for the pre- and postbuckling response. There was no noticeable difference in the buckling performance between the plate using curvilinear fibers and the plate using the straight fibers. Two reasons may explain this lack of difference: First, the design considered by Cincinnati Milacron was not designed specifically to provide high buckling resistance, as was the case with Hyer and Lee [6]. Second, only half of plies in the stacking sequence

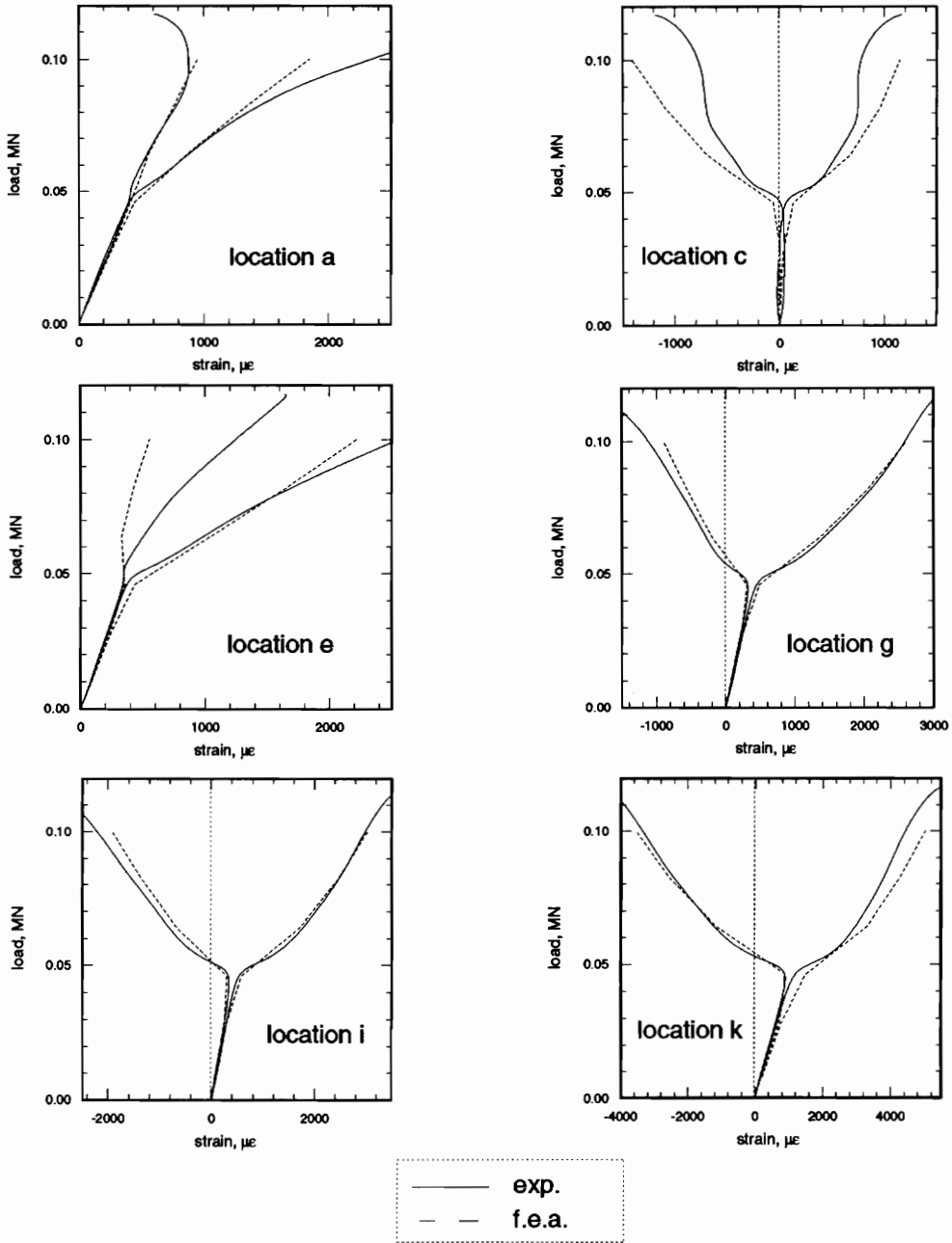


Figure 6.7: Strain gages measurements for the straight fiber plate

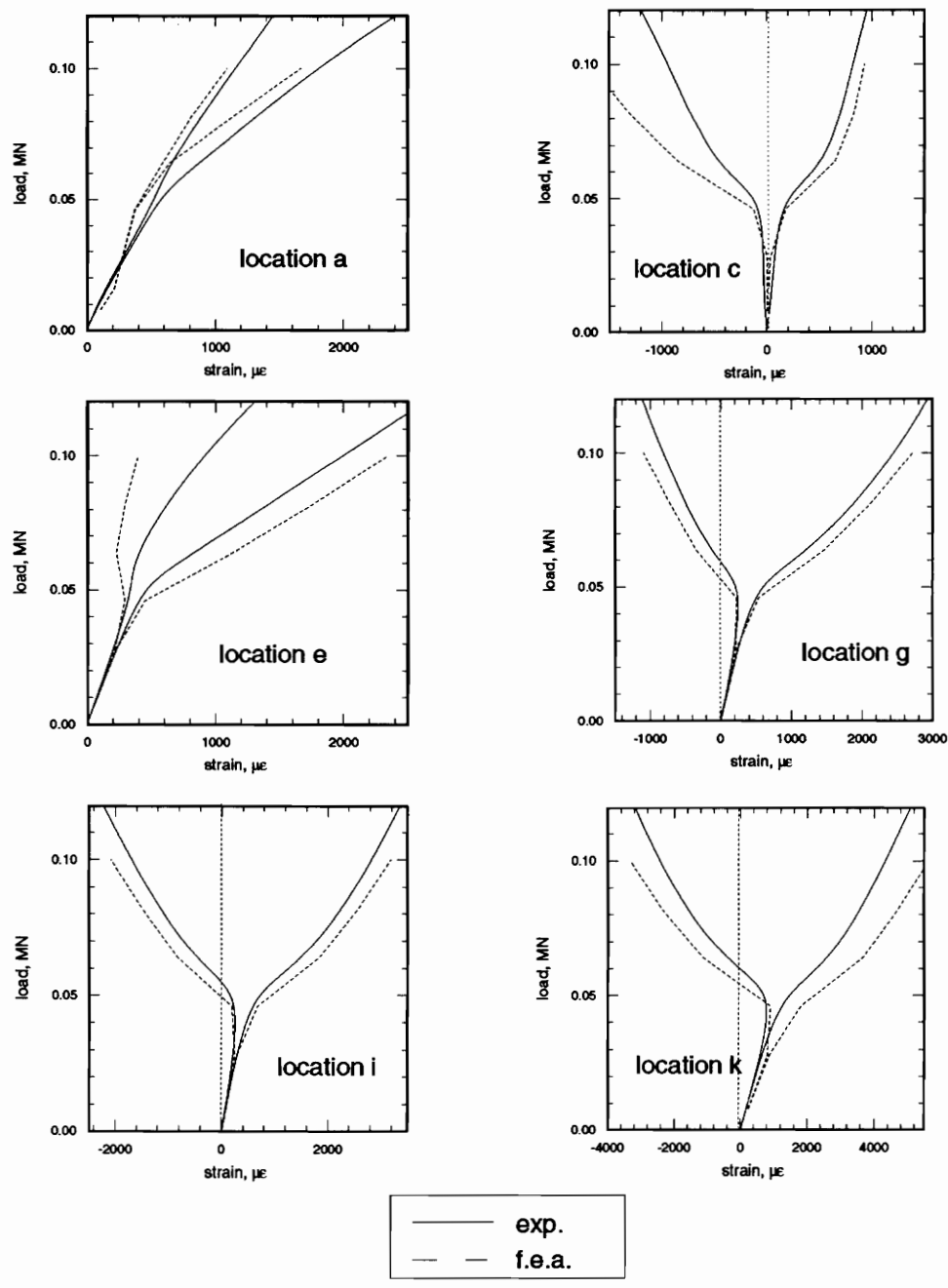


Figure 6.8: Strain gages measurements for the curvilinear fiber plate

were curvilinear. The designs considered in ref. [6] which achieved a high buckling load recommended a large percentage of curvilinear plies. Thus, the design of composite structure using a curvilinear fiber format should be studied very carefully before manufacturing if improvements in the mechanical performances are to be expected.

Chapter 7

Summary, conclusions, and recommendations

This study focused on the analyses of plates using curvilinear fiber trajectories manufactured by Cincinnati Milacron and tested at the NASA Langley Research Center. Some additional experiments with coupons cut from the plates tested in tension provided information about the plate thickness, the elastic properties, and the strengths of the material. The analyses of the plates tested in tension were conducted using finite element methods and included failure criteria. In compression, the buckling load and the postbuckling behavior of the plates were also investigated. Comparisons with test results were made.

7.1 Detailed summary and conclusions

1. The literature review summarized the content of previous work done in the field of using the curvilinear fiber format. Past research suggested that using a curvilinear fiber format may result in an important gain in tension or buckling resistance. The past work was all done using finite element analysis and most designs proposed in the literature review did not take in consideration manufacturing constraints. First, the difficulty of most approaches used included dependency of the number of design variables on finite element mesh density

and the lack of fiber continuity across finite element interfaces. Second, the proportion of curvilinear plies for designs presenting big gains in compression or tension resistance was very important (i.e., usually between 70% and 90% of the total number of plies). Such designs are very weak in other loading modes.

No experiments had been conducted to confirm these findings before Cincinnati Milacron, in collaboration with the NASA Langley Research Center, manufactured and tested plates using the curvilinear fiber format. None of the designs presented in previous work was followed by Cincinnati Milacron because of manufacturing limitations. Only half of the plies in the stacking sequence used the curvilinear fiber format.

Experimental results: In tension, the curvilinear fiber plate failed at a load 37% lower than the failure load of its straight fiber counterpart. This was an unexpected result. The buckling load of the curvilinear fiber plate was 12% higher than the buckling load of the straight fiber plate.

2. The unexpected lower load capacity of the curvilinear fiber plate in tension prompted an investigation of the properties of both the curvilinear and the straight fiber material. Two categories of mechanical testings using coupons from the remnants of the broken plates were performed. The purpose of the first set of tests was to calculate elastic properties to be used in the finite element analyses. The second set of tests was performed to investigate the strengths properties of the plates. The results showed that the curvilinear fiber plate and the straight fiber plate could be considered to be made out of the same material. With reasonable estimates of the elastic and strength properties, attention turned to the predictions of the response of the straight and curvilinear fiber tensile specimens.

3. During the experiments performed at the NASA Langley Research Center, back-to-back strain gages were placed at different locations on the plates. In general, the strains measured during the experiments and the strains computed with the finite element analyses coincided fairly well. This agreement gave credit to the engineering constants computed through the testing of coupons cut from the remnants of the tensile plates. Having in hand the finite element prediction of the strain and stress field in the plates, a FORTRAN

program was written to predict the failure modes of the plates using the maximum stress, maximum strain, and Tsai-Hill failure criteria. All the failure criteria used contradicted the experimental results. They predicted that the curvilinear fiber plate could sustain between 5-13% more load than the straight fiber plate.

This contradiction prompted an investigation into failure resulting from possible manufacturing features. Some parts of the curvilinear plies could not be laid down by the fiber placement machine and so material was placed by hand in these regions. The influence of possible material properties variations in these regions was studied. It was concluded that these manufacturing features could not reasonably explain the 37% difference between the experimental failure load of the straight fiber plate and the curvilinear fiber plate.

The difference between the experimental failure loads and the finite element predictions was explained by considering the experimental load vs. axial displacement characteristics for the two specimens. This relation showed a first fiber breakage in the straight fiber plate appearing for a load lower than the final failure load. Contrary to what happened in the curvilinear fiber plate, this first fiber breakage was not immediately followed by a total failure but the plate kept on sustaining more load. For the curvilinear fiber plate, total failure followed immediately after first fiber failure. Propagation of the failure may have been more difficult in the straight fiber plate, or some unexpected parameters appeared during the testing. By considering a first fiber breakage at a load of 0.51MN for the straight fiber plate, the experimental data and the finite element predictions coincide.

As an aside, an improved plate for tension resistance was designed using a scheme similar to the one developed by Hyer and Charette [1-4] and Charette [5]. The same stacking sequence and plate thickness as the plates manufactured by Cincinnati Milacron was considered. It was shown that the final failure load of the improved plate was 16% higher than the failure load of its straight fiber counterpart using the maximum stress criterion. The gain in tension resistance was not very important compared to other curvilinear designs presented in the literature review. Because of the lack of fiber continuity across the finite element interfaces, the design would have to be modified to be manufacturable. These

modifications would most probably lower its performances in tension resistance.

4. During the experiments in compression, the buckling load of the curvilinear fiber plate was 12% higher than the buckling load of its straight fiber counterpart. According to the finite element analyses, there was no noticeable difference in the buckling performance between the straight fiber plate and the curvilinear fiber plate. The buckling load computed by the finite element analysis matched the experimental results for the straight fiber plate within a 4% tolerance. For the curvilinear plate, the buckling load predicted by the finite element analysis was 16% lower than the experimental buckling load. This difference is reasonable considering probable variation in the plate thickness.

The postbuckling response was also investigated. This investigation included a load-displacement analysis to ensure that the eigenvalue buckling predictions already obtained was accurate. The strains measured at strain gages locations coincided fairly well with the strains computed with the finite element analyses.

7.2 Recommendations

Though prior work has shown that the curvilinear fiber format can result in significant gains for specific design objectives, these studies did not consider manufacturing constraints. Future work on the curvilinear fiber format should include process parameters. Optimization schemes should be developed taking into consideration geometrical aspects related to design and manufacturing.

Future studies could also focus on the development of new failure criteria more adapted for curvilinear fiber paths. Composite material stress-strain behavior can be linear or non-linear depending on the ply orientation of the individual ply or laminate. The presence of curvilinear plies could introduce new parameters. The present work could not explain for sure why the straight fiber plate manufactured by Cincinnati Milacron could sustain more load after the first fiber breakage. New investigations should be done in this direction.

Bibliography

- [1] Hyer, M.W. and Charette, R.F., "The Use of Curvilinear Fiber Format in Composite Structure Design," (Technical Note), *AIAA Journal*, vol. 29, no.6, pp.1011-1015, 1991
- [2] Hyer, M.W. and Charette, R.F., "Use of Curvilinear Fiber Format in Composite Structure Design," AIAA Paper 89-1404, Proceedings of the 30th Structures, Structural Dynamics, and Materials Conference, 1989
- [3] Hyer, M.W. and Charette, R.F., "Use of Curvilinear Fiber Format to Increase Structural Efficiency," SAMPE, Proceedings of the 19th International Technical Conference, pp. 190-197, 1987
- [4] Hyer, M.W. and Charette, R.F., "Innovative Design of Composite Structures: Further Studies in the Use of a Curvilinear Fiber Format to Improve Structural Efficiency," Virginia Polytechnic Institute and State University, College of Engineering Report VPI-E-88-8, 1988
- [5] Charette, R.F., "Innovative Design of Composite Structures: The Use of Curvilinear Fiber Format in Structural Design of Composites," University of Maryland Department of Mechanical Engineering, Master's Thesis, 1988
- [6] Hyer, M.W. and Lee, H.H., "The Use of Curvilinear Fiber Format to Improve Buckling Resistance of Composites Plates with Central Circular Holes," *Composite Structures*, vol. 18, pp. 236-261, 1991

- [7] Hyer, M.W., Rust, R.J., Nemeth, M.P., and Walters, W.A., "Design, Manufacturing, and Testing of Plates Utilizing Curvilinear Fiber Trajectories," Proceedings of Tenth DoD/NASA/FAA Conference on Fibrous Composites in Structural Design, Report No. NAWCADWAR-94096-60, Naval Air Warfare Center, Warminster, PA, pp. III-15 - III-34, 1994
- [8] PATRAN, PATRAN Division of PDA Engineering, Costa Mesa, CA, 1989
- [9] ABAQUS, Hibbitt, Karlson, and Sorenson, Inc. Providence, RI, 1987
- [10] ABAQUS Theory Manual, ABAQUS Version 4-6
- [11] Liu, D-H, "Stress Analysis of Pin Loaded Orthotropic Plates Using Orthotropic Photoelasticity," Ph.D. Dissertation, Virginia Polytechnic Institute and State University, Blacksburg Va, 1984
- [12] Wolfram, S., Mathematica , A System for Doing Mathematics by Computer, 2nd edition, Addison-Wesley Publishing Company, Inc., New-York, 1991
- [13] U.S. Department of Transportation, Federal, Aviation Administration, Test Methods for Composites, a State Status Report, Volume 1, Tension Test Method, June 1993, DoT/FAA/CT-93/17,1
- [14] Oplinger, D.W., Parker, B.S. , Gandhi, K.R., Lamothe, R., Foley, G., "On the Stream-line Specimen for Tension Testing of Composite Materials," Generation of Higher Composite Material Allowable Using Improved Test Coupons, ASTM STP 864, pp. 532-555, 1985
- [15] Dastin, S., Lubin, G., Munyak, J., Slobodzinski, A. "Determination of Effective [0] Properties from [0/90] Laminate Testing," Mechanical Properties and Test Techniques for Reinforced Plastic Laminates, ASTM STP 460, pp. 13-26, 1969
- [16] Cook, R.D., Malkus, D.S., Plesha, M.E., Concepts and Applications of Finite-Element Analysis, John Wiley and Sons, NY

- [17] Jones, R.M., Mechanics of Composite Materials, Hemisphere Publishing Corporation, N.Y.
- [18] Sun, C.T. and Quinn, B.J., "Evaluation of Failure Criteria Using Off Axis Laminate Specimens," Proceedings of the American Society for Composites, Ninth Technical Conference, pp. 97-105, 1994
- [19] Quinn, B.J. and Sun, C.T., "A Critical Evaluation of Failure Analysis Methods for Composite Laminates," Proceedings of Tenth DoD/NASA/FAA Conference on Fibrous Composites in Structural Design, Report No. NAWCADWAR-94096-60, Naval Air Warfare Center, Warminster, PA, pp. V-21 - V-37, 1994

Appendix A

FORTRAN program used in section 5.7

This appendix contains the listing of the program used to align the fiber angle in the curvilinear plies with the principal stress direction (see section 5.7).

```
C Yannick FIERLING SS : 231-67-1755
C
C *****
C * MAIN PROGRAM *
C * *
C * .It: Number of iteration needed to align the principal *
C * stress direction with the fiber angle in the C plie *
C * .Qa(i): fiber angle in the C ply for element i *
C * .Talf(i): principal stress direction for the element i *
C * *
C *****
C
Double precision Qa,Talf
Dimension Qa(200),Talf(200)
C
It=0
numele=200
do 10 i=1,numele
10 Qa(i)=0
30 call prg(Qa)
```

```

do 60 i=1,200
60 TAlf(i)=0
It=It+1
call FEM2D
call angle(Qa,TAlf,It)
do 20 i=1,numele
Qa(i)=TAlf(i)*180/3.1415
20 continue
Go To 30
End
C
C *****
C * Subroutine FEM2D *
C * Computes the strain field in each element at the *
C * centroidal integration point and writes the output *
C * file in ISTRESS used in the Subroutine angle *
C * *
C *****
C
SUBROUTINE FEM2D
C PROGRAM FOR STRESS ANALYSIS OF TWO-DIMENSIONAL
C LINEAR ELASTIC ORTHOTROPIC COMPOSITE STRUCTURES
C DAHSIN LIU, MARCH 1, 1983
C
COMMON /SOL/ NUMNP,NEQ,NWK,NUMEST,MIDEST,MAXEST,MK
COMMON /DIM/ N1,N2,N3,N4,N5,N6,N7,N8,N9,N10,N11,N12,N13,N14,N15
COMMON /EL/ IND,NPAR(10), NUMEG,MTOT,NFIRST,NLAST,ITWO
COMMON /VAR/ NG,MODEX
COMMON /TAPES/ IELMNT,ILOAD,IIN,IOUT,ISTRESS
C
DIMENSION TIM(5), HED(10)
DIMENSION IA(1)
EQUIVALENCE (A(1),IA(1))
C
C THE FOLLOWING TWO CARDS ARE USED TO DETERMINE THE MAXIMUM HIGH
C SPEED STORAGE THAT CAN BE USED FOR SOLUTION. TO CHANGE THE HIGH
C SPEED STORAGE AVAILABLE FOR EXECUTION CHANGE THE VALUE OF MTOT
C AND CORRESPONDINGLY COMMON A(MTOT)
C
COMMON A(500000)
MTOT = 500000
C
C DOUBLE PRECISION CARD
C ITWO = 1 SINGLE PRECISION ARITHMETIC
C ITWO = 2 DOUBLE PRECISION ARITHMETIC
C
ITWO=2
C
C THE FOLLOWING SCRATCH RILES ARE USED
C IELMNT = TAPE STORING ELEMENT DATA
C ILOAD = TAPE STORING LOAD VECTORS
C IIN = INPUT TAPE
C IOUT = OUTPUT TAPE
C
open(3,file='data2')
open(16,file='ISTRESS')
IELMNT = 1
ILOAD = 2
IIN = 3

```

```

IOUT = 4
ISTRESS= 16
C
200 NUMEST = 0
MAXEST = 0
C
C I N P U T P H A S E
C
CALL SECOND (TIM(1))
C
C READ CONTROL INFORMATION
C
READ(IIN,1000) HED,NUMNP,NUMEG,NLCASE,MODEX
IF (NUMNP.EQ.0) STOP
C
C READ NODAL POINT DATA
C
N1 = 1
N2 = N1 + 3 * NUMNP
N3 = N2 + NUMNP * ITWO
N4 = N3 + NUMNP * ITWO
N5 = N4 + NUMNP * ITWO
IF (N5.GT.MTOT) CALL ERROR (N5 - MTOT,1)
C
CALL INPUT (A(N1),A(N2), A(N3), A(N4), NUMNP, NEQ)
C
NEQ1 = NEQ + 1
C
C CALCULATE AND STORE LOAD VECTORS
C
N6 = N5 + NEQ * ITWO
C
REWIND ILOAD
C
DO 300 L= 1, NLCASE
C
READ(IIN,1010) LL,NLOAD
C
IF (LL.EQ.L) GO TO 310
STOP
310 CONTINUE
C
N7 = N6 + NLOAD
N8 = N7 + NLOAD
N9 = N8 + NLOAD * ITWO
C
IF (N9.GT.MTOT) CALL ERROR (N9 - MTOT,2)
C
CALL LOADS (A(N5),A(N6),A(N7),A(N8),A(N1),NLOAD,NEQ)
C
300 CONTINUE
C
C READ, GENERATE AND STORE ELEMENT DATA
C
N6 = N5 + NEQ
DO 10 I = N5,N6
10 IA(I)=0
IND=1
C

```

```

CALL ELCAL
C
CALL SECOND (TIM(2))
C
C S O L U T I O N P H A S E
C
C ASSEMBLE STIFFNESS MATRIX
C
CALL ADDRES (A(N2),A(N5))
C
MM = NWK/NEQ
N3 = N2 + NEQ +1
N4 = N3 + NWK * ITWO
N5 = N4 + NEQ * ITWO
N6 = N5 + MAXEST
IF (N6.GT.MTOT) CALL ERROR (N6 - MTOT,4)
C
C WRITE TOTAL SYSTEM DATA
C
C
C IN DATA CHECK ONLY MODE WE SKIP ALL FURTHER CALCULATIONS
C
IF (MODEX.GT.0) GO TO 100
CALL SECOND (TIM(3))
CALL SECOND (TIM(4))
CALL SECOND (TIM(5))
GO TO 120
C
C CLEAR STORAGE
C
100>NNL = NWK + NEQ
CALL CLEAR(A(N3),>NNL)
C
IND = 2
C
CALL ASSEM (A(N5))
C
CALL SECOND (TIM(3))
C
C TRIANGULARIZE STIFFNESS MATRIX
C
KTR = 1
CALL COLSOL (A(N3),A(N4),A(N2),NEQ,NWK,NEQ1,KTR)
C
35 CALL SECOND (TIM(4))
C
KTR = 2
IND = 3
C
REWIND ILOAD
DO 400 L=1,NLCASE
C
CALL LOADV (A(N4),NEQ)
C
C CALCULATION OF DISPLACEMENTS
C
CALL COLSOL (A(N3),A(N4),A(N2),NEQ,NWK,NEQ1,KTR)
C
CALL WRITE(A(N4),A(N1),NEQ,NUMNP)

```

```

C
C CALCULATION OF STRESSES
C
CALL STRESS (A(N5))
C
400 CONTINUE
CALL SECOND (TIM(5))
C
C PRINT SOLUTION TIMES
C
120 TT = 0.
DO 500 I = 1,4
TIM(I) = TIM(I+1) - TIM(I)
500 TT = TT + TIM(I)
C
close(16)
close(3)
C READ NEXT ANALYSIS CASE
C
C GO TO 200
C
1000 FORMAT (10A4/5I5)
1010 FORMAT (2I5)
RETURN
C
C
END
C*****
SUBROUTINE ERROR(N,I)
C
C PROGRAM
C TO PRINT MESSAGES WHEN HIGH-SPEED STORAGE IS EXCEEDED
C
COMMON/TAPES/ IELMNT,ILOAD,IIN,IOUT,ISTRESS
C
GO TO (1,2,3,4),I
C
1 WRITE(ISTRESS,2000)
GO TO 6
2 WRITE(ISTRESS,2010)
GO TO 6
3 WRITE(ISTRESS,2020)
GO TO 6
4 WRITE(ISTRESS,2030)
C
6 WRITE(ISTRESS,2050) N
2000 FORMAT (// 'NOT ENOUGH STORAGE FOR READ-IN OF ID ARRAY AND
123HNDDAL POINT COORDINATES')
2010 FORMAT (// 'NOT ENOUGH STORAGE FOR DEFINITION OF LOAD VECTORS')
2020 FORMAT (// 'NOT ENOUGH STORAGE FOR ELEMENT DATA INPUT')
2030 FORMAT (// 'NOT ENOUGH STORAGE FOR ASSEMBLAGE OF GLOBAL STRUCTUR
155HE STIFFNESS, AND DISPLACEMENT AND STRESS SOLUTION PHASE' )
2050 FORMAT (// '*** ERROR STORAGE EXCEEDED BY', I9)
RETURN
END
C*****
SUBROUTINE INPUT (ID,X,Y,Z,NUMNP,NEQ)
C
C PROGRAM

```



```

C TO READ, GENERATE, AND PRINT NODAL POINT INPUT DATA
C TO CALCULATE EQUATION NUMBERS AND STORE THEM IN ID ARRAY
C
C N=ELEMENT NUMBER
C ID=BOUNDARY CONDITION CODES (0=FREE,1=DELETED)
C X,Y,Z= COORDINATES
C KN= GENERATION CODE
C I.E. INCREMENT ON NODAL POINT NUMBER
C
IMPLICIT REAL*8(A-H,O-Z)
C
C THIS PROGRAM IS USED IN SINGLE PRECISION ARITHMETIC ON
C CDC EQUIPMENT AND DOUBLE PRECISION ARITHMETIC ON IBM
C OR UNIVAC MACHINES .ACTIVATE,DEACTIVATE OR ADJUST ABOVE
C CARD FOR SINGLE OR DOUBLE PRECISION ARITHMETIC
C
COMMON /TAPES/ IELMNT,ILOAD,IIN,IOUT,ISTRESS
DIMENSION X(1),Y(1),Z(1),ID(3,NUMNP)
C
C READ AND GENERATE NODAL POINT DATA
C
KNOLD=0
NOLD=0
C
10 READ(IIN,1000) N,(ID(I,N),I=1,3),X(N),Y(N),Z(N),KN
IF (KNOLD.EQ.0) GO TO 50
NUM=(N-NOLD) / KNOLD
NUMN=NUM-1
IF(NUMN.LT.1) GO TO 50
XNUM=NUM
DX=(X(N)-X(NOLD))/XNUM
DY=(Y(N)-Y(NOLD))/XNUM
DZ=(Z(N)-Z(NOLD))/XNUM
K=NOLD
DO 30 J=1,NUMN
KK=K
K=K + KNOLD
X(K)=X(KK)+DX
Y(K)=Y(KK)+DY
Z(K)=Z(KK)+DZ
DO 30 I=1,3
ID(I,K)=ID(I,KK)
30 CONTINUE
C
50 NOLD=N
KNOLD=KN
IF(N.NE.NUMNP) GO TO 10
C
C WRITE COMPLETE NODAL DATA
C
C NUMBER UNKNOWNNS
C
NEQ=0
DO 100 N=1,NUMNP
DO 100 I=1,3
IF (ID(I,N)) 110,120,110
120 NEQ=NEQ + 1
ID(I,N)=NEQ
GO TO 100

```

```

110 ID(I,N)=0
100 CONTINUE
C
C WRITE EQUATION NUMBERS
C
RETURN
C
1000 FORMAT (4I5,3F10.0,I5)
C
END
C*****
SUBROUTINE LOADS (R,NOD,IDIRN,FLOAD,ID,NLOAD,NEQ)
C
C PROGRAM
C TO READ NODAL LOAD DATA
C TO CALCULATE THE LOAD VECTOR R FOR EACH LOAD CASE
C AND WRITE ONTO TAPE ILOAD
C
IMPLICIT REAL * 8(A-H,O-Z)
C
C THIS PROGRAM IS USED IN SINGLE PRECISION ARITHMETIC ON
C CDC EQUIPMENT AND DOUBLE PRECISION ARITHMETIC ON IBM
C OR UNIVAC MACHINES .ACTIVATE,DEACTIVATE OR ADJUST ABOVE
C CARD FOR SINGLE OR DOUBLE PRECISION ARITHMETIC
C
COMMON /VAR/ NG, MODEX
COMMON /TAPES/ IELMNT,ILOAD,IIN,IOUT,ISTRESS
DIMENSION R(NEQ),NOD(1),IDIRN(1),FLOAD(1)
DIMENSION ID(3,1)
C
READ(IIN,1000) (NOD(I),IDIRN(I),FLOAD(I),I=1,NLOAD)
IF (MODEX.EQ.0) RETURN
C
DO 210 I=1,NEQ
210 R(I)=0.
C
DO 220 L=1,NLOAD
LN=NOD(L)
LI=IDIRN(L)
II=ID(LI,LN)
IF (II) 220,220,240
240 R(II) = R(II)+ FLOAD(L)
C
220 CONTINUE
C
WRITE (ILOAD) R
C
200 CONTINUE
C
1000 FORMAT(2I5,F15.5)
RETURN
END
C*****
SUBROUTINE ELCAL
C
C PROGRAM
C TO LOOP OVER ALL ELEMENT GROUPS FOR READING,
C GENERATING AND STORING THE ELEMENT DATA
C

```

```

COMMON /SOL/ NUMNP,NEQ,NWK,NUMEST,MIDEST,MAXEST,MK
COMMON /EL/ IND,NPAR(10),NUMEG,MTOT,NFIRST,NLAST,ITWO
COMMON /TAPES/ IELMNT,ILOAD,IIN,IOUT,ISTRESS
COMMON A(1)
C
REWIND IELMNT
C
C LOOP OVER ALL ELEMENT GROUPS
C
DO 100 N=1,NUMEG
C
READ(IIN,1000) NPAR
C
CALL ELEMNT
C
IF (MIDEST.GT.MAXEST) MAXEST=MIDEST
C
WRITE (IELMNT) MIDEST,NPAR,(A(I),I=NFIRST,NLAST)
C
100 CONTINUE
C
RETURN
C
1000 FORMAT (20I5)
C
END
C*****
SUBROUTINE ELEMNT
C
C PROGRAM
C TO CALL THE APPROPRIATE ELEMENT SUBROUTINE
C
COMMON /EL/ IND,NPAR(10),NUMEG,MTOT,NFIRST,NLAST,ITWO
C
NPAR1=NPAR(1)
C
GO TO (1,2,3),NPAR1
C
1 CALL TRUSS
RETURN
C
C OTHER ELEMENT TYPES WOULD BE CALLED HERE, IDENTIFYING
C EACH ELEMENT TYPE BY A DIFFERENT NPAR(1) PARAMETER
C
2 RETURN
C
3 RETURN
C
END
C*****
SUBROUTINE COLHT (MHT,ND,LM)
C
C PROGRAM
C TO CALCULATE COLUMN HEIGHTS
C
COMMON /SOL/ NUMNP,NEQ,NWK,NUMEST,MIDEST,MAXEST,MK
DIMENSION LM(1),MHT(1)
C
LS=100000

```

```

DO 100 I=1,ND
IF(LM(I)) 110,100,110
110 IF(LM(I)-LS) 120,100,100
120 LS=LM(I)
100 CONTINUE
C
DO 200 I=1,ND
II=LM(I)
IF(II.EQ.0) GO TO 200
ME=II - LS
IF(ME.GT.MHT(II)) MHT(II)=ME
200 CONTINUE
C
RETURN
END
C*****
SUBROUTINE ADDRES(MAXA,MHT)
C
C PROGRAM
C TO CALCULATE ADDRESSES OF DIAGONAL ELEMENTS IN BANDED
C MATRIX WHOSE COLUMN HEIGHTS ARE KNOWN
C
C MHT = ACTIVE COLUMN HEIGHTS
C MAXA = ADDRESSES OF DIAGONAL ELEMENTS
C
COMMON/SOL/ NUMP,NEQ,NWK,NUMEST,MIDEST,MAXEST,MK
DIMENSION MAXA(2),MHT(1)
C
C CLEAR ARRAY MAXA
C
NN=NEQ + 1
DO 20 I=1,NN
20 MAXA(I)=0
C
MAXA(1)=1
MAXA(2)=2
MK=0
IF (NEQ.EQ.1) GO TO 100
DO 10 I=2,NEQ
IF (MHT(I).GT.MK) MK=MHT(I)
10 MAXA(I+1)=MAXA(I) + MHT(I) + 1
100 MK=MK + 1
NWK=MAXA(NEQ+1) - MAXA(1)
C
RETURN
END
C*****
SUBROUTINE CLEAR(A,N)
C
C PROGRAM
C TO CLEAR ARRAY A
C
IMPLICIT REAL*8(A-H,O-Z)
C
C THIS PROGRAM IS USED IN SINGLE PRECISION ARITHMETIC ON
C CDC EQUIPMENT AND DOUBLE PRECISION ARITHMETIC ON IBM
C OR UNIVAC MACHINES .ACTIVATE,DEACTIVATE OR ADJUST ABOVE
C CARD FOR SINGLE OR DOUBLE PRECISION ARITHMETIC
C

```

```

DIMENSION A(1)
DO 10 I=1,N
10 A(I)=0.
RETURN
END
C*****
SUBROUTINE ASSEM (AA)
C
C PROGRAM
C TO CALL ELEMENT SUBROUTINES FOR ASSEMBLAGE OF THE
C STRUCTURE STIFFNESS MATRIX
C
COMMON /EL/ IND, NPAR(10),NUMEG,MTOT,NFIRST,NLAST,ITWO
COMMON /TAPES/ IELMNT,ILOAD,IIN,IOUT,ISTRESS
DIMENSION AA(1)
C
REWIND IELMNT
C
DO 200 N=1,NUMEG
READ(IELMNT)NUMEST,NPAR,(AA(I),I=1,NUMEST)
C
CALL ELEMNT
C
200 CONTINUE
RETURN
C
END
C*****
SUBROUTINE ADDBAN (A,MAXA,S,LM,ND)
C
C PROGRAM
C TO ASSEMBLE UPPER TRIANGULAR ELEMENT STIFFNESS INTO
C COMPACTED GLOBAL STIFFNESS
C
C A = GLOBAL STIFFNESS
C S = ELEMENT STIFFNESS
C ND = DEGREE OF FREEDOM IN ELEMENT STIFFNESS
C S(1) S(2) S(3) ...
C S = S(ND+1) S(ND+2) ...
C S(2*ND) ...
C
C A(1) A(3) A(6) ...
C A = A(2) A(5) ...
C A(4) ...
C
IMPLICIT REAL*8(A-H,O-Z)
C
C THIS PROGRAM IS USED IN SINGLE PRECISION ARITHMETIC ON
C CDC EQUIPMENT AND DOUBLE PRECISION ARITHMETIC ON IBM
C OR UNIVAC MACHINES .ACTIVATE,DEACTIVATE OR ADJUST ABOVE
C CARD FOR SINGLE OR DOUBLE PRECISION ARITHMETIC
C
DIMENSION A(1),MAXA(1),S(1),LM(1)
C
NDI=0
DO 200 I=1,ND
II=LM(I)
IF(II) 200,200,100
100 MI=MAXA(II)

```

```

KS=I
DO 220 J=1,ND
JJ=LM(J)
IF(JJ) 220,220,110
110 IJ=II - JJ
IF(IJ)220,210,210
210 KK=MI + IJ
KSS=KS
IF(J.GE.I) KSS=J + NDI
A(KK)=A(KK) + S(KSS)
220 KS=KS +ND -J
200 NDI=NDI + ND - I
C
RETURN
END
C*****
SUBROUTINE COLSOL(A,V,MAXA,NN,NWK,NNM,KKK)
C
C PROGRAM
C TO SOLVE FINITE ELEMENT STATIC EQUILIBRIUM EQUATIONS IN
C CORE, USING COMPACTED STORAGE AND COLUMN REDUCTION SCHEME
C
C - INPUT VARIABLES -
C A(NWK) = STIFFNESS MATRIX STORED IN COMPACTED FORM
C V(NN) = RIGHT-HAND-SIDE VECTOR
C MAXA(NNM)= VECTOR CONTAINING ADDRESSES OF DIAGONAL
C ELEMENTS OF STIFFNESS MATRIX IN A
C NN = NUMBER OF EQUATIONS
C NWK = NUMBER OF ELEMENTS BELOW SKYLINE OF MATRIX
C NNM = NN + 1
C KKK = INPUT FLAG
C EQ. 1 TRIANGULARIZATION OF STIFFNESS MATRIX
C EQ. 2 REDUCTION AND BACK-SUBSTITUTION OF LOAD VECTOR
C IOUT = NUMBER OF OUTPUT DEVICE
C
C - OUTPUT VARIABLES -
C A(NWK) = D AND L - FACTORS OF STIFFNESS MATRIX
C V(NN) = DISPLACEMENT VECTORS
C
C
C THIS PROGRAM IS USED IN SINGLE PRECISION ARITHMETIC ON
C CDC EQUIPMENT AND DOUBLE PRECISION ARITHMETIC ON IBM
C OR UNIVAC MACHINES .ACTIVATE,DEACTIVATE OR ADJUST ABOVE
C CARD FOR SINGLE OR DOUBLE PRECISION ARITHMETIC
C
COMMON /TAPES/ IELMNT,ILOAD,IIN,IOUT,ISTRESS
DIMENSION A(NWK),V(1),MAXA(1)
C
C PERFORM L*D*L(T) FACTORIZATION OF STIFFNESS MATRIX
C
IF(KKK-2)40,150,150
40 DO 140 N=1,NN
KN=MAXA(N)
KL=KN+1
KU=MAXA(N+1) -1
KH=KU-KL
IF(KH)110,90,50
50 K=N-KH
IC=0

```

```

KLT=KU
DO 80 J=1,KH
IC=IC + 1
KLT=KLT -1
KI=MAXA(K)
ND=MAXA(K+1) - KI - 1
IF(ND)80,80, 60
60 KK=MIN0(IC,ND)
C=0.
DO 70 L=1,KK
70 C=C+A(KI+L)*A(KLT+L)
A(KLT)=A(KLT)-C
80 K=K+1
90 K=N
B=0.
DO 100 KK=KL,KU
K=K - 1
KI=MAXA(K)
C=A(KK)/A(KI)
B=B +C*A(KK)
100 A(KK)=C
A(KN)=A(KN) -B
110 IF(A(KN)) 120,120,140
120 STOP
140 CONTINUE
RETURN
C
C REDUCE RIGHT-HAND-SIDE VECTOR
C
150 DO 180 N=1,NN
KL=MAXA(N) + 1
KU=MAXA(N+1) - 1
IF(KU-KL)180,160,160
160 K=N
C=0.
DO 170 KK=KL,KU
K=K -1
170 C=C+A(KK)*V(K)
V(N)=V(N) -C
180 CONTINUE
C
C BACK-SUBSTITUTE
C
DO 200 N=1,NN
K=MAXA(N)
200 V(N)=V(N)/A(K)
IF (NN.EQ.1) RETURN
N=NN
DO 230 L=2,NN
KL=MAXA(N) + 1
KU=MAXA(N+1) - 1
IF(KU-KL)230,210,210
210 K=N
DO 220 KK=KL,KU
K=K -1
220 V(K)=V(K)-A(KK)*V(N)
230 N=N-1
RETURN
END

```

```

C*****
SUBROUTINE LOADV (R,NEQ)
C
C PROGRAM
C TO OBTAIN THE LOAD VECTOR
C
IMPLICIT REAL*8(A-H,O-Z)
C
C THIS PROGRAM IS USED IN SINGLE PRECISION ARITHMETIC ON
C CDC EQUIPMENT AND DOUBLE PRECISION ARITHMETIC ON IBM
C OR UNIVAC MACHINES .ACTIVATE,DEACTIVATE OR ADJUST ABOVE
C CARD FOR SINGLE OR DOUBLE PRECISION ARITHMETIC
C
COMMON /TAPES/ IELMNT,ILOAD,IIN,IOUT,ISTRESS
DIMENSION R(NEQ)
C
READ(ILOAD) R
C
RETURN
END
C*****
SUBROUTINE WRITE(DISP,ID,NEQ,NUMNP)
C
C PROGRAM
C TO PRINT DISPLACEMENTS
C
IMPLICIT REAL*8(A-H,O-Z)
C
C THIS PROGRAM IS USED IN SINGLE PRECISION ARITHMETIC ON
C CDC EQUIPMENT AND DOUBLE PRECISION ARITHMETIC ON IBM
C OR UNIVAC MACHINES .ACTIVATE,DEACTIVATE OR ADJUST ABOVE
C CARD FOR SINGLE OR DOUBLE PRECISION ARITHMETIC
C
COMMON /TAPES/IELMNT,ILOAD,IIN,IOUT,ISTRESS
DIMENSION DISP(NEQ),ID(3,NUMNP)
DIMENSION D(3)
C
C PRINT DISPLACEMENTS
C
IC=4
DO 100 II=1,NUMNP
IC=IC +1
IF(IC.LT.56) GO TO 105
IC=4
105 DO 110 I=1,3
110 D(I)=0.
C
DO 120 I=1,3
KK=ID(I,II)
IL=I
120 IF(KK.NE.0) D(IL)=DISP(KK)
C
100 continue
RETURN
C
END
C*****
SUBROUTINE STRESS (AA)
C

```



```

C PROGRAM
C TO CALL THE ELEMENT SUBROUTINE FOR THE COLCULATION OF STRESSES
C
COMMON /VAR/ NG, MODEX
COMMON /EL/ IND,NPAR(10),NUMEG,MTOT,NFIRST,NLAST,ITWO
COMMON /TAPES/ IELMNT,ILOAD,IIN,IOUT,ISTRESS
DIMENSION AA(1)
C
C LOOP OVER ALL ELEMENT GROUPS
C
REWIND IELMNT
C
DO 100 N=1,NUMEG
NG=N
C
READ(IELMNT) NUMEST,NPAR,(AA(I),I=1,NUMEST)
C
CALL ELEMNT
C
100 CONTINUE
C
RETURN
END
C*****
SUBROUTINE TRUSS
C
C PROGRAM
C TO SET UP STORAGE AND CALL THE TRUSS ELEMENT SUBROUTINE
C
COMMON /SOL/ NUMNP,NEQ,NWK,NUMEST,MIDEST,MAXEST,MK
COMMON /DIM/ N1,N2,N3,N4,N5,N6,N7,N8,N9,N10,N11,N12,N13,N14,N15
COMMON /EL/ IND,NPAR(10),NUMEG,MTOT,NFIRST,NLAST,ITWO
COMMON /TAPES/ IELMNT,ILOAD,IIN,IOUT,ISTRESS
COMMON A(1)
C
EQUIVALENCE (NPAR(2),NUME),(NPAR(3),NUMMAT)
C
NFIRST=N6
IF(IND.GT.1) NFIRST=N5
N101=NFIRST
N102=N101 + 16*NUME
N103=N102 + 8*NUME*ITWO
N104=N103 + 8*NUME*ITWO
N105=N104 + NUMMAT*ITWO
N106=N105 + NUMMAT*ITWO
N107=N106 + NUMMAT*ITWO
N108=N107 + NUMMAT*ITWO
N109=N108 + NUMMAT*ITWO
N110=N109 + NUMMAT*ITWO
N111=N110 + NUME
NLAST=N111
C
IF (IND.GT.1) GO TO 100
IF (NLAST.GT.MTOT) CALL ERROR(NLAST-MTOT,3)
GO TO 200
100 IF (NLAST.GT.MTOT) CALL ERROR(NLAST-MTOT,4)
C
200 MIDEST=NLAST - NFIRST
C

```

```

CALL RUSS (A(N1),A(N2),A(N3),A(N4),A(N4),A(N5),A(N101),A(N102),
1A(N103),A(N104),A(N105),A(N106),A(N107),A(N108),A(N109),A(N110))
C
RETURN
C
END
C*****
SUBROUTINE RUSS (ID,X,Y,Z,U,MHT,LM,XX,YY,A1,A2,A3,A4,A5,A6,MATP)
C
C PROGRAM
C TRUSS ELEMENT SUBROUTINE
C
IMPLICIT REAL*8(A-H,O-Z)
C
C THIS PROGRAM IS USED IN SINGLE PRECISION ARITHMETIC ON
C CDC EQUIPMENT AND DOUBLE PRECISION ARITHMETIC ON IBM
C OR UNIVAC MACHINES. ACTIVATE, DEACTIVATE OR ADJUST ABOVE
C CARDS FOR SINGLE OR DOUBLE PRECISION ARITHMETIC
C
COMMON /SOL/ NUMNP,NEQ,NWK,NUMEST,MIDEST,MAXEST,MK
COMMON /DIM/ N1,N2,N3,N4,N5,N6,N7,N8,N9,N10,N11,N12,N13,N14,N15
COMMON /EL/ IND,NPAR(10),NUMEG,MTOT,NFIRST,NLAST,ITWO
COMMON /VAR/ NG,MODEX
COMMON /TAPES/ IELMNT,ILOAD,IIN,IOUT,ISTRESS
COMMON A(1)
C
REAL A
C
DIMENSION X(1),Y(1),Z(1),ID(3,1),LM(16,1),MATP(1),U(1),MHT(1)
DIMENSION XX(8,1),YY(8,1),A1(1),A2(1),A3(1),A4(1),A5(1),A6(1)
DIMENSION DR(3),IPS(1)
DIMENSION EPSX(3,3),EPSY(3,3),GAMA(3,3)
DIMENSION S(136),SS(16,16),UU(8),VV(8)
DIMENSION AX(3),H(3),E(8),F(8),PNXSI(8),PNXIT(8)
DIMENSION SIGX(3,3),SIGY(3,3),TUXY(3,3)
C
EQUIVALENCE (NPAR(1),NPAR1),(NPAR(2),NUME),(NPAR(3),NUMMAT)
C
C ND = NUMBER DEGREE OF FREEDOM PER EACH ELEMENT
C AX = GAUSSIAN INTEGRATION POINTS
C H = GAUSSIAN INTEGRATION WEIGHTS
C XX = X COORDINATE OF NODE
C YY = Y COORDINATE OF NODE
C MTYP = NUMBER OF MATERIAL TYPE AT EACH ELEMENT
C NUMMAT= TOTAL NUMBER OF MATERIAL TYPES
C A1,A2,A3,A4,A5,A6 = A11,A12,A16,A22,A26,A66 ARE EXTENSIONAL MATRIX
C I1,I2,I3,I4,I5,I6,I7,I8 ARE NODE ORDER STARTS FROM THE RIGHT-UPPER
C CORNER OF AN ELEMENT AND COUNTED COUNTER-CLOCKWISELY
C
ND=16
C
AX(1)=0.774596669241483D0
AX(2)=0.000000000000000D0
AX(3)=-0.774596669241483D0
H(1)=0.5555555555555556D0
H(2)=0.8888888888888889D0
H(3)=0.5555555555555556D0
C
GO TO (300,610,900),IND

```

```

C
C READ AND GENERATE ELEMENT INFORMATION
C
300 DO 10 I=1,NUMMAT
READ(IIN,9000)N,A1(N),A2(N),A3(N),A4(N),A5(N),A6(N)
9000 FORMAT(I5,6F11.0)
10 CONTINUE
C
N=1
100 READ(IIN,1020) M,I1,I2,I3,I4,I5,I6,I7,I8,MTYP,KG
1020 FORMAT(11I5)
IF (KG.EQ.0) KG=1
120 IF(M.NE.N) GO TO 200
MY=MTYP
KKK=KG
C
C SAVE COORDINATE SYSTEM
C
200 XX(1,N)=X(I1)
YY(1,N)=Y(I1)
XX(2,N)=X(I2)
YY(2,N)=Y(I2)
XX(3,N)=X(I3)
YY(3,N)=Y(I3)
XX(4,N)=X(I4)
YY(4,N)=Y(I4)
XX(5,N)=X(I5)
YY(5,N)=Y(I5)
XX(6,N)=X(I6)
YY(6,N)=Y(I6)
XX(7,N)=X(I7)
YY(7,N)=Y(I7)
XX(8,N)=X(I8)
YY(8,N)=Y(I8)
C
MATP(N)=MY
C
C LM = DEGREE OF FREEDOM IN X,Y DIRECTIONS PER EACH NODE
C
DO 390 L=1,16
390 LM(L,N)=0
DO 391 LK=1,2
LM(LK,N)=ID(LK,I1)
LM(LK+2,N)=ID(LK,I2)
LM(LK+4,N)=ID(LK,I3)
LM(LK+6,N)=ID(LK,I4)
LM(LK+8,N)=ID(LK,I5)
LM(LK+10,N)=ID(LK,I6)
LM(LK+12,N)=ID(LK,I7)
LM(LK+14,N)=ID(LK,I8)
391 CONTINUE
C
CALL COLHT (MHT,ND,LM(1,N))
C
IF (N.EQ.NUME) RETURN
N=N+1
I1=I1+KKK
I2=I2+KKK
I3=I3+KKK

```

```

I4=I4+KKK
I5=I5+KKK
I6=I6+KKK
I7=I7+KKK
I8=I8+KKK
C
IF (N.GT.M) GO TO 100
GO TO 120
C
C DEVELOP STIFFNESS MATRIX OF EIGHT-NODED ELEMENT
C
610 DO 611 N=1,NUME
MY=MATP(N)
A11=A1(MY)
A12=A2(MY)
A16=A3(MY)
A22=A4(MY)
A26=A5(MY)
A66=A6(MY)
DO 612 I=1,16
DO 612 J=1,16
SS(I,J)=0.D0
612 CONTINUE
C
DO 102 L=1,3
XA=AX(L)
DO 102 K=1,3
YA=AX(K)
C
XJ11=0.D0
XJ12=0.D0
XJ21=0.D0
XJ22=0.D0
C
C PARTIAL PHI OVER PARTIAL XSI
C
PNXSI(1)=(2.D0*XA+YA+2.D0*XA*YA+YA*YA)/4.D0
PNXSI(2)=(-2.D0*XA-2.D0*XA*YA)/2.D0
PNXSI(3)=(2.D0*XA-YA+2.D0*XA*YA-YA*YA)/4.D0
PNXSI(4)=(-1.D0+YA*YA)/2.D0
PNXSI(5)=(2.D0*XA+YA-2.D0*XA*YA-YA*YA)/4.D0
PNXSI(6)=(-2.D0*XA+2.D0*XA*YA)/2.D0
PNXSI(7)=(2.D0*XA-YA-2.D0*XA*YA+YA*YA)/4.D0
PNXSI(8)=(1.D0-YA*YA)/2.D0
C
C PARTIAL PHI OVER PARTIAL ETA
C
PNXIT(1)=(2.D0*YA+XA+XA*XA+2.D0*XA*YA)/4.D0
PNXIT(2)=(1.D0-XA*XA)/2.D0
PNXIT(3)=(2.D0*YA-XA+XA*XA-2.D0*XA*YA)/4.D0
PNXIT(4)=(-2.D0*YA+2.D0*XA*YA)/2.D0
PNXIT(5)=(2.D0*YA+XA-XA*XA-2.D0*XA*YA)/4.D0
PNXIT(6)=(-1.D0+XA*XA)/2.D0
PNXIT(7)=(2.D0*YA-XA-XA*XA+2.D0*XA*YA)/4.D0
PNXIT(8)=(-2.D0*YA-2.D0*XA*YA)/2.D0
C
C ELEMENTS OF JACOBIAN
C
DO 52 KK=1,8

```

```

XJ11=XJ11+PNXSI(KK)*XX(KK,N)
XJ12=XJ12+PNXSI(KK)*YY(KK,N)
XJ21=XJ21+PNXIT(KK)*XX(KK,N)
XJ22=XJ22+PNXIT(KK)*YY(KK,N)
52 CONTINUE
C
C DETERMINANT OF JACOBIAN
C
AVXJ=(XJ11*XJ22)-(XJ12*XJ21)
C
C INVERSE OF JACOBIAN
C
STJ11=XJ22/AVXJ
STJ12=-XJ12/AVXJ
STJ21=-XJ21/AVXJ
STJ22=XJ11/AVXJ
C
C E(I): PARTIAL PHI OVER PARTIAL X
C
DO 12 I=1,8
E(I)=STJ11*PNXSI(I)+STJ12*PNXIT(I)
12 CONTINUE
C
C F(I): PARTIAL PHI OVER PARTIAL Y
C
DO 13 I=1,8
F(I)=STJ21*PNXSI(I)+STJ22*PNXIT(I)
13 CONTINUE
C
C STIFFNESS MATRIX OF EIGHT-NODED ELEMENT: 16 BY 16
C
DO 90 I=1,8
DO 90 J=1,8
KI=I*2-1
KJ=J*2-1
SS(KI,KJ)=SS(KI,KJ)+(A11*E(I)*E(J)+A16*F(I)*E(J)+
*A16*E(I)*F(J)+A66*F(I)*F(J))*AVXJ*H(L)*H(K)
SS(KI+1,KJ)=SS(KI+1,KJ)+(A12*F(I)*E(J)+A16*E(I)*E(J)+
*A26*F(I)*F(J)+A66*E(I)*F(J))*AVXJ*H(L)*H(K)
SS(KI,KJ+1)=SS(KI,KJ+1)+(A16*E(I)*E(J)+A66*F(I)*E(J)+
*A12*E(I)*F(J)+A26*F(I)*F(J))*AVXJ*H(L)*H(K)
SS(KI+1,KJ+1)=SS(KI+1,KJ+1)+(A26*F(I)*E(J)+A66*E(I)*E(J)+
*A22*F(I)*F(J)+A26*E(I)*F(J))*AVXJ*H(L)*H(K)
90 CONTINUE
102 CONTINUE
C
C TRANSFORM SS(I,J) INTO S(IJ)
C
IJ=0
DO 95 I=1,16
DO 95 J=I,16
IJ=IJ+1
S(IJ)=SS(I,J)
95 CONTINUE
C
CALL ADDBAN (A(N3),A(N2),S,LM(1,N),ND)
C
611 CONTINUE
RETURN

```

```

C
C STRESS CALCULATION
C
C EPSX = EPSILON X
C EPSY = EPSILON Y
C GAMA = GAMA XY
C SIGX = SIGMA X
C SIGY = SIGMA Y
C TUXY = TAU XY
C
900 DO 663 N=1,NUME
C
DO 664 I=1,8
UU(I)=0.D0
VV(I)=0.D0
664 CONTINUE
C
DO 666 I=1,3
DO 666 J=1,3
EPSX(I,J)=0.D0
EPSY(I,J)=0.D0
GAMA(I,J)=0.D0
666 CONTINUE
C
MY=MATP(N)
A11=A1(MY)
A12=A2(MY)
A16=A3(MY)
A22=A4(MY)
A26=A5(MY)
A66=A6(MY)
C
DO 655 L=1,3
XA=AX(L)
DO 655 K=1,3
YA=AX(K)
C
XJ11=0.D0
XJ12=0.D0
XJ21=0.D0
XJ22=0.D0
C
C PARTIAL PHI OVER PARTIAL XSI
C
PNXSI(1)=(2.D0*XA+YA+2.D0*XA*YA+YA*YA)/4.D0
PNXSI(2)=(-2.D0*XA-2.D0*XA*YA)/2.D0
PNXSI(3)=(2.D0*XA-YA+2.D0*XA*YA-YA*YA)/4.D0
PNXSI(4)=(-1.D0+YA*YA)/2.D0
PNXSI(5)=(2.D0*XA+YA-2.D0*XA*YA-YA*YA)/4.D0
PNXSI(6)=(-2.D0*XA+2.D0*XA*YA)/2.D0
PNXSI(7)=(2.D0*XA-YA-2.D0*XA*YA+YA*YA)/4.D0
PNXSI(8)=(1.D0-YA*YA)/2.D0
C
C PARTIAL PHI OVER PARTIAL ETA
C
PNXIT(1)=(2.D0*YA+XA+XA*XA+2.D0*XA*YA)/4.D0
PNXIT(2)=(1.D0-XA*XA)/2.D0
PNXIT(3)=(2.D0*YA-XA+XA*XA-2.D0*XA*YA)/4.D0
PNXIT(4)=(-2.D0*YA+2.D0*XA*YA)/2.D0

```

```

PNXIT(5)=(2.D0*YA+XA-XA*XA-2.D0*XA*YA)/4.D0
PNXIT(6)=(-1.D0+XA*XA)/2.D0
PNXIT(7)=(2.D0*YA-XA-XA*XA+2.D0*XA*YA)/4.D0
PNXIT(8)=(-2.D0*YA-2.D0*XA*YA)/2.D0
C
C ELEMENTS OF JACOBIAN
C
DO 53 KK=1,8
XJ11=XJ11+PNXSI(KK)*XX(KK,N)
XJ12=XJ12+PNXSI(KK)*YY(KK,N)
XJ21=XJ21+PNXIT(KK)*XX(KK,N)
XJ22=XJ22+PNXIT(KK)*YY(KK,N)
53 CONTINUE
C
C DETERMINANT OF JACOBIAN
C
AVXJ=(XJ11*XJ22)-(XJ12*XJ21)
C
STJ11=XJ22/AVXJ
STJ12=-XJ12/AVXJ
STJ21=-XJ21/AVXJ
STJ22=XJ11/AVXJ
C
C E(I): PARTIAL PHI OVER PARTIAL X
C
DO 771 I=1,8
E(I)=STJ11*PNXSI(I)+STJ12*PNXIT(I)
771 CONTINUE
C
C F(I): PARTIAL PHI OVER PARTIAL Y
C
DO 772 I=1,8
F(I)=STJ21*PNXSI(I)+STJ22*PNXIT(I)
772 CONTINUE
C
C CALCULATION OF STRAIN
C
KK=LM(1,N)
IF (KK.EQ.0) GO TO 801
UU(1)=U(KK)
C
801 KK=LM(2,N)
IF (KK.EQ.0) GO TO 802
VV(1)=U(KK)
C
802 KK=LM(3,N)
IF (KK.EQ.0) GO TO 803
UU(2)=U(KK)
C
803 KK=LM(4,N)
IF (KK.EQ.0) GO TO 804
VV(2)=U(KK)
C
804 KK=LM(5,N)
IF (KK.EQ.0) GO TO 805
UU(3)=U(KK)
C
805 KK=LM(6,N)
IF (KK.EQ.0) GO TO 806

```

```

VV(3)=U(KK)
C
806 KK=LM(7,N)
IF (KK.EQ.0) GO TO 807
UU(4)=U(KK)
C
807 KK=LM(8,N)
IF (KK.EQ.0) GO TO 808
VV(4)=U(KK)
C
808 KK=LM(9,N)
IF (KK.EQ.0) GO TO 809
UU(5)=U(KK)
C
809 KK=LM(10,N)
IF (KK.EQ.0) GO TO 810
VV(5)=U(KK)
C
810 KK=LM(11,N)
IF (KK.EQ.0) GO TO 811
UU(6)=U(KK)
C
811 KK=LM(12,N)
IF (KK.EQ.0) GO TO 812
VV(6)=U(KK)
C
812 KK=LM(13,N)
IF (KK.EQ.0) GO TO 813
UU(7)=U(KK)
C
813 KK=LM(14,N)
IF (KK.EQ.0) GO TO 814
VV(7)=U(KK)
C
814 KK=LM(15,N)
IF (KK.EQ.0) GO TO 815
UU(8)=U(KK)
C
815 KK=LM(16,N)
IF (KK.EQ.0) GO TO 816
VV(8)=U(KK)
C
816 DO 655 LK=1,8
EPSX(L,K)=EPSX(L,K)+UU(LK)*E(LK)
EPSY(L,K)=EPSY(L,K)+VV(LK)*F(LK)
GAMA(L,K)=GAMA(L,K)+(UU(LK)*F(LK)+VV(LK)*E(LK))
655 CONTINUE
C
C STRESS-STRAIN RELATIONSHIP
C
DO 667 L=1,3
DO 667 K=1,3
SIGX(L,K)=A11*EPSX(L,K)+A12*EPSY(L,K)+A16*GAMA(L,K)
SIGY(L,K)=A12*EPSX(L,K)+A22*EPSY(L,K)+A26*GAMA(L,K)
TUXY(L,K)=A16*EPSX(L,K)+A26*EPSY(L,K)+A66*GAMA(L,K)
667 CONTINUE
C
LK=0
DO 668 L=1,3

```



```

DO 668 K=1,3
LK=LK+1
if (LK.eq.5) THEN
WRITE(16,9095)N,EPX(L,K),EPSY(L,K),GAMA(L,K)
9095 FORMAT(1X,1X,I5,3E18.6)
endif
668 CONTINUE
C
663 CONTINUE
9090 FORMAT(///,32X,26H STRESS RESULTANTS ,28X,
122H STRAINS ,//7HELEMENT,1X,5H N0DE,5X,
214H ** N-X ** ,4X,14H ** N-Y ** ,4X,14H ** N-XY ** ,2X,
314H * EPSILON-X * ,5X,14H * EPSILON-Y * ,3X,14H * GAMA-XY * )
RETURN
END
C*****
SUBROUTINE SECOND(TIM)
C
C SUBROUTINE TO OBTAIN TIME
C
TIM=FLOAT(II)
RETURN
END
C*****
C *****
C * MAIN PROGRAM *
C *
C * .Ite: Number of iteration needed to align the principal*
C * stress direction with the fiber angle in the C plie *
C * .Palf(i): fiber angle in the C ply for element i *
C * .Qlf(i): principal stress direction for the element i *
C * .T: transformation matrix *
C * .EPS: strain *
C * .SIG: stress *
C * .S: Compliance matrix *
C * .Q: Stiffness matrix *
C * .QT: Reduced stiffness matrix *
C * .E1, E2, v12, G12: material properties *
C *****
C SUBROUTINE TO COMPUTE THE ANGLES
SUBROUTINE ANGLE(Palf,Qlf,Ite)
double precision Qlf,Palf,S,Q,T,INVT,QT,O,EPS,STR,E1,E2,v12,G12,
- A,EPX1,EPX2,EPX3,Qalf,Sub,Qnge,SIG1,SIG2,SIG3
DIMENSION EPX1(200),EPX2(200),EPX3(200),Qlf(200),Palf(200),
- Qalf(200),Sub(200),Qnge(200),S(3,3),Q(3,3),T(3,3),
- INVT(3,3),QT(3,3),EPS(3),STR(3),SIG1(200),SIG2(200),
- SIG3(200)
open(16,file='ISTRESS')
open(25,file='angle')
numele=200
C
E1=130.E9
E2=10.66E9
V12=0.263
G12=3.88E9
CALL PUTZERO(S)
S(1,1)=1./E1
S(2,2)=1./E2
S(3,3)=1./G12

```

```

S(1,2)=-V12/E1
S(2,1)=S(1,2)
CALL PUTZERO (Q)
A=S(1,1)*S(2,2)-S(1,2)*S(1,2)
Q(1,1)=S(2,2)/A
Q(1,2)=-S(1,2)/A
Q(2,1)=Q(1,2)
Q(2,2)=S(1,1)/A
Q(3,3)=G12
C
do 406 i=1,numele
C
O=PalF(i)*3.1415926/180
Call PUTZERO (QT)
CALL CALCUL(T,O)
CALL INVERT(T,INVT)
CALL PROD(Q,INVT,QT)
READ(16,*)ki,EPS1(i),EPS2(i),EPS3(i)
do 12 j=1,3
EPS(j)=0
STR(j)=0
12 Continue
EPS(1)=EPS1(i)
EPS(2)=EPS2(i)
EPS(3)=EPS3(i)
call PRODMV(EPS,QT,STR)
SIG1(i)=STR(1)
SIG2(i)=STR(2)
SIG3(i)=STR(3)
Qlf(i)=0
PP=2*SIG3(i)
QQ=SIG1(i)-SIG2(i)
if (QQ.eq.0) GOTO 406
Qalf(i)=0.5*ATAN2(PP,QQ)
Sub(i)=Qalf(i)-PalF(i)
If (Sub(i).le.0.005.and.Sub(i).ge.-0.005) Then
k=k+1
Qlf(i)=PalF(i)
Endif
If (Sub(i).ge.0.005.or.Sub(i).le.-0.005) Then
Qlf(i)=Qalf(i)
Endif
406 Continue
If (k.ge.195) Then
do 408 i=1,200
Qnge(i)=Qlf(i)*180/3.145
408 write(25,407)i,Qnge(i),Ite
407 format(I5,f13.3,I5)
stop
Endif
C
C do 501 i=1,200
C 501 write(16,502)i,Qlf(i)*180/3.145
C 502 format(I5,f13.3)
C
close(16)
close(25)
RETURN
End

```

```

C *****
C * *
c * Program to convert ABAQUS input file to FEM2D *
c * input file. *
c * *
C *****
SUBROUTINE PRG(TE)
integer L1,L2
double precision EE1,E2,V12,G12,S,Q,T,TT,
- ST,QT,INVT,MA,TETA,O,TE
dimension x(663),y(663),z(663)
dimension m1(200),m2(200),m3(200),m4(200),
1 m5(200),m6(200),m7(200),m8(200)
dimension num(200),bc(200),ind(200),nbcx(700),
- nbcy(700),nbcz(700),jfnod(17),jfd(17),fnor(17)
dimension S(3,3),Q(3,3),T(3,3),TT(3,3),INVT(3,3),
- ST(3,3),QT(3,3),ZZ(100),EE1(200),E2(200),
- V12(200),G12(200),TETA(200),TE(300),MA(3,3),
- N(200)
open(15,file='data1')
open(3,file='data2')
numele=200
numnod=663
numf=17
numbc=104
njunk=1
kcode=0
write (3,9)
9 format('first try to write the main program which will be able to
1d')
read(15,*)numnod,njunk,njunk,njunk
write(3,10)numnod,njunk,njunk,njunk
10 format(i5,i5,i5,i5)
do 100 k=1,numnod
100 read(15,*)k,nbcx(k),nbcy(k),nbcz(k),x(k),y(k),z(k),kcode
read(15,*)jn,numf
do 112 i=1,numf
112 read (15,*) jfnod(i),jfd(i),fnor(i)
do 400 k=1,numele
400 read(15,*)k,m1(k),m2(k),m3(k),m4(k),
1 m5(k),m6(k),m7(k),m8(k),k,kcode
do 600 k=1,numnod
600 write(3,620)k,nbcx(k),nbcy(k),nbcz(k),x(k),y(k),z(k),kcode
620 format(4i5,3f10.8,i5)
write(3,650)1,numf
650 format(2I5)
do 630 k=1,numf
630 write(3,640)jfnod(k),jfd(k),fnor(k)
640 format(2I5,f15.5)
write(3,660)1,numele,numele
660 format(3I5)
DO 144 I=1,176
N(I)=16
144 CONTINUE
DO 155 I=177,200
N(I)=56
155 CONTINUE
H=0.00028
DO 44 L1=1,16

```

```

EE1(L1)=130.E9
E2(L1)=10.66E9
V12(L1)=0.263
G12(L1)=3.88E9
44 CONTINUE
DO 55 L2=17,56
EE1(L2)=23.58E9
E2(L2)=23.58E9
V12(L2)=0.09176
G12(L2)=4.14E9
55 CONTINUE
DO 222 K=1,numele
TETA(1)=45
TETA(2)=-45
TETA(3)=TE(K)
TETA(4)=TE(K)
TETA(5)=0
TETA(6)=90
TETA(7)=TE(K)
TETA(8)=TE(K)
TETA(9)=TE(K)
TETA(10)=TE(K)
TETA(11)=90
TETA(12)=0
TETA(13)=TE(K)
TETA(14)=TE(K)
TETA(15)=-45
TETA(16)=45
DO 133 J=17,56
TETA(J)=0
133 CONTINUE
CALL PUTZERO(MA)
CALL PUTZERO(S)
DO 70 L=1,N(K)
S(1,1)=1.0/EE1(L)
S(2,2)=1./E2(L)
S(3,3)=1./G12(L)
S(1,2)=-V12(L)/EE1(L)
S(2,1)=S(1,2)
A=S(1,1)*S(2,2)-S(1,2)*S(1,2)
Q(1,1)=S(2,2)/A
Q(1,2)=-S(1,2)/A
Q(2,1)=Q(1,2)
Q(2,2)=S(1,1)/A
Q(3,3)=G12(L)
O=TETA(L)*3.1415926/180
CALL CALCUL(T,O)
CALL INVERT(T,INVT)
CALL TRANS(T,TT)
CALL PROD(S,TT,ST)
CALL PROD(Q,INVT,QT)
DO 111 I=1,3
DO 101 J=1,3
MA(I,J)=MA(I,J)+QT(I,J)*H
101 CONTINUE
111 CONTINUE
70 CONTINUE
WRITE (3,700) K,MA(1,1),MA(1,2),MA(1,3),
- MA(2,2),MA(2,3),MA(3,3)

```

```

700 FORMAT(I5,6f11.0)
222 CONTINUE
do 800 k=1,numele
800 write(3,810)k,m1(k),m2(k),m3(k),m4(k),
1 m5(k),m6(k),m7(k),m8(k),k,kcode
write(3,803)
803 format('first try to write the may program which will be able to
1d' )
write(3,804)0,0,0,0
804 format(4I5)
810 format(11i5)
close(15)
close(3)
RETURN
END
C**** TO INITIALIZE THE MATRIX AT ZERO *****
C
SUBROUTINE PUTZERO (B)
C
DOUBLE PRECISION B
dimension B(3,3)
C
DO 10 I=1,3
DO 20 J=1,3
B(I,J)=0
20 CONTINUE
10 CONTINUE
RETURN
END
C
C**** TO COMPUTE THE TRANSFORMATION MATRIX *****
C
SUBROUTINE CALCUL(T,O)
DOUBLE PRECISION T,SN,C,O
dimension T(3,3)
SN=DSIN(O)
C=DCOS(O)
T(1,1)=C*C
T(1,2)=SN*SN
T(1,3)=2*SN*C
T(2,1)=T(1,2)
T(2,2)=T(1,1)
T(2,3)=-2*SN*C
T(3,1)=-SN*C
T(3,2)=-T(3,1)
T(3,3)=C*C-SN*SN
RETURN
END
C
C**** TO INVERT T *****
C
SUBROUTINE INVERT(B,INVB)
DOUBLE PRECISION Z1,Z2,B,DET,INVB,COF
dimension B(3,3),INVB(3,3),COF(3,3)
C
Z1=B(1,1)*B(2,2)*B(3,3)+B(2,1)*B(3,2)*B(1,3)+B(3,1)*B(1,2)*B(2,3)
Z2=B(3,1)*B(2,2)*B(1,3)+B(2,1)*B(1,2)*B(3,3)+B(1,1)*B(3,2)*B(2,3)
DET=Z1-Z2
COF(1,1)=B(2,2)*B(3,3)-B(3,2)*B(2,3)

```

```

COF(1,2)=B(3,1)*B(2,3)-B(2,1)*B(3,3)
COF(1,3)=B(2,1)*B(3,2)-B(3,1)*B(2,2)
COF(2,1)=B(3,2)*B(1,3)-B(1,2)*B(3,3)
COF(2,2)=B(1,1)*B(3,3)-B(3,1)*B(1,3)
COF(2,3)=B(3,1)*B(1,2)-B(1,1)*B(3,2)
COF(3,1)=B(1,2)*B(2,3)-B(2,2)*B(1,3)
COF(3,2)=B(2,1)*B(1,3)-B(1,1)*B(2,3)
COF(3,3)=B(1,1)*B(2,2)-B(2,1)*B(1,2)
DO 10 I=1,3
DO 20 J=1,3
INVB(I,J)=COF(J,I)/DET
20 CONTINUE
10 CONTINUE
RETURN
END
C
C*** TO TRANSPOSE T *****
C
SUBROUTINE TRANS(B,BT)
C
DOUBLE PRECISION B,BT
DIMENSION B(3,3),BT(3,3)
DO 10 I=1,3
DO 20 J=1,3
BT(I,J)=B(J,I)
20 CONTINUE
10 CONTINUE
RETURN
END
C
C*** TO COMPUTE THE PRODUCT OF 3 MATRIX *****
C
SUBROUTINE PROD (B,D,E)
DOUBLE PRECISION B,D,E
DIMENSION B(3,3),D(3,3),E(3,3)
DO 10 I=1,3
DO 20 J=1,3
E(I,J)=0
DO 30 K=1,3
DO 40 L=1,3
E(I,J)=E(I,J)+D(I,K)*D(J,L)*B(K,L)
40 CONTINUE
30 CONTINUE
20 CONTINUE
10 CONTINUE
RETURN
END
C
C*****
SUBROUTINE PRODMV(VA,MAT,VB)
C
DOUBLE PRECISION VA,VB,MAT
DIMENSION VA(3),VB(3),MAT(3,3)
C
DO 800 I=1,3
VB(I)=0
DO 801 J=1,3
VB(I)=MAT(I,J)*VA(J)+VB(I)
801 CONTINUE

```

```
800 CONTINUE  
RETURN  
  
END
```

Appendix B

Sample of an ABAQUS input file

This appendix contains an ABAQUS input file used to study the postbuckling response of the straight fiber plate having two edges clamped. This input file is known to be compatible with ABAQUS version 5.2.

```
*HEADING
BUCK
** NEUTRAL FILE GENERATED ON: 23-SEP-94 16:33:14 PATABA VERSION: 3.1A
**
** NODE DEFINITIONS
**
*NODE
1, .457300007E+00, .215000004E+00, .000000000E+00
2, .457392931E+00, .211236179E+00, .000000000E+00
3, .457672894E+00, .207468569E+00, .000000000E+00
4, .458135098E+00, .203747571E+00, .000000000E+00
5, .458777696E+00, .200064704E+00, .000000000E+00
.
.
.
529, .479750007E+00, .000000000E+00, .000000000E+00
530, .493187517E+00, .000000000E+00, .000000000E+00
531, .506624997E+00, .000000000E+00, .000000000E+00
532, .520062506E+00, .000000000E+00, .000000000E+00
533, .533500016E+00, .000000000E+00, .000000000E+00
**
** NODE SETS FROM NAMED COMPONENTS
```



```

**
*NSET, NSET=SNODE
261 262 263 264 265 266 267 268 270 271 272 273 274 275 276
277
**
** ELEMENT DEFINITIONS
**
*ELEMENT, TYPE=S8R5 , ELSET=PID0
1, 3, 1, 27, 29, 2, 18, 28, 19
2, 5, 3, 29, 31, 4, 19, 30, 20
3, 7, 5, 31, 33, 6, 20, 32, 21
4, 9, 7, 33, 35, 8, 21, 34, 22
5, 11, 9, 35, 37, 10, 22, 36, 23
.
.
.
155, 499, 497, 521, 523, 498, 511, 522, 512
156, 501, 499, 523, 525, 500, 512, 524, 513
157, 503, 501, 525, 527, 502, 513, 526, 514
158, 505, 503, 527, 529, 504, 514, 528, 515
159, 507, 505, 529, 531, 506, 515, 530, 516
160, 509, 507, 531, 533, 508, 516, 532, 517
*EQUATION
2
SNODE,1,-1.0,269,1,1.0
** ELEMENT PROPERTIES
* SHELL SECTION, ELSET=PID0, COMPOSITE
0.000252,3,MAT,PL45
0.000252,3,MAT,PLM45
0.000756,3,MAT,ZERO
0.000252,3,MAT,PL90
0.001008,3,MAT,ZERO
0.000252,3,MAT,PL90
0.000756,3,MAT,ZERO
0.000252,3,MAT,PLM45
0.000252,3,MAT,PL45
* MATERIAL, NAME=MAT
* ELASTIC, TYPE=LAMINA
130E9,10.66E+09,0.263,3.88E+09,3.88E+09,3.5E+09
* ORIENTATION, NAME=PL45
1,0,0,0,1,0
3,45
* ORIENTATION, NAME=PLM45
1,0,0,0,1,0
3,-45
* ORIENTATION, NAME=ZERO
1,0,0,0,1,0
3,0
* ORIENTATION, NAME=PL90
1,0,0,0,1,0
3,90
**
** LOAD CASE 1
**
*STEP,NLGEOM
LOAD CASE 1
*STATIC
.08, 1.
**

```

```
*CLOAD, OP=NEW
269, 1, 50000.0000
422, 3, -25.0000
**
*BOUNDARY, OP=NEW
1, 2,, 0.0
1, 4,, 0.0
1, 6,, 0.0
18, 2,, 0.0
18, 4,, 0.0
.
.
.
532, 5,, 0.0
533, 1,, 0.0
533, 3,, 0.0
533, 5,, 0.0
533, 6,, 0.0
*NODE FILE, SUMMARY=NO
U
*NODE FILE,SUMMARY=NO
CF
*NODE PRINT, SUMMARY=NO
U,CF1

*END STEP
```

VITA

Yannick P.H. FIERLING was born in Sarreguemines, France, on February 1st 1971. He attended public school in Petit-Rederching and completed his high-school education in a math section in 1989. He spent the 2 next years studying mathematics in the “Faculté des Sciences” in Nancy. In 1991, he joined the Engineering School in Compiègne (U.T.C.). In September 1992, he was awarded a scholarship from the European Community to spend 4 months in Stuttgart (Germany). In June 1993, he was selected by his school to pursue his education in the United States. Granted the Lavoisier Scholarship from the “Ministère des Affaires Etrangère Française” for his program of study, he enrolled at Virginia Polytechnic Institute and State University in the Department of Engineering Science and Mechanics.